Final Report to the Air Force Office of Scientific Research
March, 2008
Grant Number FA9550-05-1-0079

Noise Identification In A Hot Transonic Jet Using Low-Dimensional Methods

André M. Hall, *Jeremy T. Pinier, †Mark N. Glauser‡
Syracuse University, 149 Link Hall, Syracuse, NY 13244

Lawrence Ukeiley§
University of Florida, 1350 N. Poquito Road, Shalimar, FL 32579

*Ph.D. Candidate, Dept. of Mech. & Aerospace Eng.
†Research Aerospace Engineer, NASA Langley Research Center, Hampton, VA 23681.
‡Professor, Dept. of Mech. & Aerospace Eng.
§Assistant Professor, Mech. & Aerospace Engineering

20080604028

REPORT DOCUMENTATION PAGE

Form Approved
OMB No. 0704-0188

Public reporting burden for this collection of information is estimated to average 1 hour per response, including the time for reviewing instructions, searching data sources, gathering and maintaining the data needed, and completing and reviewing the collection of information. Send comments regarding this burden estimate or any other aspect of this collection of information, including suggestions for reducing this burden to Washington Headquarters Service, Directorate for Information Operations and Reports, 1215 Jefferson Davis Highway, Suite 1204, Arlington, VA 22202-4302, and to the Office of Management and Budget, Paperwork Reduction Project (0704-0188) Washington, DC 20503.
PLEASE DO NOT RETURN YOUR FORM TO THE ABOVE ADDRESS.

1. REPORT DATE *(DD-MM-YYYY)*	2. REPORT TYPE	3. DATES COVERED *(From - To)*
	Final Technical Report	1 Jan 2005 – 31 Dec 2007

4. TITLE AND SUBTITLE

Noise Identification In a Hot Transonic Jet Using Low-Dimensional Methods

5a. CONTRACT NUMBER

FA9550-05-1-0079

5b. GRANT NUMBER

5c. PROGRAM ELEMENT NUMBER

6. AUTHOR(S)

Dr. Mark N. Glauser

5d. PROJECT NUMBER

5e. TASK NUMBER

5f. WORK UNIT NUMBER

7. PERFORMING ORGANIZATION NAME(S) AND ADDRESS(ES)

Mechanical Aerospace and Manufacturing Engineering
Syracuse University
149 Link Hall
Syracuse NY 13244

8. PERFORMING ORGANIZATION REPORT NUMBER

9. SPONSORING/MONITORING AGENCY NAME(S) AND ADDRESS(ES)

Air Force Office of Scientific Research (AFOSR)
875 N. Arlington St., Rm. 3112
Arlington, VA 22203
Dr John Schmisseur/NA

10. SPONSOR/MONITOR'S ACRONYM(S)
AFOSR

11. SPONSORING/MONITORING AGENCY REPORT NUMBER
N/A

12. DISTRIBUTION AVAILABILITY STATEMENT

DISTRIBUTION A: Approved for public release; distribution unlimited.

AFRL-SR-AR-TR-08-0292

13. SUPPLEMENTARY NOTES

14. ABSTRACT

The goal of this effort has been to identify the dominant source of the radiated aero-acoustic noise produced by high-speed, heated jets and develop control strategies to reduce it. To that end, two acoustically matched Mach 0.6 jets, at temperature ratio Tr=0.93 (cold) and Tr=1.7 (hot) are examined. The use of non-intrusive Particle Image Velocimetry (PIV) to sample the flow, allowed a true measure of the velocity field to be realized without fear of corrupting the radiated noise field intrinsic to each jet. The low-order modal dominance of each was determined using Proper Orthogonal Decomposition (POD), highlighting the low-dimensional nature of this highly turbulent flow field.

15. SUBJECT TERMS

16. SECURITY CLASSIFICATION OF:	17. LIMITATION OF ABSTRACT	18. NUMBER OF PAGES	19a. NAME OF RESPONSIBLE PERSON

Contents

I Introduction 3

II Jet Noise 4
- A The acoustic analogy . . . 4
- B Hot jets . . . 5
- C Far-field noise . . . 6

III Objective 7

IV Low-dimensional Jet Analysis 8
- A Experiment . . . 8
  - 1 Facility . . . 8
  - 2 Instrumentation . . . 9
- B Cold study . . . 12
- C Hot study . . . 13
- D Near-field pressure . . . 13
- E Far-field acoustic signature . . . 16
- F Near-field and acoustic far-field coupling . . . 24
- G Source velocity field . . . 26
  - 1 Single-point statistics . . . 26
  - 2 Reynolds stresses . . . 31
  - 3 POD analysis . . . 35
  - 4 Modal structure . . . 38
  - 5 Velocity field reconstruction . . . 43
- H Noise source statistics . . . 45
- I Conclusions . . . 52
  - 1 Discussion . . . 54

V Dynamical Systems Modeling 55
- A Measuring flow dynamics . . . 56
- B Dual-time PIV experiment . . . 56
- C Low-order dynamical system development . . . 58
- D Conclusions and recommendations . . . 60

In an effort to identify the dominant source of the radiated aero-acoustic noise produced by high-speed, heated jets and develop control strategies to reduce it, two primary experiments are led in parallel using a 2 inch diameter nozzle operating at Mach 0.6: I) An investigation of the aeroacoustic sources of two 'acoustically matched' Mach 0.6 jets, at temperature ratio of Tr=0.93 and Tr=1.7, is conducted to identify distinctions in contribution to the acoustic far-field spectrum. The fluctuating pressure sampled near the exit of the jet(x/D=2, $r/D \simeq$1), is shown to sense the dominant flow features intrinsic to each velocity field. POD analysis of the velocity fields reveals the presence of larger scaled, more energetic structures in the hot jet, as well as a dominant Fourier-column mode-like structure, and a Fourier-helical mode-like structure in the cold jet. Fourth order correlations of the self noise contributions are shown to be dominant in both jets, with the hot jet exhibiting a greater shear noise efficiency, and cold, a greater self noise contribution. The low frequency emission of the shear noise terms is linked to the increase in the acoustic spectrum of the hot jet at these frequency, where as the decrease at high frequency is characteristic of the self noise weighting. The pronounced effect of increased low frequency noise is not deemed likely as solely resulting from the changes in the contribution of the shear noise sources, and as such, points to the contribution of the second entropy source term. II)A dual-time PIV investigation of the sound producing region (x/D=3 thru 10), (Tr=0.93), is performed to capture the instantaneous Eulerian acceleration field. An identification method is implemented to solve for the coefficients of the ordinary differential equation (ODE) derived from a Galerkin projection of the Navier-Stokes equations onto a basis of POD eigenfunctions, describing the evolution of the flow. An extensive database of the velocity and acceleration fields is used as *training* data for the development of an empirical low-order dynamical system (LODS), for eventual use in closed-loop flow control applications. These predictive models show a good agreement with the original data when the truncation of the system is minimized. It is found beneficial to retain more modes in a quadratic model than to increase the order of the system, which restricts the number of modes that can be used in the modeling. The higher modes are found to be responsible for much of the higher frequency content in the models, which make them more representative of the actual flow.

I. Introduction

Since its advent, and throughout it's life cycle from gas turbine to combustion, the jet engine has been the focus of numerous research efforts. Of particular interest is the mechanism by which the exhausted plume generates noise. At the heart of this problem is the challenge of deciphering what events in these high-speed flows are most efficient at radiating highly intense acoustic pressure fluctuations, that translate to the far-field as broadband noise. The noise due to current military and commercial high-speed jet aircraft engines can reach upwards of 120 (dB) on take off (depending on proximity), with the exhausted plume being the most significant contributor.[2] With regulations pertaining to noise from commercial jet aircraft becoming more stringent, efforts to mitigate noise levels are a major concern. Military applications remain focused on improving stealth technology on a range of aircraft, from unmanned air vehicles (UAV) to fighter aircraft. Where radar signature is now minimized on the most recent aircraft, their noise signature has yet to be considerably altered.

The noise 'source' in jets has been characterized by the generation, subsequent interaction, and evolution of the coherent turbulence structure within the shear layer produced by the mixing between the high-momentum, high-temperature core jet flow and the lower-speed, cold entrained flow, as cited by Ffowcs Williams & Kempton.[3] Research at the most fundamental level involves the use of circular nozzles (coaxial, over, ideally, and under expanded) and primarily cold (ambient temperature) core flow. The seemingly subtle differences between cold and hot jets can prove to be extremely complex in the experimental arena, as solutions to Lighthill's wave equation for noise caused by unsteady fluid motion, involves making certain assumptions that do not apply at the elevated temperatures at which realistic engine cycles occur. Terms that can simply be deemed negligible under the assumption of being small in the cold jet, must now be included through measurement. Unfortunately for the researcher, the development of measurement tools lags behind the necessity for required information. We must therefore rely on numerical tools such as Direct Numerical Simulation (DNS) and Large Eddy Simulation (LES) to provide answers. These tools provide solutions to the equations of motion, but at times leaves much to be desired in terms of the physical flow

dynamics, as full 3-D simulations are costly both in capital and time. Many studies have recently moved towards using this information to validate experimental results. However, in the case of gleaning insight into the turbulent mixing mechanism responsible for noise generation in the hot jet, the coupling of numerical and experimental data appears to be the only current solution.

The area of flow control, geared toward the reduction of jet noise, is in its early stages of development. Currently implemented strategies consist of passive control devices, commonly known as chevrons or tabs. These serve to enhance mixing between the high-momentum, high-temperature core jet flow and the lower-speed, cold entrained flow. These devices have shown some promise in reducing the noise radiated by these high-speed jet exhausts without compromising the thrust efficiency, notably, reducing low frequency noise at aft angles while increasing high frequency noise at broadside angles relative to the jet. However, significant noise mitigation has yet to be achieved.

Flow control at the first stages of the design process is needed for such complex problems where so many disciplines come into play; from propulsion to thermodynamics, turbulence, acoustics and control theory. The more realizable alternative of 'active' flow control has now gained considerable focus. To date, active flow control techniques for jet noise reduction have not yet provided enough consistency and cost-efficiency to be found in industrial applications. Development of theses strategies represents the solution with the most potential for furthering and optimizing the noise reduction capability provided by passive techniques. Ultimately, both active and passive flow control techniques could be complementary in accomplishing this challenging goal.

II. Jet Noise

The turbulent motion of shear flows has long proved challenging to researchers. On the heels of the work of Sir James Lighthill in identifying the mechanism by which sound is generated aerodynamically,[6] and Ffowc Williams & Kempton[3] reporting that jet noise production was biased towards the contribution of large-scale turbulence, many groups set out to identify orderly patterns in the flow as 'sources' of sound, in hopes of controlling it.

The establishment of Lighthill's aerodynamic noise theory[6,7] stands as one of the more significant contributions to identifying the role of shear flows in generating vortical structures, and the noise caused by this unsteady fluid motion. An acoustic approximation to momentum transport, Lighthill's theory describes the production of 'aero-acoustic' noise by high-speed jets through the time dependent kinematics which generate pressure fluctuations as they evolve downstream of the jet exit, ultimately radiating to the far field as noise. Solutions to Lighthill's wave equation realizes the far-field fluctuating quantities (*i.e.* acoustic pressure, density), but involves making certain assumptions that do not apply at the elevated temperatures at which realistic engine cycles occur. Where the axisymmetric jet is of concern, it is the factors surrounding the propagation of this sound to the far-field, as well as the entropy contribution in heated jets, that remains not clearly identifiable.

A. The acoustic analogy

Lighthill's aerodynamic noise theory[6,7] identifies a relationship between the sound source in free shear flows and the resulting distribution of external pressure/density fluctuations. An analogy is drawn between the non-linear equations of motion and the linear theory of acoustics to form the inhomogeneous wave equation,

$$\frac{\partial^2 \rho}{\partial t^2} - a_0^2 \nabla^2 \rho = \frac{\partial^2 T_{ij}}{\partial x_i \partial x_j} \tag{1}$$

where the left hand side of the equation represents acoustic wave propagation, and on the right the 'source' term, Lighthill stress tensor T_{ij} is defined as,

$$T_{ij} = \rho u_i u_j + (p - a_0^2 \rho)\delta_{ij} - \tau_{ij} \tag{2}$$

In the simple case of a cold, subsonic jet the stress tensor can be reduced to the contribution of the reynolds stresses only,

$$T_{ij} = \rho u_i u_j \tag{3}$$

by a series of assumptions. Firstly, τ_{ij} the viscous stress tensor, can generally be neglected as jet noise is considered to be driven by an inviscid process.[24] Secondly, for mildly heated isothermal jets the term commonly referred to as the 'entropy' term $(p - a_0^2\rho)\delta_{ij}$ is also considered small, as $(p' = a_0\rho')$ is an accurate isentropic assumption in isothermal jets, and neglected.[74] The solution to Lighthill's wave equation for far-field pressure fluctuation can be expressed in free space as the volume integral,

$$p(\mathbf{x}, t) = \frac{1}{4\pi} \int_V \frac{\partial^2 T_{ij}}{\partial x_i \partial x_j} (\mathbf{y}, \tau) \frac{d\mathbf{y}}{|\mathbf{x} - \mathbf{y}|} \tag{4}$$

for the contribution resulting from V, an average eddy volume. The variables $\mathbf{x}$ and $\mathbf{y}$ are location of observation reference point, and fluid volume respectively, and $\tau = t - \frac{|x-y|}{a_0}$ is the retarded time.

Lilley[19] in an attempt to include flow variables associated with the propagation of sound through the flow field (and subsequent interaction of sound waves and flow, *flow-acoustic interaction*) established that contrary to Lighthill's original formulation involving only terms of quadrupole nature, there existed a component of the pressure-density relationship more appropriately represented by dipole sources. The term $(p - a_0^2\rho)\delta_{ij}$ argued by Lighthill to be associated with non-isentropic density fluctuations produced by viscous effects was shown to also have an isentropic component, resulting in an important dipole noise source in the presence of density/temperature fluctuations. Howe[20] in a reformulation with emphasis placed on this 'excess' noise of hot jets found terms of similar dipole-like contribution, discussed in further detail later in the next section.

B. Hot jets

Most effort toward the identification of turbulent sources of sound and development of jet noise theory has been focused on the subsonic, cold jet due to it measurable characteristics. However, at the elevated temperatures at which realistic engine cycles occur, it has been shown that noise sources are altered, whereby entropy fluctuations are now prominent, producing a noticeably different far-field spectrum.

The assumption previously made in Lighthill's acoustic analogy regarding the $(p - a_0^2\rho)\delta_{ij}$ term, no longer holds with the addition of heat. Lighthill briefly discussed that in the heated jet, this term could be replaced by $[1 - (a_0^2/a^2)]\nabla^2 p$, and quadrupole type sources could again be assumed, however this formulation was later shown to be incomplete. In attempts to adapt Lightill's original theory to flows with mean flow-acoustic interaction (*i.e.* sources in a convecting medium) researchers (Lilley,[19] Goldstein,[17] Howe[20]) derived an inhomogeneous, convective wave equation from the Navier-Stokes equations. Mainly varying in assumptions made and choice of independent variables in the final approximation to far-field pressure, these theories result in greater complexity involving solutions to the full unsteady equations of motions.

Howe,[20] in a reformulation with emphasis placed on the 'excess' noise arising in heated flow, used the velocity potential and stagnation enthalpy as independent variables to derive an analogy relating the stagnation enthalpy to vorticity and specific entropy. To demonstrate its application, a model problem is considered in which the rate of heat energy absorption by a fluid particle can be expressed in terms of the temperature gradient across the fluid,

$$\rho T \frac{DS}{Dt} = \text{div}(K \,\text{grad}\, T) \tag{5}$$

where K denotes the thermal conductivity of the fluid and S specific entropy. Combining the continuity equations and (Eqn. 5), and through a series of assumptions limiting the thermodynamic quantities to first order, the acoustic equation can now be written as,

$$\left(\frac{1}{a_0^2}\frac{\partial^2}{\partial t^2} - \nabla^2\right)\frac{p}{\rho} = \frac{\partial}{\partial t}\left(\frac{1}{c_p}\frac{\partial S'}{\partial t}\right) \tag{6}$$

where S' represents the fluctuating component of specific entropy, and p acoustic pressure perturbations. A solution for the radiated pressure field resulting from this expansion and contraction of the fluid is then realized, through the use of an appropriate Green's function.

$$\frac{p}{\rho_0} \simeq \int \frac{\partial}{\partial \tau}\left(\frac{1}{c_p}\frac{\partial S'}{\partial \tau}(y_1,\tau)\right) G(x_1,y_1;t,\tau)dy_1 d\tau \tag{7}$$

Similar results for the far-field pressure were obtained in the alternative matched expansions analysis of Landau & Lifshitz.[37] Although a simple model, the contribution of entropy fluctuations to far-field sound is highlighted. Howe[20] concluded that these fluctuations only radiate noise in the presence of a mean flow pressure gradient.

Lush *et al.*[36] also showed the plausible existence of an additional entropy fluctuation source in heated flows by application of the isentropic relationship, $S = c_v \ln(p/\rho^\gamma) + const$, for a perfect gas, where S is entropy and $\gamma = c_p/c_v$. From this,

$$\frac{\partial \rho}{\partial t} = \frac{1}{a^2}\frac{\partial p}{\partial t} - \frac{\rho}{c_p}\frac{\partial S}{\partial t} \tag{8}$$

The time derivative of the $(p - a_0^2\rho)$ term from Lighthill's stress tensor then becomes,

$$\frac{\partial}{\partial t}(p - a^2\rho) = \left(1 - \frac{a_0^2}{a^2}\right)\frac{\partial p}{\partial t} + \frac{\rho a_0^2}{c_p}\frac{\partial S}{\partial t} \tag{9}$$

where $a = (\gamma p/\rho)^{\frac{1}{2}}$ is local sound speed. The derivation highlights the importance of the second term on the right, as large temperature gradients between core flow and ambient entrained flow would invariably create large entropy fluctuations. It also validates the assumption that allows the $(p - a_0^2\rho)$ term to be neglected as small in cold jets, as $a = a_0$ and entropy is generally considered uniform $(dp - a_0^2 d\rho)$ across the flow field.

C. Far-field noise

Even with this additional 'source' present, the overall contribution of heat to the far-field noise is ultimately a function of exit velocity. To illustrate this effect, the acoustic Mach number is introduced, $M_a = U/a_0$, where U is the jet exit velocity and a_0 the ambient sound speed. At fixed acoustic Mach numbers less than 0.7, the overall sound pressure level radiated by an axisymmetric jet is shown to increase with the addition of heat, and decrease above $M_a > 0.7$ (Tanna,[38] Fisher *et al.*[39]). This is rather counter intuitive as the dominant source term in the cold jet $\rho u_i u_j$, (Reynolds stress term) would no doubt decrease in magnitude with decrease in density ρ, resulting from the addition of heat. Ribner,[22] after observing limited noise reduction in jets of varying density due to heating, suggested that the source density played little role in affecting the overall noise of hot jets, and that the entropy fluctuations must dominate in these flows.

The addition of heat affects jets moving at lower velocity, through a significant contribution of entropy fluctuations, manifest as an increase in the radiated sound. However, at higher velocity, this effect is diminished as the resulting overall sound pressure level is decreased. The Reynolds stress term seemingly now the driving mechanism, as decreases in the magnitude of the source density (in the absence of additional sources), would result in a reduction of the radiated noise. A second interesting point of contention arises as the frequency content of the far-field spectrum of low Mach number, heated jets is examined. Conversely to that of the cold jet, a larger angular distribution over which radiation occurs is seen, owing to an increased magnitude in the refractive 'cone of silence' region. The increase in the overall sound pressure level is also shown to coincide with increases in the lower frequencies and a decrease in higher frequencies. This coincides with the perception that the acoustic sources consist of quadrupoles and dipoles, with the contributions of quadrupoles dominant in the cold jet.

Fisher *et al.*[39] suggested that with the addition of heat, the additional entropy fluctuation source exhibited a dominant contribution of dipole-like sources. Based on these observations, Morfey *et al.*[40] modeled the the noise radiated from hot jets using quadrupole sources, with temperature fluctuation terms of dipole

order, representing the effect of heating. The resulting spectrum showed differences in shape at an angle of 90^o with the jet axis, with peak frequency of the dipole terms lower than that of the quadrupole. This again is consistent with the shift to lower frequency, previously exhibited in hot jets, leading to the fluctuating entropy source term $(p - a_0^2\rho)$ being dubbed as the '2nd dipole source term'. In Goldstein's[18] formulation of the acoustic analogy, it is also noted that the 'enthalpy flux term' corresponds to a dipole source. Viswanathan,[41] an opponent to this view, studied extensively the affect of jet temperature on radiated noise (including analysis of previously reported data) and concluded that the observed changes in spectral shape were in fact an effect due to Reynolds number and possible rig-noise contamination. This contention among researchers leaves no universally accepted theory in regards to the mechanisms at work in hot jets.

III. Objective

The goal of this effort has been to identify the dominant source of the radiated aero-acoustic noise produced by high-speed, heated jets and develop control strategies to reduce it. To that end, two acoustically matched Mach 0.6 jets, at temperature ratio Tr=0.93 (cold) and Tr=1.7 (hot) are examined. The use of non-intrusive Particle Image Velocimetry (PIV) to sample the flow, allowed a true measure of the velocity field to be realized without fear of corrupting the radiated noise field intrinsic to each jet. The low-order modal dominance of each was determined using Proper Orthogonal Decomposition (POD), highlighting the low-dimensional nature of this highly turbulent flow field.

The near-field pressure signature surrounding the jet is sampled by an azimuthal array of fifteen pressure transducers, at a downstream location of 2 diameters. The predominantly hydrodynamic signature is shown to correlate well with the far-field acoustic response. The contribution to the far-field acoustic spectrum, was determined by sampling the acoustic signature of each jet, using an arc array of six microphones. These quantities are simultaneously sampled in order to examine the process by which sound generated by the axisymmetric jet radiates to the far-field. The low-dimensional nature of the source field (column mode in the hot jet, and helical in the cold), was resonated by the near-field pressure, and also sensed by the far-field microphones. This consistency between all three measurements, source velocity field, near-field pressure, and far-field acoustics, highlights the strong relationship between source generation mechanism and the subsequent propagation of fluctuating pressure, both as hydrodynamic disturbances and far-field acoustic disturbances.

The Reynolds stresses are weighed to glean some insight into the entropy source term's contribution to the overall radiated noise field. Where noise production is concerned, the Reynolds stresses can be viewed as a simplified representation of the Lighthill's stress tensor, $T_{ij} = \rho u_i u_j$. Although not a valid approximation to the complete source term, with the addition of heat, the weighting of these terms can be telling. The increased magnitudes consistently seen in the hot jet would seem to indicate a clear relationship between these stresses and trends observed in overall sound pressure level. However, as this term scales with density, the vast difference in mean density in each jet (ρ_{cold}=1.428 and ρ_{hot}=0.759) demonstrates that further consideration of theses terms is needed. As such, the Reynolds stress terms contribution to noise generation in the hot jet would be diminished as compared to the cold jet, again suggesting the presence of an additional acoustic source with the addition of heat.

The acoustic source strength is sought in an investigation of the quadrupole correlations, following the formulation of Proudman[68] and Ribner.[69] The acoustic power output, or intensity, in the far-field can be expressed as fourth order space-time statistics, calculated directly from the fluctuating source quantities. Terms involving the mean velocity component of the dominant flow direction in the jet are deemed shear noise, and those only of fluctuating quantities, self noise. This is more clearly articulated as noise contribution from turbulence-mean flow interaction and turbulence-turbulence interaction, respectively. There individual contribution is examined to determine the dominant flow interaction mechanism in each jet. As the formulation assumes isotropic turbulence and neglects the contribution of the second source term, $(p - a_0^2\rho)$, which has been shown to scale with increases in temperature fluctuation, from these results the contribution of the Reynolds stress term(s) is qualitatively compared in both jets to infer as to the contribution of the second source term.

The task of controlling the dominant sources of radiated noise is undertaken, firstly, by modeling the flow field dynamics using the full, unsteady equations of motion as a basis. PIV measurements in a longitudinal plane (x,y) can be performed to demonstrate the evolution of flow structures as they convect within the shear layer. However, streamwise vorticity is an important quantity in the jet flow, being responsible for much of the dynamics, and found to be linked to noise production.[17] Therefore, in the present study measurements are performed in the cross-flow plane of the jet, *i.e.* the plane perpendicular to the jet centerline. The measurement plane is traversed downstream by discrete increments to cover a measurement volume extending from the near jet exit (x/D=3) to beyond the region of collapse of the potential core which occurs between 5 and 6 jet diameters downstream. At this location, turbulence intensity reaches a maximum and the near-field pressure dynamics seem to relate best with the far-field sound, as shown by Hall *et al.*[52] . To capture and rebuild the dynamics of the flow, a low-dimensional experimental approach is taken here, in which a large database of the acceleration field (and thereby the velocity field) is needed. Since the velocity data contains the information described by the Navier-Stokes equations, a system of ordinary differential equations (ODE's) is fit to the data to provide a dynamical system capable of predicting the low order dynamics of the jet flow field, given an initial condition. This capability carries interest for flow control applications where a dynamical estimate of the state of the flow can be of great use in conjunction with direct measurement.

IV. Low-dimensional Jet Analysis

In many aspects, research involving the complex flows associated with turbulence has been limited by the development of measurement/computational tools. The complexity of the full non-linear equations of motion makes numerical results such as direct numerical simulations (DNS) limited, even with improved processing power and speed of computers. Experiments, relying on measurement prove futile in many cases, as necessary flow properties are at times impossible to acquire without corruption. Leaving techniques such as those incorporating modeling and statistics at the forefront of the development of new theories. These set of experiments couples measurements and statistics to glean insight into the source velocity characteristics, near-field pressure signature, and acoustic features, distinct to both the cold and hot jet.

A. Experiment

Two separate sets of experiments were carried out at Mach 0.6 exit velocity, with varying core flow temperatures, to quantify the effect of elevated temperature on the aeroacoustic sources. The first at a temperature of 20^oC (293^oK) which will be referred to as the ***cold jet*** and a second at 243^oC (516^oK) referenced as the ***hot jet***. In both studies, the ambient conditions were held constant at T=20^oC and p=$1bar$.

1. Facility

All experiments are conducted in the Syracuse University Skytop Anechoic Chamber, located at Syracuse Universitys Skytop campus. The facility, is approximately 30 years old, having been constructed in the early seventies under the leadership of Dosanjh *et al.*[47] and designed specifically with the purpose of conducting aeroacoustic studies. All exterior walls, flooring and ceiling are constructed of reinforced 30.5cm thick concrete. The chamber, encompassing $206m^3$, is acoustically treated using high-density fibreglass wedges on all interior walls, with a cut-off frequency of $150Hz$. The interior of the chamber can be seen in Figure 1. A detailed description of the facility and it's outfitted equipment is presented by Tinney *et al.*[48]

The experimental jet rig in Figure 2 is comprised of three main parts, two stainless steel sections, joined at a flange connection, and a machined nozzle. The nozzle interior utilizes a matched 5th order polynomial profile for the contraction from 15.2cm pipe to a 5.08cm exit diameter. The mounting stand, fashioned from carbon steel I-beams and designed to allow for expansion of piping at elevated temperatures, completes the experimental jet rig. The stand compensates for this growth using several high strength linear rails providing a rigid single degree of freedom system, in the direction of flow.

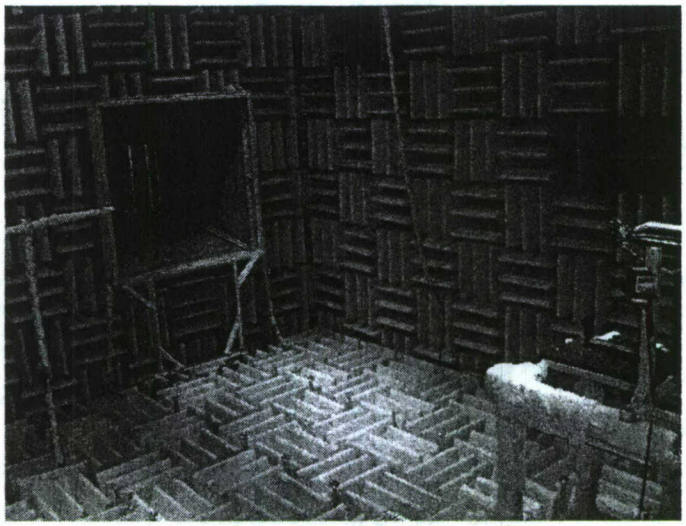

Figure 1. Interior of Syracuse University Skytop Anechoic Chamber.

The power plant of the facility is comprised of a $100hp$, two-stage (2 piston) *Joy* compressor, housed in a separate building. Operating as a blow-down facility, the compressed air is stored in five tanks with a volumetric capacity of $6.2m^3$ each, to a maximum pressure of approximately $3400kPa$. Once at pressure, desired exit flow rates of the jet rig can be achieved. This is done through the use of a robust, industrial grade *Allen Bradley, Pro-Logix Control* (PLC) system, which drives the flow process and monitors/controls much of the equipment (*i.e.* industrial make-up air unit, electric heater, flow-sense switch, numerous pressure transducers, compressed air tank pressure and throttle, and exhaust fan). As input sources to the jet rig operation are the storage tanks' pressure, static pressure in the nozzle, and both plenum and chamber, pressure and temperature. From a dedicated PC, the supply tanks pressure can be monitored until sufficient pressure is reached. Once at pressure, a user defined exit velocity, in terms of Mach number, is achieved based on the ratio of static* pressure in the nozzle to chamber pressure. The pneumatically actuated valve controlling the air supply is then throttled to a corresponding percentage opening, giving the prescribed exit velocity. The operational time of the jet facility, based on maximum pressure, is just below twenty minutes when discharging at Mach 0.85, for the $50.8mm$ nozzle.

Governing the flow process, and maintaining conditions during experiments, are a series of inputs from pressure transducers and thermocouples, used to monitor the flow's properties. The pressure ratio used to control flow rate is given by a set of in-pipe and chamber transducers. This ratio drives a diaphragm-actuated, sliding-stem control valve to maintain a desired exit velocity. The static pressure* used in the ratio to determine the exit Mach number, has been shown by Tinney *et al.*,[48] to be a valid approximation to the total pressure used in the isentropic relationship,

$$\frac{p_0}{p} = \left(1 + \frac{\gamma - 1}{2} M^2\right)^{\gamma/\gamma - 1} \tag{10}$$

where p_0 and p are total and ambient pressure, respectively. The calibration between the nozzle static pressure (transducer) and total pressure (pitot probe) reveals a nearly linear relationship between the two, exhibiting minimal differences. The ratio of pipe static pressure to ambient can therefore be used in place of total to ambient as specified by Eq. 10 above.

2. *Instrumentation*

The near-field pressure is acquired using an azimuthal array of fifteen *Kulite* model XCE-093-5G transducers. These are positioned in a array at two diameters downstream from the jet exit, equally spaced at 24^o apart,

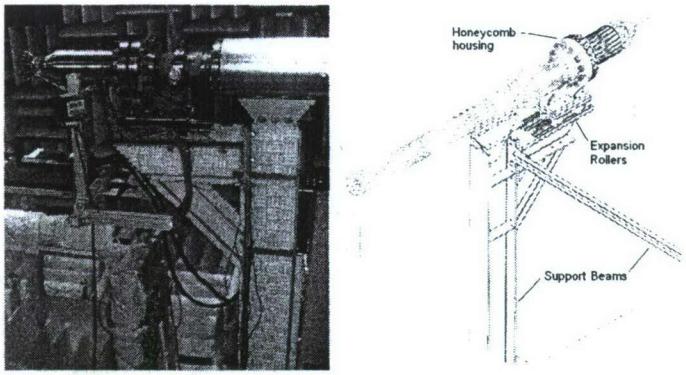

Figure 2. Experimental jet rig (left) left-side view (right) right-side schematic drawing.

and approximately $1cm$ outside the spreading shear layer. The array is mounted to the nozzle using a cap fitted with a series of holders. Their orientation is pictured in Figure 3. The frequency response of these transducers is $150kHz$, with dynamic range DC to $50kHz$, and a $20mV/6.8kPa$ sensitivity. Their small size, (shaft diameter $2.36\text{x}10^{-2}cm$) makes them an ideal measurement tool, evoking minimal obstruction of flow characteristics. These are continuously sampled at $40{,}960Hz$ and sub-sampled during analysis in blocks of 8192 samples, giving a frequency resolution of $\mathrm{d}f{=}5Hz$.

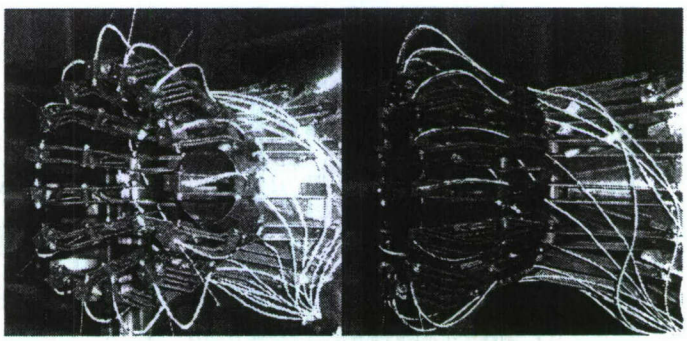

Figure 3. Azimuthal array of *Kulite* transducers.

To sample the far-field acoustic characteristics, six *G.R.A.S. Type 40BE* prepolarized, free-field microphones are used. The frequency response is $4Hz$ to $100kHz(+/-1dB)$ or $10Hz$ to $40kHz(+/-2dB)$, with dynamic range $166dB(ref20\mu Pa)$ and a sensitivity of $4mV/Pa$. These front-vented microphones are capably of operating at temperatures ranging from -5^oC to 120^oC. Excitation is provided by a *G.R.A.S. Type 26CB* preamplifier with a frequency response range between $4Hz$ to $100kHz$ with an uncertainty of $\pm 0.2dB$. These are positioned on a boom marking an arc fixed at 85 jet diameters from jet centerline. The array of microphones are then mounted on threaded rods extending from the boom, placing there diaphragms on an arc of 75 diameters. The array is pictured in Figure 4, with its orientation also diagramed. The downstream microphone (mic. 6) is positioned at an angle of ϕ=15^o from the jet centerline and arrayed at 15^o thereafter, with the sixth (mic. 1) at ϕ=90^o from jet exit.

Heating the jet core flow is achieved using a 470kW *Chromalox* electric circulation heater. The heater utilizes of series of sheathed rods that power on and off, as needed, to achieve the desired user input temperature. It's operation is controlled by the PLC system, with a necessary requirement being the output of a flow-sense switch, to prevent damage to the rods. The output temperature, measured by a thermocouple

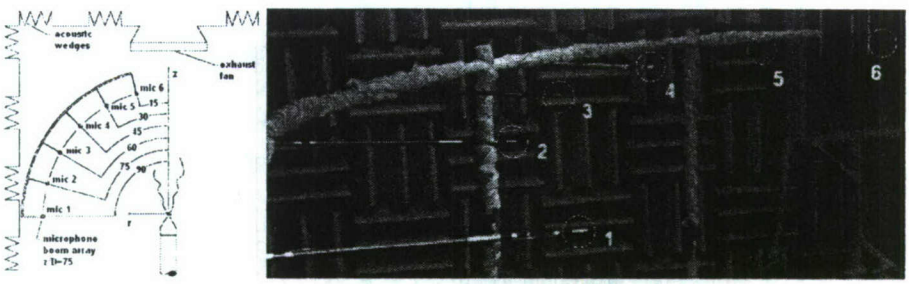

Figure 4. Boom array of far-field microphones.

upstream of the jet rig, is a function of a number of components. The outside air temperature that supplies the compressor, flow's properties as it exits the storage tanks, and the initial temperature of the heater all play a role. As the flow is heated through convection, this delicate balance inhibits a user prescribed output temperature, but rather only allows a heater coil temperature to be defined. A nozzle exit flow temperature of 538^oC (1000^oF) can be achieved, at a flow rate of $41.3m^3/min$.

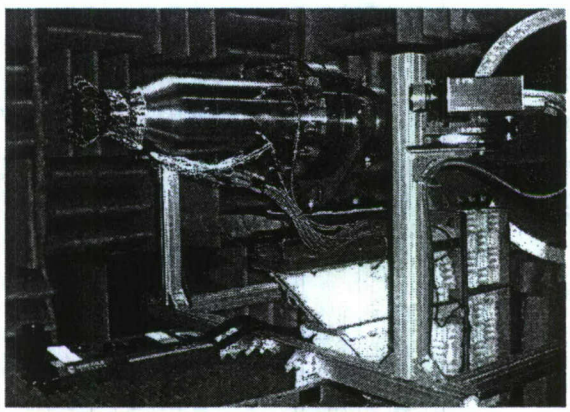

Figure 5. PIV setup, showing camera orientation and laser positioning.

A *Dantec Dynamics* 3-component, stereoscopic PIV system is used to acquire the jet's velocity field. The system incorporates two *HiSense* 8-bit resolution CCD cameras (1280x1024 pixels), a pair of pulsed *New Wave Research* $200mJ$ Nd:YAG lasers, and an optical laser sheet generator. The cameras are positioned at an angle of 45^o with jet centerline, mounted just upstream of the jet rig (at a height inline with the piping), on either side. The laser sheet illuminates the field from beneath in the radial-azimuthal $(r-\theta)$ plane, perpendicular to the jet exit. This orientation, shown in Figure 5, establishes the streamwise direction (x), as the out-of-plane component of the velocity field. The iterative correlation scheme used to resolve the image pairs captured by each camera, gives in plane particle displacement, and is thus a two component representation of the spreading shear layer. The single resultant velocity maps (one from each camera) are transformed to realize the third component, based on out-of-plane displacement. This orientation allows a greater limit of measurable velocity range, as the time step between laser pulses, is now not a direct function of jet streamwise velocity. Acquiring the strong mean flow in this direction would directly limit the system, as particle displacement within a given interrogation area would be large; requiring very short duration between captured images. In this high speed, Mach 0.6 flow, a duration of $5\mu s$ between pulses was used resulting in particle displacement on the order of a millimeter (laser sheet thickness of $5mm$). The system's positioning is fixed, including both cameras and laser sheet generator, and mounted on a single degree of freedom traverse. As an initial calibration locates camera positioning with reference to laser sheet, this limits

the need to recalibrate the system at different downstream sampling locations.

A key component in studies involving the use of optics based measurement tools, is seeding. To seed the core flow, a PIVTEC, twelve Laskin nozzle seeder, with olive oil as its fuel, is used in the cold study. Its design allows pressures upwards of 10bar, well above the back pressure experienced from injecting into the jet piping. Median particle sizing is on the order of $1\mu m$. For the hot study, a seeder was designed in-house, using a *3M* ceramic microsphere particulate seeding medium. The pressure vessel included two angled injection ports to promote mixing and a fine $10\mu m$ mesh before the exit port to prevent particles from clumping. An ad hoc investigation of the mean particle sizing revealed a value on the order of 1-$10\mu m$. The coflow is also seeded in both studies, providing a uniform distribution of particles in the entrainment region as well. A *TSI* model-9307 oil droplet generator is used, first filling the plenum, then pushed by the make-up air unit into the circular co-flow duct surrounding the jet piping. This seeder also uses olive oil as its seeding medium. Based on manufacture specifications, the median particle size on the order of $1\mu m$. These sizes are optimal based on discussions of Melling[49] on the effect of tracer particle sizing and other aspects relevant to optical measurements tools.

The sampling of the instrumentation mentioned above is accomplished through the use of a National Instruments PXI system, with a 866MHz NI-8175 embedded controller. The system houses three NI-4472 boards, each with eight available 24-bit resolution channels, and all with independent analog to digital converter. Of the twenty-four available, fifteen channels are dedicated to the *Kulite* transducers, six to the *G.R.A.S*, and one to the timing of the *Dantec Dynamics* PIV system. The system is capable of continuous sampling, streaming all channels simultaneously at rates above $50kHz$. The sampling rate of $40{,}960Hz$ used falls well within these limits. A *Krohn-Hite* model filter is used as a signal conditioner before acquisition of the far-field microphones. The filters attenuate at a rate of $24dB/octave$ and have a maximally flat (Butterworth) amplitude response. The high pass setting of $100Hz$, is intended to eliminate possible low-frequency vibrations from the boom array. A $20dB$ gain is also applied.

B. Cold study

In an attempt to examine the effect of temperature on the aeroacoustic sources of the jet, a cold study was first performed to serve as a 'control' case. At an exit Mach number of 0.6, the core flow was held constant at approximately 20^oC. Based on isentropic flow relationships,[50]

$$\frac{p_0}{p} = \left(1 + \frac{\gamma - 1}{2} M^2\right)^{\frac{\gamma}{\gamma - 1}} \tag{11}$$

$$\frac{T_0}{T} = 1 + \frac{\gamma - 1}{2} M^2 \tag{12}$$

the nozzle total to static pressure ratio (NPR) is 1.2755, with temperature ratio of 1.072. However, as is the case in jet acoustic studies, a new temperature ratio and Mach number are defined and will be referred to as the acoustic temperature ratio (Tr) and Mach number (M_a). Where Tr is defined by the ratio of jet total temperature at exit over the ambient temperature and M_a as the ratio of jet exit velocity to ambient sound speed (a_∞). For completeness, the jet Mach number is expressed as M_j.

$$Tr = \frac{T_0}{T} \tag{13}$$

$$M_a = \frac{U_j}{a_\infty} \tag{14}$$

$$M_j = \frac{U_j}{a_j} \tag{15}$$

indices referenced as 0-(total), j-(jet), ∞-(ambient)

The relevant properties of the cold study are itemized in Table 4 below. Velocity measurements are acquired at half diameter increments from 4.5-$10D$, with ambient conditions held constant at T=20^oC and p=$1bar$, by use of the co-flow system. Throughout the remainder of the document, this study is referenced as the ***cold jet***.

Table 1. Cold Study

T_∞	Tr	M_a	M_j	NPR	Re
20^oC (293^oK)	0.93	0.6	0.6	1.2755	6.9x10^5

C. Hot study

In the second set of experiments, the jet's core flow temperature is increased to 243^oC (516^oK). As the acoustic properties in the jet are a function of both exit velocity and temperature, the exit velocity (U_j) must be held constant to isolate the effect of temperature. The properties of air change at elevated temperature, so to maintain a constant exit velocity translates into lowering the jet Mach number; whereby the sound speed in Eq.15 increases with increases in temperature, as a result of a decrease in fluid density. In this instance, it is prudent to use the acoustic Mach number, coupled with a temperature ratio as a measure of the jet's exit conditions. The study is thus described as an investigation of the acroacoustic sources of an 'acoustically matched' Mach 0.6 jet, at varying temperature ratio.

The air exiting the compressor, stored in the large tanks powering the jet, must be heated upstream of it's exit. As it convects over the sheathed rod of the electric heater, only a coil temperature can be determined. Based on the velocity of the air in the upstream piping, a setting of approximately 315^oC was necessary to achieve an average temperature of 243^oC, over the duration of a single run of approximately 16 minutes. In-pipe temperature is measured by the thermocouple positioned just upstream of a honeycomb flow straightener, housed within the connection of piping and nozzle. The relevant properties of the hot study are itemized in Table 2 below. The jet Mach number now falls to 0.44 and Reynolds number almost half of

Table 2. Hot Study

T_∞	Tr	M_a	M_j	NPR	Re
243^oC (516^oK)	1.7	0.6	0.44	1.142	2.8x10^5

the cold study, however remaining a turbulent flow field still within the compressible flow regime. Velocity measurements are again acquired at half diameter increments from 4.5-10D, with ambient conditions held constant at T=20^oC and p=$1bar$, by use of the co-flow system. This study is hereafter referenced as the ***hot jet***. Any increase in chamber temperature or pressure was indiscernible to measurement tools, *i.e.* thermocouple positioned at the base of the jet rig and transducer on chamber floor. There was also no noticeable expansion of the jet piping under the described thermal loading.

D. Near-field pressure

The averaged power spectral density of the sampled fluctuating pressure surrounding the cold jet is now examined.

$$S_{pp}^{(j)}(f) = \frac{1}{T}\left\langle p_j(f) p_j^*(f) \right\rangle \tag{16}$$

(*) denotes the complex conjugate
Similar shapes are echoed by each transducer as a transfer function, derived based on the averaged amplitude spectrum over all transducers, is applied prior to the following analysis. The similar orientation of the transducers and the mean azimuthal invariance of the axisymmetric jet, dictates that all averaged power spectral densities will be identical. The application of the transfer function has negligible impact, as the transformed signal simply experiences an amplitude modulation, retaining all phasing and frequency characteristics.

The data is analyzed using methodology presented in the Arndt *et al.*[29] investigation of the pressure field surrounding the turbulent jet. A simple model based on a point-source solution to the spherical wave equation

was utilized in order to divide the pressure fluctuations into two forms: propagating or acoustic fluctuations (in phase with the velocity fluctuations), and non-propagating or hydrodynamic fluctuations (out of phase by 90° with the velocity). Using the assumption that long wavelength disturbances are associated with large sources and that short wavelength disturbances are associated with small sources, an expression is derived for the intensity of the hydrodynamic field (for a constant wave number $\omega = a_o k$) which would have a spatial decay of $I \propto r^{-6}$, where r denotes a radial distance outward from the center of the source (mixing layer centerline). While at constant r, in the inertial subrange, the spectral variation would be something of the order of $I \propto k^{-2/3}k^{-6} \propto k^{-6.67}$. More importantly, it is demonstrated that the transition between these two slopes (the hydrodynamic near field and the acoustic far field regions of the pressure) was frequency dependent and occurred predominantly around kr=2, exhibiting a $I \propto k^{-2}$ slope. This analysis has been revisited more recently by Hall *et al.*[52] and Coiffet *et al.*[51] who revealed strong interaction mechanisms between the reactive and propagative components of the pressure field just outside of the rotational mixing layer region of a Mach 0.85 & 0.30 round jet, respectively.

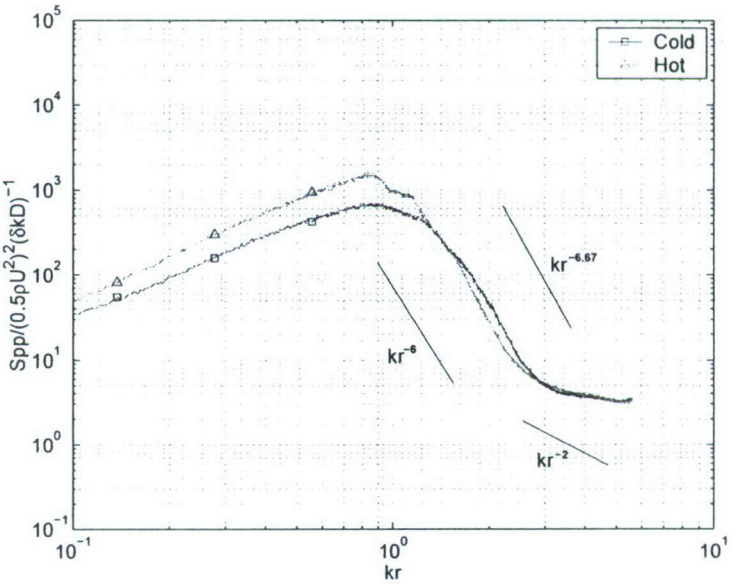

Figure 6. Transformed near-field pressure spectra, x/D=2, $r/D \simeq$1 (*all 15 transducers lay ontop each other*).

The non-dimensional spectral densities, normalized by dynamic head $(0.5\rho U_j^2)^2$, are presented in Figure 6. These are averaged over 200 blocks of 8192 data points, equivalent to 40 seconds of sampled data, at an acquisition rate of $40{,}960Hz$. *Unless otherwise noted, all presented spectra are analyzed using these criteria.* The slope exhibits a roll-off consistent with that of hydrodynamic spectral variations, and does manifest a bifurcation in concurrence with Arndt *et al.*,[29] however at $kr = 3$, not $kr = 2$. This has been the matter of some contention among researchers. In the plot presented, there is also only a small region, following the $kr = 3$ separation which exhibits a slope near kr^{-2}. The positioning of the transducers (x/D=2 and $r/D \simeq$1, just outside the spreading shear layer) may play a role here, as Ko & Davies[30] and Lau *et al.*[5] have reported evidence regarding the absence of visible vortices or the radially inward entrainment of velocity in the near lip region of the flow field. Suggesting that the development of the source field at this location is premature. In separate measurements acquired at a downstream location x/D=8, and several radial locations (r/D=1.9 to 2.68), this dissemblance between the reactive (hydrodynamic) and propagative (acoustic) components of the pressure field is more clearly articulated. This location is known to lie within the dominant sound production region, exhibiting a larger amount of energy with k^{-2} roll-off slope, indicating the presence of an acoustic source. This analysis dictates that care must be taken, where sensing of the deterministic sources of sound near the jet exit is concerned. At the present measurement location of x/D=2, although seemingly unlikely to apprehend a realizable acoustic signature until some distance downstream where the propagating

acoustic signature is dominant, x/D=6-10, it is demonstrated that much information can be gleaned from this near lip region. This is examined in greater detail in the coupling of the near and far-field pressure.

Also clearly illustrated in Figure 6, is the marked increase in low frequency energy seen in the fluctuating pressure spectra of the hot jet, accompanied by a slight decrease at high frequency. With the lowered Re of the hot jet, 2.8x10^5 from 6.9x10^5, it may be expected that less fluctuations would exist as the jet moves towards more laminar behavior. However, an increase in the pressure fluctuations is observed, p_{rms}=0.3163 in the cold jet and p_{rms}=0.4179 in the hot. It is well known that due to increased spatial growth rate of instability waves in hot jets, increased mixing is manifest. This feature is reflected here in the spectra, by an increase in energy. The phenomenon observed suggests that there is an increased low frequency contribution of the dominant structures near the jet exit in the hot jet, which is sensed by the surrounding pressure near-field.

Additional features of the pressure field are shown in Figure 7, comprising the coherency spectra between the azimuthal array of probes of both the cold and hot jets. The spectra is averaged over all azimuthal separation, as correlations are evaluated with each probe as the $\theta = 0$ coordinate and then averaged over similar $\Delta\theta$ separation. The plots only show the first 180 degrees of separation, as the coherency at greater $\Delta\theta$ separation, lie on similar curves. The curves peak at small azimuthal separation ($\Delta\theta = 24$), then decrease with increasing separation, suggesting the presence of a dominant Fourier-azimuthal helical mode structure. Similar coherency is exhibited at nearly 78% in the cold jet, and just over 72% in the hot jet. However, at larger $\Delta\theta$ separation, the hot jet exhibits a stronger correlation, more indicative of an axisymmetric column mode structure. This trend suggests the presence of differing dominant modal contribution in each jet. There is also a marked difference in the dominant frequency at which these peaks occurs. In the cold jet (7a), a more broadband peak persists, centered at approximately St_D=0.5. The hot jet (7b), exhibits a more distinct peak, over all separation, at a lower St_D near 0.3, suggesting that a greater distribution of scales is present in the cold jet.

To further investigate the observed trends, the distribution of the modal characteristics of the near-field pressure correlation is presented. The cosine transform is not utilized, for purposes of computational ease and time. Instead, the real-part of the cross-spectra, Fourier transformed in azimuth ($\Delta\theta \rightarrow m$), is presented (*only positive modes*, $+m$). Striking in Figure 8, is the scarcity of higher azimuthal modal energy that has been shown to govern the primary features of the turbulent source field, as only the first two modes (0&1) exhibit a significant amount of energy, in both the cold and hot jet. This modal behavior has also been shown by Petersen,[9] Arndt,[29] and Hall *et al.*[54]

The azimuthal mode spectra illustrates a similar picture as did the coherency, where the dominant peak frequencies in the cold jet span a greater range than seen in the hot jet. Mode 0, appears to peak at approximately St_D=0.4, then just below that value in the hot jet. This trend is echoed at higher mode number. In the modal distribution of both jets, the column mode peaks at higher frequency, then a progressively lower frequency is exhibited at each consecutive mode number. Although more broadband than its hot counterpart, the peak observed in the mode 0 spectra exhibits a more distinct shape, when compared to the broad peaks exhibited at higher mode number, in both jets. It is of note to highlight that the energy content of each does however differ greatly, with mode 0 of the hot jet more than doubling that of the cold.

The total azimuthal modal energy content is presented in Figure 9, where

$$F_{pp} = \int_T S_{pp}(m, f)df \tag{17}$$

Conclusions can now be drawn as to the distinct dominant structures present in each jet. The energy distribution is summed over positive and negative modes ($\pm m$) here, as to only view the positive contribution of the modes would give misleading information. The axisymmetric column mode is shown to dominate the flow field in Figure 8, however it is demonstrated here, as suggested by the coherency plots, that the second mode (helical mode) has a significant contribution as well. This is especially noticeable in the case of the cold jet Figure 9a, where the mode 0 & 1 contributions are nearly identical. In the hot jet there is a marked

distinction between the contribution of these two modes. Modes 0 & 1, account for nearly 75% of the total energy in both the cold and hot jet, with the hot jet exhibiting 40% more overall energy. The distribution in each case is highlighted in Table 3 below, suggesting that the presence of the stronger helical mode in the cold study, may gives rise to the broadening of peaks exhibited in the coherency spectra (Figure 7a). The more even distribution over the modes suggests a greater distribution in the dominant scales. As such, the narrow-band peak present in the coherency curves of the hot jet, coinciding with a dominant mode 0 contribution, dictates the presence of a consistently larger scaled structure.

Table 3. Modal energy distribution (*percentage of total*).

Cold	Hot
mode 0: 38%	mode 0: 45%
mode 1: 37%	mode 1: 31%

From this, it can also be inferred that, it is the presence of the helical mode which significantly diminishes the strength of the coherency at larger separation ($\Delta\theta$=48-168). The hot jet exhibits greater coherency at these separation, as the column mode's contribution is more pronounced here (*an entirely helical structure would be largely uncorrelated at 180 degrees of separation, where as a column structure would be well correlated over all separation*). The low frequency energy increase seen in the fluctuating pressure power spectral density can therefore be linked to the presence of a dominant axisymmetric column mode 0. The peak value of St_D=0.4 seen in the mode spectra is consistent with the low frequency peak observed in both the power and coherency spectra presented.

E. Far-field acoustic signature

Similarly to the investigation of the near-field pressure, the spectral densities of the far-field, or acoustic, pressure signature are presented in Figure 10, though as a function of wavenumber, not kr. ($H_{mm}(f)$ *is calculated in similar fashion as* $S_{pp}(f)$ *using Eq.* 16). The radial location is neglected as only the characteristics of the spectral variations in the signal are of concern. As can be expected, the curves depict a slope primarily scaling with a slower decay of $I \propto k^{-2}$, consistent with that of a dominant acoustic field.

In both the cold and hot jet, at shallow aft angles (15-30 degrees from jet centerline, corresponding to microphones 5 & 6) the signal exhibits larger magnitude, than at large aft angles (75-90 degrees corresponding to microphones 1 & 2). This is consistent with the directional nature of the jet's far-field radiated spectrum. As the noise source is deemed as the interaction of turbulent fluid convecting with the bulk mean flow, the distinct far-field acoustic spectrum of the jet is a result of a distorted radiated field from a point source. The magnitude of the resulting field is enhanced in the direction of convection. Where the hot jet is concerned, there is a noticeably larger increase exhibited over the range of microphones, seen predominantly at shallow aft angles, with only the downstream microphones positioned from ϕ=15-45^o, exhibiting significant change. As jet noise is known to scale with velocity, at a fixed exit velocity ($M_a^{(Cold)} = M_a^{(Hot)}$) between the two experiments, this increase can be attributed to a marked contribution of acoustic energy from an additional (*entropy*) source due to heating, in-line with the theory of hot jets. This is in direct relation to the diminishing of the Reynolds stress source term ($\rho u_i u_j$) with decreases in fluid density. The normalization by $(0.5\rho U_j^2)^2$ carried out here is similar to that of Mollo-Christensen & Narasimha,[55] who used the jet's dynamic head to establish a non-dimensional similarity relationship for the spectra of emitted sound. As the Reynolds stress source term can be thought to scale with (ρU_j^2), the normalized spectra presented can ultimately be thought of as depicting only the contribution of the second entropy source term ($p - a_0^2\rho$).

In this regard, the spectra presented in Figure 11a highlights this contribution in the cold and hot jet at microphone locations ϕ=15^o & 90^o. There is a clear increased contribution in the hot jet at low frequency, and a decrease at high frequency, with a maximum difference seen at St_D=0.2, at the ϕ=15^o microphone location. This is consistent with the low frequency energy of the dipole like distribution of the second

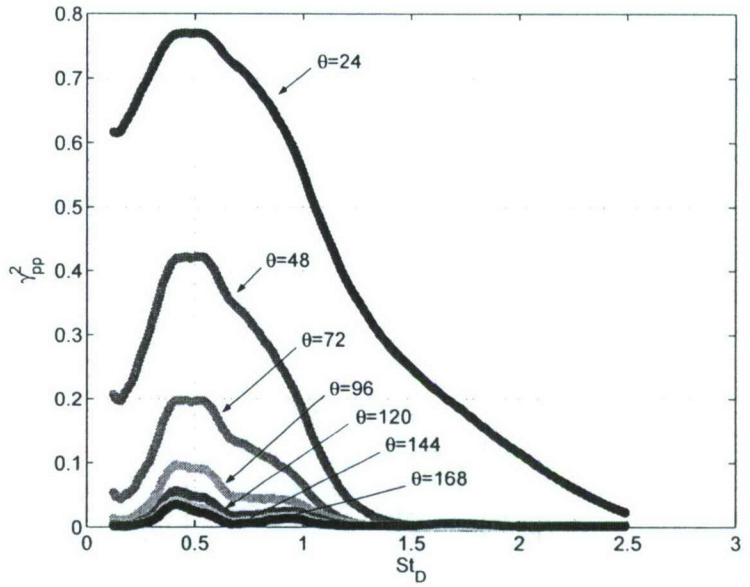

(a)

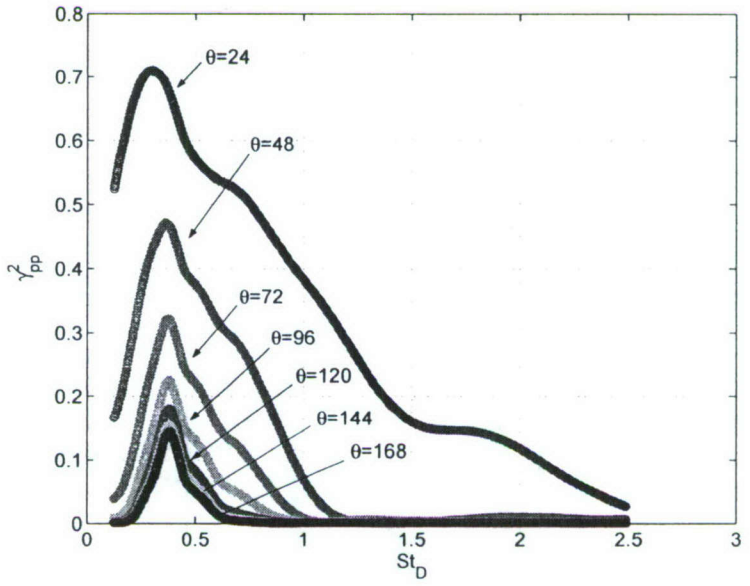

(b)

Figure 7. Coherency spectra over first 180 degrees of separation. (a)Cold jet. (b)Hot jet.

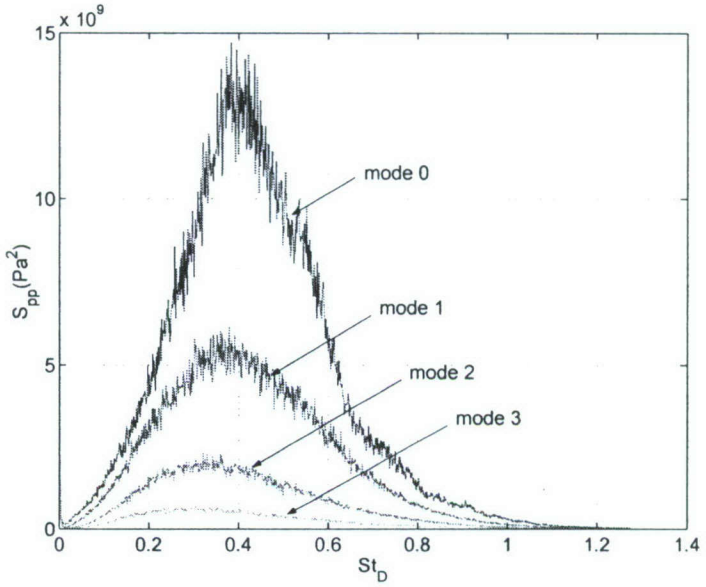

(a)

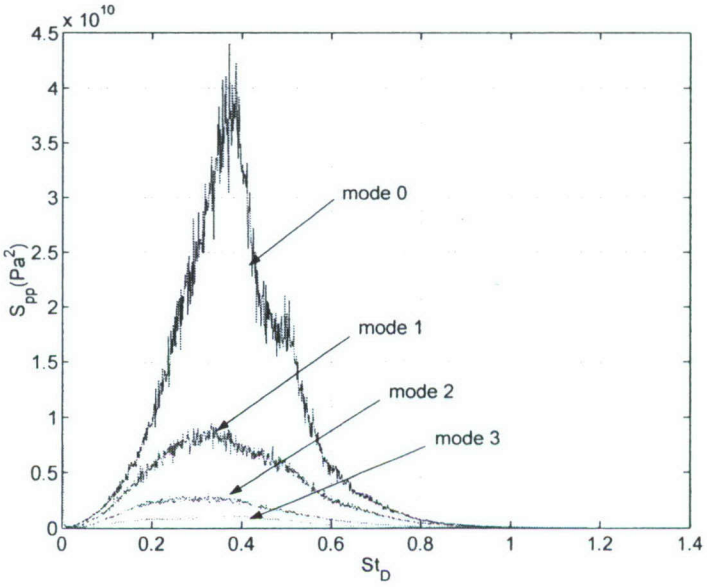

(b)

Figure 8. Azimuthal mode contribution to cross-spectra (*modes 0-3*). (a)Cold jet. (b)Hot jet.

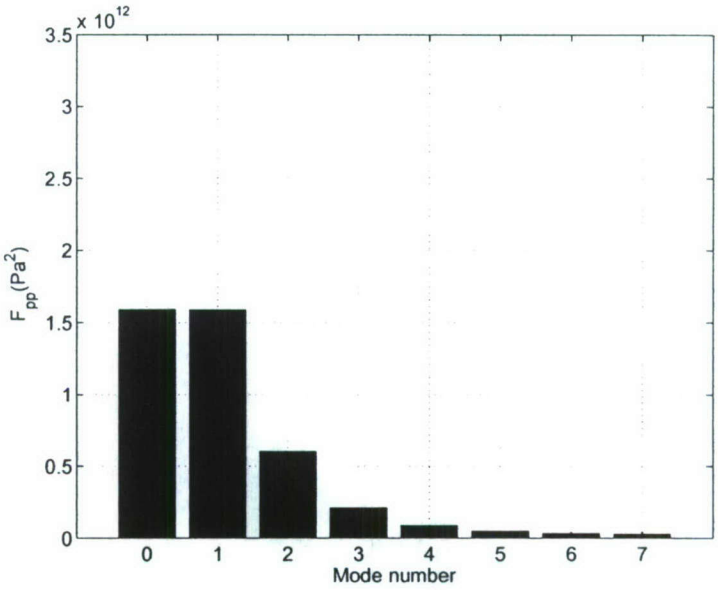

(a)

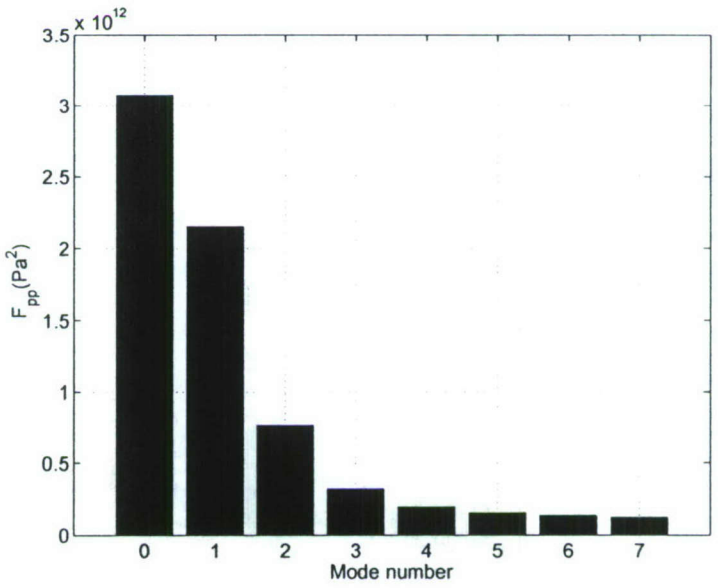

(b)

Figure 9. Modal energy content (*summed over ±modes*). (a)Cold jet. (b)Hot jet.

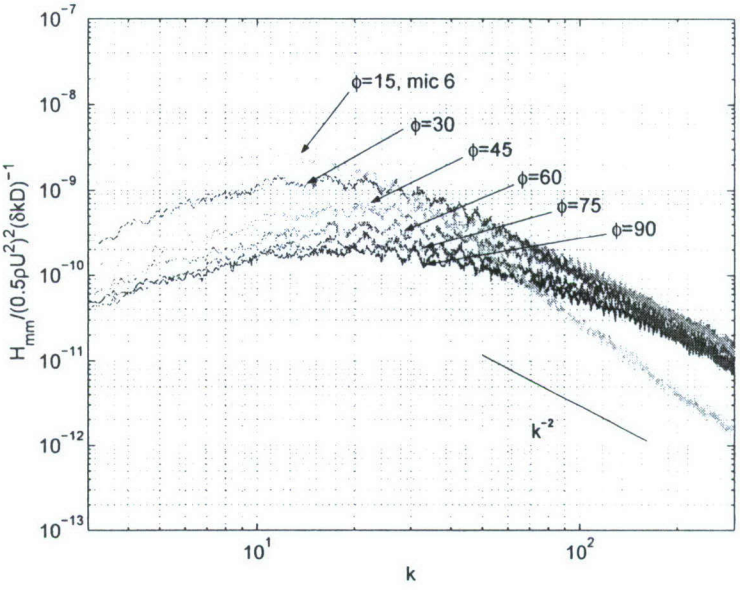

(a)

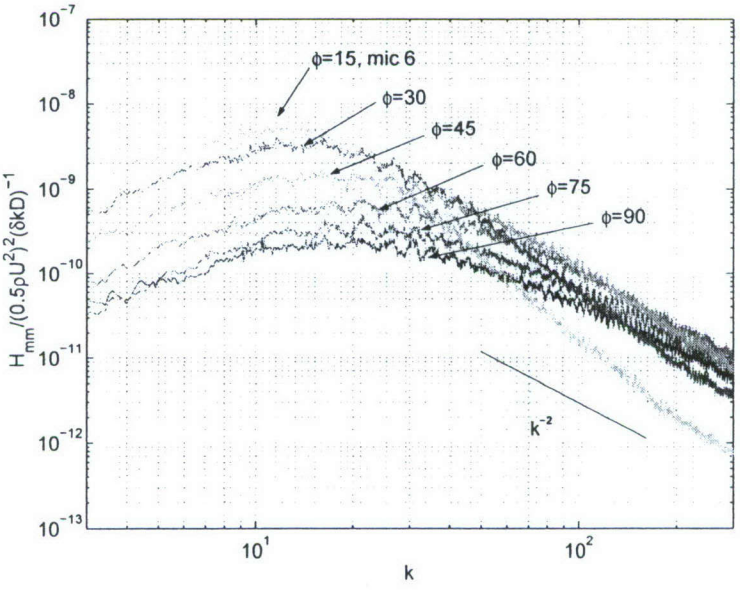

(b)

Figure 10. Normalized far-field spectra. (a)Cold jet. (b)Hot jet.

source term as modeled by Morfey *et al.*[40] The increase as a measure of sound pressure level is depicted in Figure 11b. There is a greater disparity in noise level seen between the two microphones in the hot jet, as the cold jet exhibits only a change of $\sim 10dB$ and hot jet $\sim 14dB$, over the range of aft angles from ϕ=15° through ϕ=90°. Again, the maximum change occurs near the St_D=0.2 value.

The decrease in high frequency contribution seen in the comparison of the two microphone locations (ϕ=15° & ϕ=90°), exhibiting the maximum and minimum change, respectively, suggests that the apparent increase in acoustic energy may more correctly be described as a redistribution over the range of frequencies. The 'shift' in the acoustic spectrum is further highlighted in Figure 12, demonstrating the contribution of each microphone location over a range of frequencies from $St_D = 0.2$, where the spectra peak, to St_D=3.0, where the magnitude diminishes. More clearly seen here, at low frequency ($St_D = 0.2$), the hot jet exhibits a larger noise contribution over all microphones, peaking at the downstream microphone (ϕ=15°). At high frequency ($St_D = 3.0$), the opposite is seen as the cold jet contributes more noise, at all microphones, peaking at ϕ=75°. In the range of frequencies between these two states, a region of transition is seen as a marked decrease in magnitude is observed at the downstream microphone, with increasing frequency. At the lowest frequency presented, the noise level is a maximum for both jets, with larger magnitudes exhibited in hot jet at all angles. The contribution then diminishes with increasing frequency, more drastically in the hot jet, ultimately falling below the values of the cold jet at all microphones at St_D=3.0. An effect which is shown to begin at the ϕ=15° microphone location and cascade to consecutive locations (increasing ϕ separation). The ΔdD difference between St_D=0.2 and 0.3 is approximately $35dB$ in the hot jet, at ϕ=15°, and near $29dB$ in the cold jet. The largest aft angle, ϕ=90°, exhibiting only a $14dB$ and $11dB$ change over similar frequency range, in hot and cold jet, respectively.

A striking result is the similar distribution over all microphone locations seen for both the cold an hot jet, as similar trends are illustrated in each set of curves. Where suggested previously that only shallow aft angles experience a redistribution of acoustic energy, it is apparent here that all microphone locations exhibit an increase in the amount of low frequency noise detected and a reduction in high frequency noise, in the hot jet. Consistent with the amplitude changes seen at low frequency in the spectral densities, a larger increase in noise level at low frequency is demonstrated at shallow aft angles. The largest low frequency difference between the cold and hot jet is seen at St_D=0.2 and ϕ=30°, of $\sim 5dB$. Also notable, however not as clearly discernable from the spectra, is the larger decrease in high frequency noise at large aft angle, again $\sim 4dB$ seen at St_D=3.0 at ϕ=75°. This coupled with the more pronounced changes in amplitude with increasing frequency seen at shallow aft angles, substantiates the notion that these angles are dominated by low frequency noise contribution. At high frequency, the higher noise levels seen at large aft angles, suggests that the opposite is also an accurate assumption.

An examination of the overall sound pressure level of both jets, shown in Figure 13, reveals that not only is the acoustic energy redistributed to different frequencies, but there exists an overall increase in the level of noise produced by the hot jet at nearly all observed angles, when integrated over frequency.

$$SPL(f) = 10\log_{10}\left(\frac{H_{mm}(f)}{p_{ref}^2}\right) \tag{18}$$

$$OASPL = 10\log_{10}\left(\frac{p_{rms}^2}{p_{ref}^2}\right) \tag{19}$$

where,

$$p_{rms}^2 = p_{var} = \int_T H_{mm}(f)df \tag{20}$$

This trend is consistent with experimental findings of Viswanathan[27] and Tanna,[38] and computational work of Bodony & Lele.[56] The largest increases of approximately $2dB$ is seen at shallow aft angle, the ϕ=30° microphone location exhibiting a maximum ΔdB, falling nearly linearly with increasing separation to ϕ=90°, where a slight decrease of nearly half a dB is observed. Again affirming that the low frequency noise is

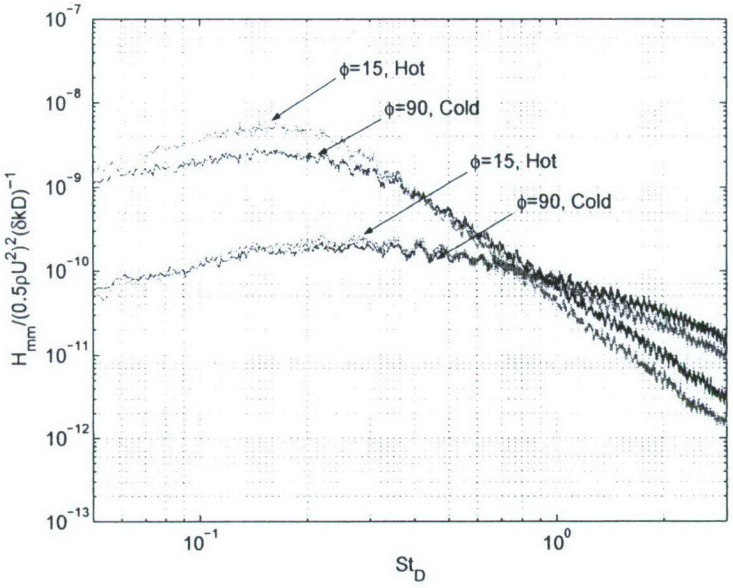

(a)

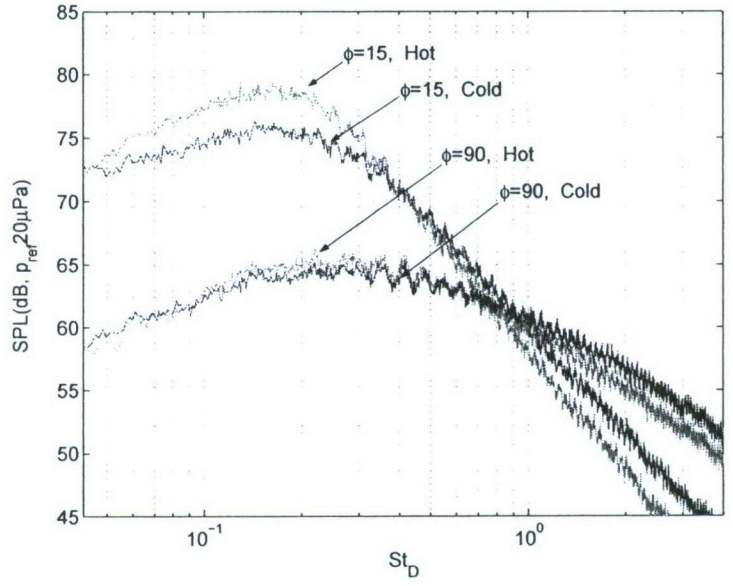

(b)

Figure 11. (a)Normalized far-field pressure spectral density of microphones positioned at ϕ=15^o & 90^o (b) and sound pressure level spectral density.

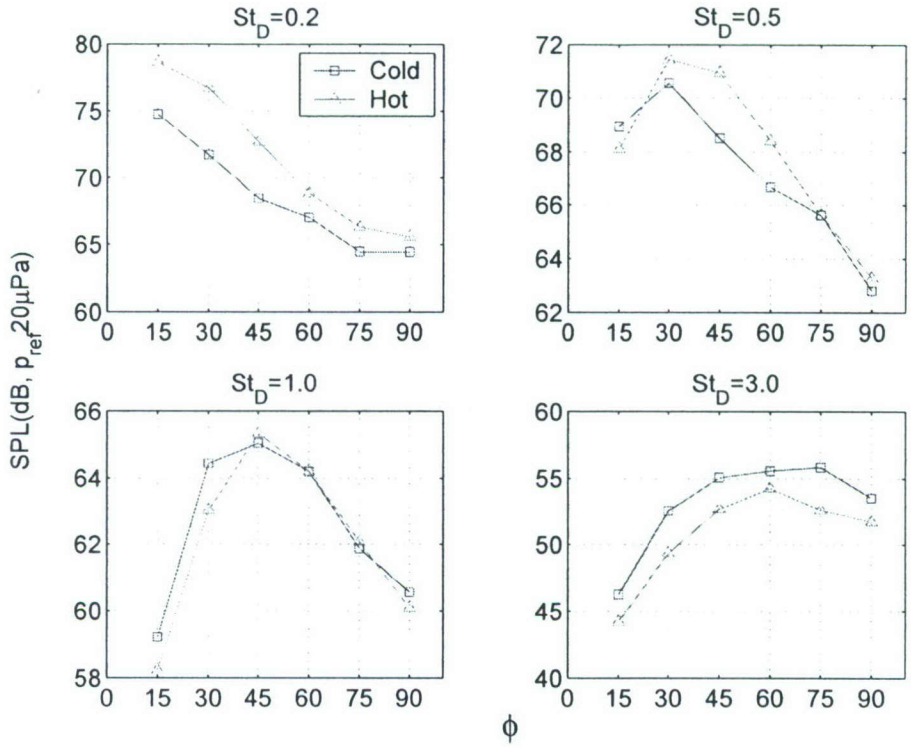

Figure 12. Sound pressure level distribution over all microphone locations as a function of St_D.

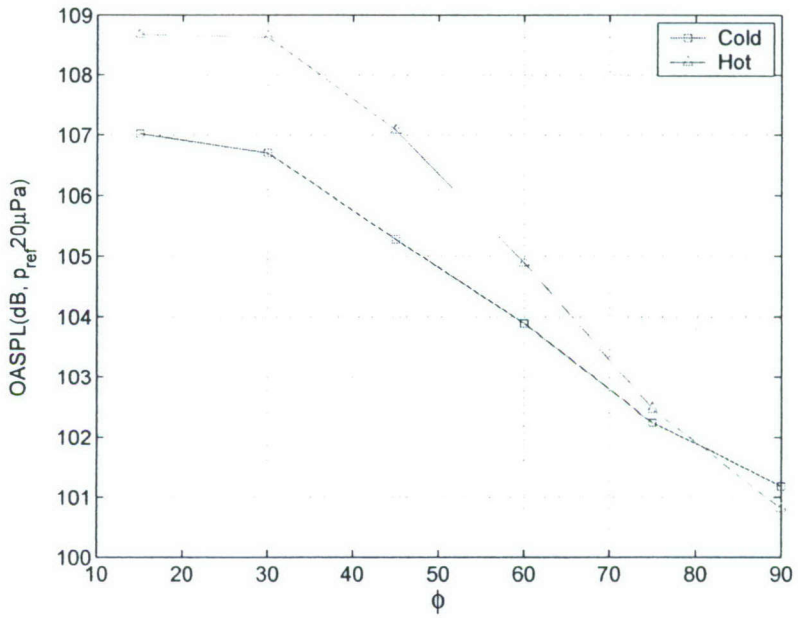

Figure 13. Overall sound pressure level distribution of microphone locations.

prevalent at shallow aft angles and high frequency, at large aft angles, as the high frequency noise decrease in the hot jet is depicted here in the ϕ=90° microphone location.

Tam *et al.*[23] has attributed the directional distribution of the axisymmetric jet's far-field acoustic spectrum to a contribution from two independent components of the flow-field, of varying length-scales and time-scales. Although jet's far-field spectrum is thought to be governed by the contribution of large-scale structures, Tam & Auriault[57] established the 'fine' or small scales (FS), importance to the weaker and more broadband distribution seen at large aft angles, having fairly uniform directivity. The larger structures (LS) are shown to contribute to the dominant, more narrow-band spectra seen at shallow aft angles. Universal similarity noise spectrum for each component empirically derived from an examination over a wide range of databases, has demonstrated similar results as experimental measurements, Viswanathan;[27] the LS spectrum fitting measured spectra radiated in the downstream direction at shallow aft angle and the FS spectrum fitting that observed at large aft angle. As a hypothesis for this, it proposed that the rapid non-linear decay of instability waves with the collapse of the potential core region, result in an intense Mach wave-like radiation in the downstream direction (wavy-wall theory). As the dominant structures in this region are large scaled, it is concluded that it is predominantly their contribution which is responsible for the observed noise in this direction.

However, currently there is no widely accepted theory to interpret the mechanism responsible for the change in spectral shape at shallow and large aft angles. Objections coming from Ribner[58] and Fisher,[59] bolster first principles of jet noise theory, emphasizing that this pattern is based on refraction effects of mean velocity gradients. The predicted 'figure-eight' pattern elongated by convective amplification, resulting in the dominant distribution seen at shallow aft angles. Fisher[59] points out the lack of consistency between the universal FS and LS spectra with hot jets at low acoustic Mach number, where the spectra shows an decrease in noise levels, rather than an increase. This is also echoed by Viswanathan,[41] who although not a supporter of the intrinsic mechanism driving the shifting of frequencies in hot jets, shows discrepancy between measured data and LS similarity spectra for a low Mach number jet over a range of temperature ratios.

At the present M_a=0.6 study, there is however evidence seemingly supporting the FS and LS theory. The spectra in both cold and hot jet are of similar shape, with a pronounced increase in low frequency and decrease in high frequency contribution observed in the hot jet. The properties of the hot jet are such that increased mixing, due to increased spatial growth rate of instability waves, results in an increased contribution of large scaled structures. The shift to a dominant low frequency column mode observed in the near-field pressure signature, along with the increase in low frequency acoustic energy seen predominantly at shallow aft angles, may serves as evidence of the the large scale's contribution predominantly to the shallow aft angles. This will be examined further in the next section, coupling the near and far-field pressure, as well as in the analysis of the source velocity field.

F. Near-field and acoustic far-field coupling

Although the near-field azimuthal array does not lie within the well establish 'noise source region' of 6-10D (at x/D=2 and $r/D \simeq$1), the pressure signature may still be used to garner information about the acoustic far-field. An analysis is now undertaken to examine the relationship between the two fields, with the aim of extracting distinctions in dominant frequency of the structure of each jet.

The two signals exhibit weak coherence, at a maximum of less than 10% with the in-plane transducer (θ=90°) and the downstream microphone 6, at ϕ=15°, in both the cold and hot jet. As a result, coherency plots are not presented here. The magnitude of the cross-spectral densities, instead, are evaluated using only the in-plane transducer and microphones 1 & 6 (ϕ=90° & 15°, respectively). These are calculated as follows, *(k=1-6, denotes microphone location, j=1, denote in-plane transducer)*

$$G_{mp}(f) = \frac{1}{T}\left\langle p_k(f) p_j^*(f) \right\rangle \tag{21}$$

The frequencies over which these signals are coherent, intuitively should coincide with those exhibited over the range of k^{-2} slope seen in both the near-field spectra (Fig. 6) and far-field spectra (Fig. 10), indicating

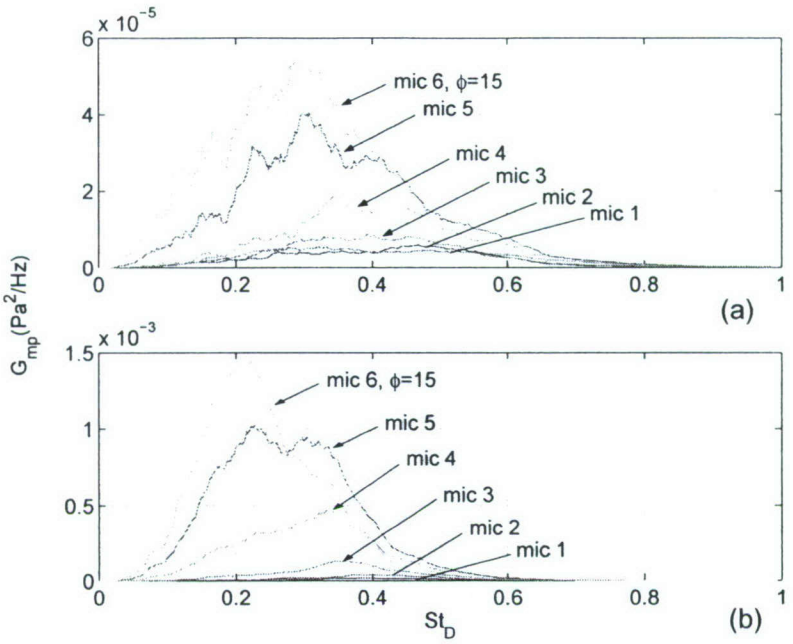

Figure 14. Near-field and acoustic far-field pressure cross-spectra (*single in-plane transducer*). (a)Cold jet. (b)Hot jet.

an acoustic signature. This is not the case, as the amplitude of the cross-spectra, shown in Figure 14, demonstrates a pronounced peak over a range of St_D=0.2-0.5. These peaks corresponding instead to the range of frequencies spanning the peak energy containing regions of each signal (near-field and far-field spectra). However an examination of the extremely low magnitudes confirms trends in the coherency spectra alluded to earlier, of the weak correlation between the two signals. A 10% filter is applied to the curves for clearer presentation. It is interesting to note that the correlated energy, however limited in magnitude, is a result of a predominantly hydrodynamic near-field signature with the acoustic far-field. The existence of this correlation suggests that the pressure measured here exhibits some signature of the acoustic source. A similar result has recently been shown by Hall *et al.*[52]

In comparing the two plots of the cold and hot jet, a more broadband signature is again seen in the cold, exhibiting a weaker correlation. The hot jet demonstrates a more narrow distribution over frequency, falling to negligible magnitude near St_D=0.4, where the cold extends to a higher value of St_D=0.6 (*as compared to peak energy*). Of particular importance is the increase in peak frequency with increasing aft angle separation, seen in both jets, in concert with a decrease in correlated energy. As results shown in the analysis of the far-field pressure indicate, the dominant frequency of the acoustic signature also increases with increasing aft angle separation. The peak exhibited here at ϕ=15^o (mic 6), coincides with the dominant low-frequency component exhibited in the near-field pressure signal, shown earlier. This trend suggests a relationship with the energy content of the column mode of the near-field pressure. The hot jet, exhibiting a greater correlation here, has demonstrated a larger amount of energy in mode 0 (*dominant modal contribution*), where its contribution in the cold jet is diminished (*similar modal contribution as the helical mode*), and exhibits lesser correlation.

To investigate this, a modal decomposition is performed in similar fashion as in the analysis of the near-field pressure, using the real-part of thecross-spectra, Fourier transformed in azimuth ($\Delta\theta \rightarrow m$). All transducer locations in θ, and a single microphone location in ϕ, are used to realize an azimuthal modal distribution, as a function of each microphone location. The first four modes are displayed for both the cold and hot jet, again. The trend previously observed in the cross-spectra is echoed in the modal distribution,

with the cold jet demonstrating correlation over larger frequency range and the hot jet showing larger magnitudes at both microphone locations. A shift to lower frequency with increasing aft angle separation is again seen in both jets, as the peaks at microphone 1 (ϕ=90^o), occur at higher frequency, near St_D=0.4, and fall to St_D=0.2 at microphone 6 (ϕ=15^o). The correlated energy is also consistently greater at microphone 6. In examining the modal contribution across the two studies, the mode 0 contribution in the hot jet at microphone 6, demonstrates a considerably greater increase in amplitude, nearly quadrupling it's cold counterpart, where as at microphone 1 (ϕ=90), a doubling effect is seen. This is consistent with the increase in low frequency noise seen at all microphone locations in the far-field acoustic spectra, more prominently seen however, at shallow aft angle. The magnitude of all others modes remains nearly consistent for both jets. The decrease in higher frequency energy at larger aft angles in the hot jet acoustic spectrum, is not clearly seen here, though it can be inferred from the trends of the curves. At mic 6, the curves extend to higher frequency in the cold jet (St_D=1.3) than in the hot jet (St_D=0.9). A more pronounced change may be evident, were it not for the lack of correlated energy at the higher frequencies exhibited in the acoustic far-field St_D >1. Recalling that the decrease in high frequency noise contribution was not clearly exhibited until St_D=3 in Figure 12.

The directional dependence of the far-field spectrum with frequency is highlighted in this analysis. It is also shown that it is the low-frequency, large-scale column mode 0, prevalent in the near-field signature, that drives the correlation with the far-field, especially at shallow aft angles. (*Trends behave similarly to the downstream pressure and acoustic field coupling seen in Hall et al.*[52]). At a maximum correlation with the downstream microphone positioned at ϕ=15^o, it is suggested that the increased contribution of mode 0 seen in the hot jet, is responsible for the increase in low frequency acoustic energy observed at shallow aft angles. At increasing aft angles, the correlation between the signals decreases, as these angles have been linked to the high frequency contribution of the 'fine-scale' turbulence structures. Conversely, these results imply that it is the higher ordered modal structures that contribute to high frequency noise.

The traditional quadrople distribution of jet noise does not account for the fluctuating entropy source term $(p - a_0^2\rho)$, as modeled by Morfey *et al.*[40] to exhibit a dipole-like distribution. Its demonstrated contribution of low-frequency energy to the acoustic spectrum makes this a viable candidate in accounting for the shift in the acoustic spectrum to low frequency, and the overall increase in noise level of low Mach number heated jets. Where the reduction of the overall sound pressure level seen at M_a >0.7 is concerned, much research is left to be done.

G. Source velocity field

The fluctuating velocity fields of both the cold and hot jet are now compared in an analysis aimed at identifying the dominant features, intrinsic to each, that contribute to sources of noise . The use of stereoscopic PIV to sample the velocity field allows superior spatial resolution as compared to other tools. However it's low sampling rate, makes acquisition of temporal time scales, in high Reynolds number flows, difficult. Thus the sampling rate used ($1Hz$), was chosen to ensure statistically independent snapshots, rather than attempting to resolve dominant time scales.

1. Single-point statistics

The mean velocity profiles at all measured locations (x/D=4.5-10) are shown in Figure 16a, comprising an average over a minimum of 1980 vector snapshots. The average centerline velocity at the furthest upstream location is reported at $204m/s$ for the cold jet and $199m/s$ in the hot jet. As the present study fixes acoustic Mach number, and thus exit velocity, these values are in concert with expected the $U_j = M_a/a_\infty$=$204m/s$ at M_a=0.6. Although the average velocity exhibited in the hot jet is well within the uncertainty of the measurement, it is now *assumed* that this value corresponds to a premature centerline decay, a known feature of hot jets. Due to limitations in optical access near the jet exit, experimental verification was not possible. However, previous measurement using LDA and PIV have reported centerline values of $203m/s$ and 202m/s, respectively. The following presentation of the mean statistics follows in this assumption, whereby the centerline velocity of the cold jet ($U_{cl}^{(cold)}$), is utilized for all normalization.

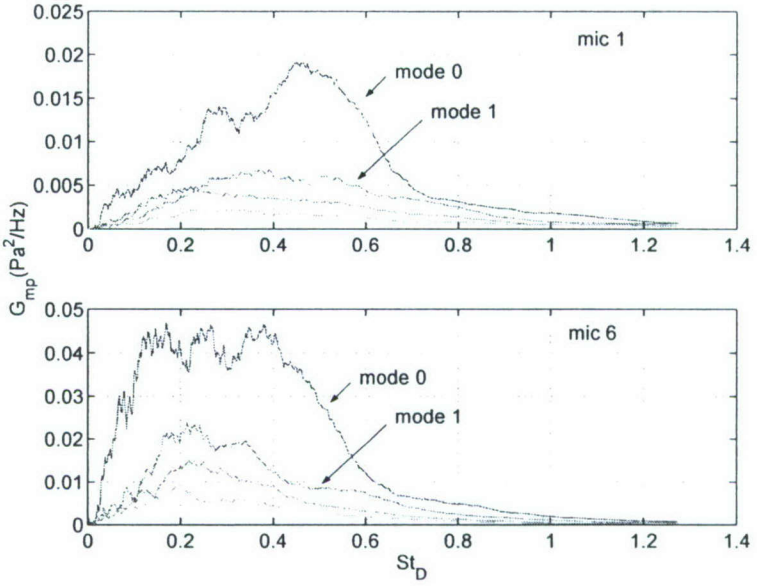

(a)

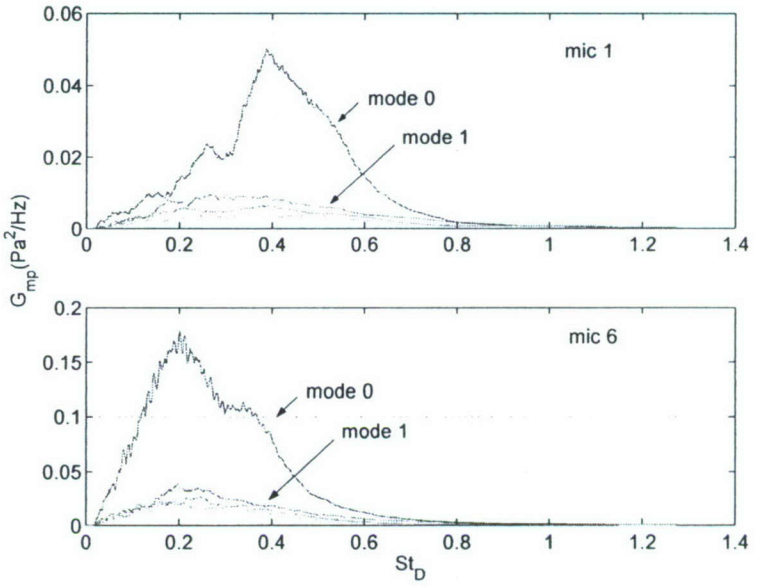

(b)

Figure 15. Modal distribution of near-field pressure and acoustic far-field cross-spectra. (a)Cold jet. (b)Hot jet.

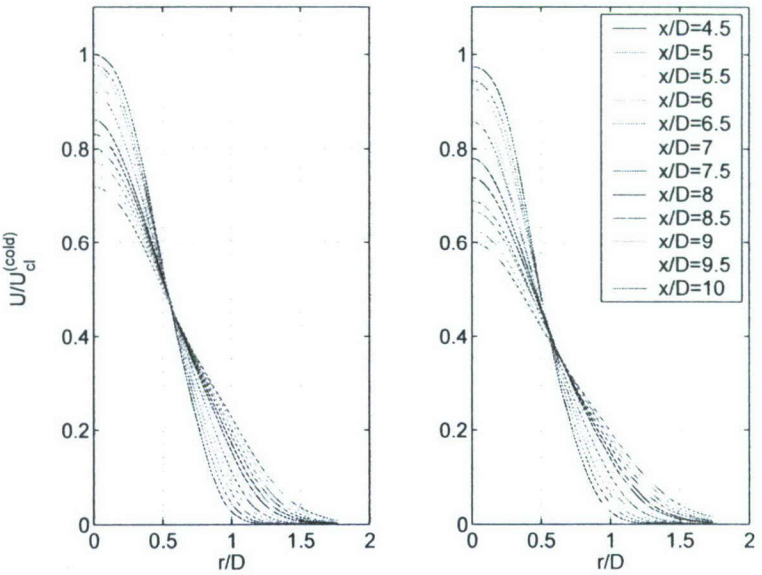

(a)

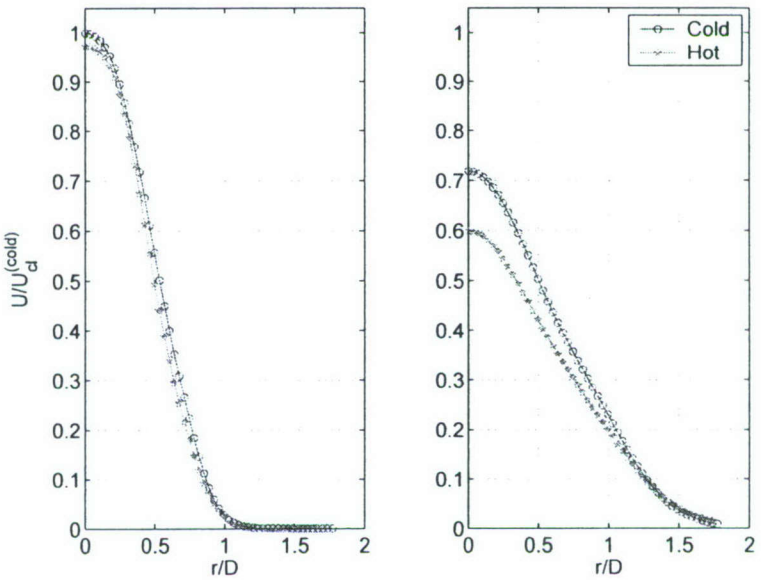

(b)

Figure 16. (a)Mean velocity distribution of (left)hot jet and (right)cold jet. (b)Mean velocity distribution of both jets at (left)x/D=4.5 and (right)x/D=10.

Apparent in the profiles is the more rapid decrease in centerline velocity with downstream distance, seen in the hot jet, indicative of an increased decay rate, as seen by Tanna,[38] Bridges & Wernet,[60] and Lew *et al.*[61] Recently, Panda *et al.*[72] showed through measurement, that with the addition of heat, the axisymmetric jet exhibits increased density fluctuations, which is linked to an increased growth/spreading rate. This is not seen here, as both sets of curves extend to similar radial locations at similar streamwise location. From the curves, a spreading rate near 7.5^o, $(0.13x)$ is calculated. However, the rapid decay of the hot jet is shown in Figure 16b to decrease the half-width of the curves near their apex, and as such produces a larger inner shear layer (*greater potential core collapse angle*). Ultimately, a larger mixing layer is exhibited in the hot jet.

The trend observed indicating a shorter potential core length, is investigated further as the centerline velocity of each jet is presented as a function of streamwise location in Figure 17a and tabulated in the Table 4 below, *recalling again that U_{cl} refers to that exhibited by the cold jet at x/D=4.5.* With the criteria

Table 4. Centerline Velocity

x/D	$\%U_{cl}$ **Cold Jet**	$\%U_{cl}$ **Hot Jet**
4.5	100	97.41
5	97.94	94.49
5.5	97.20	92.79
6	94.12	88.76

of $0.95U_{cl}$ indicating the collapse of the potential core region, the curves indicate that the hot jet collapses further upstream, near x/D=5, while the cold jet is seen to persist until x/D=6.

The Witze[62] correlation parameter is an effective means of comparing jets of varying temperature and Mach number, minimizing compressibility effects, defined by,

$$W = 2\kappa \left(\frac{x - x_c}{D}\right) \left(\frac{\rho_\infty}{\rho_j}\right)^{\frac{1}{2}} \tag{22}$$

where

$$\kappa = 0.08(1 - 0.16 * U_{cl}/a_\infty)^{-0.22} \tag{23}$$

Here x_c refers to potential core length defined as axial location of $0.95U_{cl}$, ρ_j and ρ_∞ are jet and ambient density respectively, a_∞ the ambient sound speed, and D is jet diameter. The curves collapse rather well, not surprisingly, considering the *fairly* low temperature ratio and small range over which measurements are acquired. The streamwise velocity curves are also plotted using the similarity variable $\eta(x) = (r - r_{0.5})/x$, where $r_{0.5}$ marks the location of $0.5U_{cl}$, in Figure 17b. The profiles for each jet collapses well, onto a similar curve. The region of disparity seen between $\eta(x)$=-0.1 to -0.05 indicates a lost of similarity consistent with the collapsing of the potential core region. The collapse of the curves using these various scaling, shows the data to be accurate to first order.

The turbulence intensities for both the cold and hot jet are presented in Figures 18a & b, as a function of radial distance r/D and $\eta(x)$. Streamwise locations of x/D=4.5, 6 & 8, are chosen, corresponding to the existence, collapse, and fully mixed potential core region. The top curves corresponding to the streamwise component (u), middle, the radial (v), and bottom, tangential/azimuthal (w). When referenced against previous measurements, these values fall slightly below those reported, at just over 11% for the streamwise component and 6% for the in-plane velocities (16% streamwise, 7% radial and azimuthal from LDA, and 15% streamwise, 7% radial and azimuthal from PIV). There is an increase in turbulence levels seen in the hot jet as the streamwise component increases to nearly 13%, with a slight increase in magnitude seen in the other velocity components [38,60,61,56] The increased mixing of the hot jet is again apparent as the turbulence levels at the centerline no longer fall at x/D=8, as in the cold jet, signifying a completely mixed region.

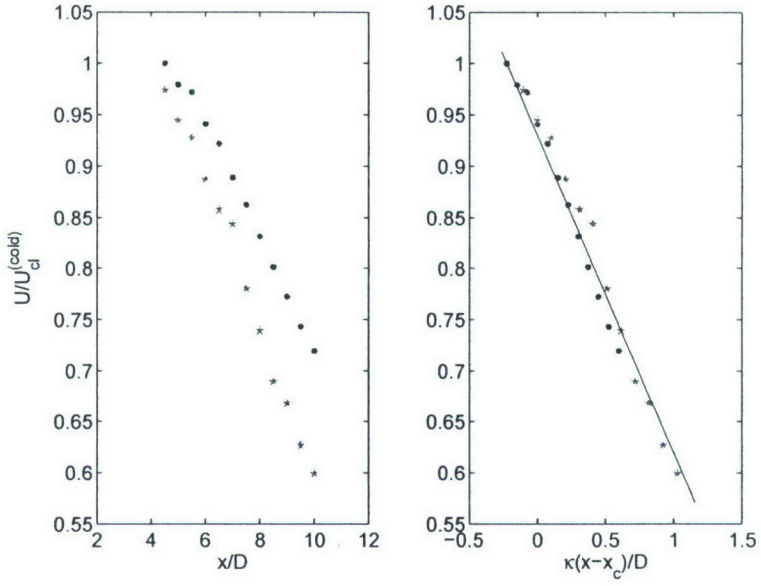

(a)

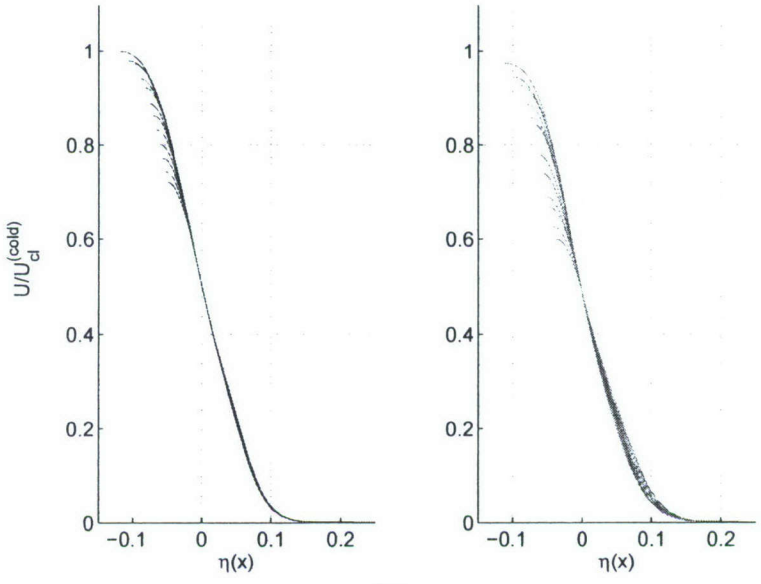

(b)

Figure 17. (a)Mean centerline velocity decay (left)x/D scaling and (right)Witze scaling. (b)Collapsed streamwise velocity profiles of (left)cold jet and (right)hot jet, using $r_{0.5}$ scaling.

The diminished magnitudes are coupled with evidence of pronounced turbulent fluctuations along the edge of the outer shear layer. The disturbance is confined to a radial location along the low-speed side of the mixing layer and appears to grows with the jet's evolution. This is more prominent in the streamwise component, indicating the presence of a 'streamwise disturbance. It's influence is less prominent in the hot jet where an increased turbulence intensity is exhibited. Recalling the placement of the transducer array near the jet exit (x/D=2, $r/D \simeq 1$) in Figure 3, it is clear that it's positioning is the most likely culprit of this disturbance, generating streamwise vortices acting similarly to a chevron/microjet nozzle. The holders for the individual transducer probes consist of small aluminum blocks that are held in place by two thin, flat sheet metal strips, on either side. These are screwed together, clamping the blocks in between. These thin strips act as knife edges, perturbing the entrained air near the jet lip.

Arakeri *et al.*[64] have reported decreases in turbulence intensity with the use of microjets, with injection as minimal as 1% of mean core flow. Alkislar *et al.*[63] concluded that this influence, although generating strong streamwise vorticity initially, decayed rapidly with downstream distance confining, it to a smaller region of the jet.In the present case, the array's positioning ensures there is no penetration into the core flow of the jet, resulting only in a perturbation of the outer edge of the forming shear layer, with disturbances confined to this region. Therefore, no change is exhibited in the mean statistics and the increased growth rate with respect to the natural jet is also not seen here, as comparisons of mean velocity profiles and shear layer thickness to experiments in the same facility at similar Mach number are nearly completely matched.

2. Reynolds stresses

With the predisposition of investigating acoustic source features, the normalized Reynolds stresses for the axial location $x/D = 8$, lying within the noise producing region, are presented in Figures 19 & 20. These are computed using,

$$\xi_{ij}(r, r', \theta) = \frac{\langle u_i(r, \theta, t_s) u_j(r', \theta + \Delta\theta, t_s) \rangle}{U_{cl}^2} \tag{24}$$

where t_s denotes snapshot time step, U_{cl}, the jet exit centerline velocity, and index notation is adopted, as (u_1,u_2, and u_3) replaces the previous (u,v,w) notation (*corresponding to streamwise, radial, and tangential directions, respectively*). The $< . >$ signifies an average over snapshot timing, as well as similar $\Delta\theta$ separation.

Although the full Reynolds stress matrix is available, only the radial grid representing the normal stresses (ξ_{ii}) at a separation of $\Delta\theta$=0, are presented in the contours in Figure 19. The streamwise, or axial, stresses are shown to dominate the flow field, with the radial stresses consistently exhibiting the largest spatial range. The peaks in the curves of the cold jet are centered along the turbulent mixing layer ($r = r' = 0.5$), while the hot jet demonstrates a trend consistent with a more rapid decay of potential core region, as peaks have moved closer toward the centerline at this downstream location. Consistent with this, the length scales are shown be larger in the hot jet, as compared to it's cold counterpart.

At an azimuthal separation $\Delta\theta$=0°, along the line r=r' (*i.e. the diagonal of the contours*), similar curves as depicted by the turbulence intensities presented previously can be realized. These are presented in the set of curves beneath the stress contours. (*Note that magnitudes of the y-axis, although similar, are of different scaling for* σ/U_{cl} *and* ξ). Paralleling the increased turbulence levels, the axial stresses in the hot jet demonstrate an increased contribution with the addition of heat. It is important to again highlight the similar spreading rates, as the curves reach a minimum at similar values along the horizontal axis in both sets of curves. The shear stress components are presented in Figure 20, illustrating that only the ξ_{12} term has a significant amount of energy. Similar trends are observed here, as the magnitude of the stresses and spatial length scales are again greater in the hot jet.

Where noise production is concerned, the Reynolds stresses can be viewed as a simplified representation of the Lighthill's stress tensor, $T_{ij} = \rho u_i u_j$. Although not a valid approximation to the complete source term with the addition of heat, the weighting of these terms can be examined to give a measure of there contribution to overall noise production. The increased magnitudes consistently seen in the hot jet would

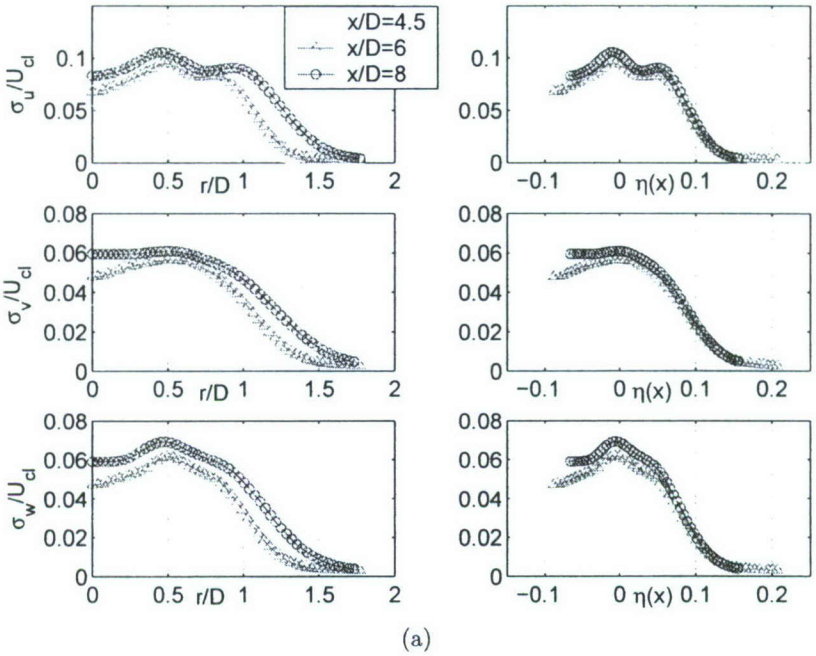

(a)

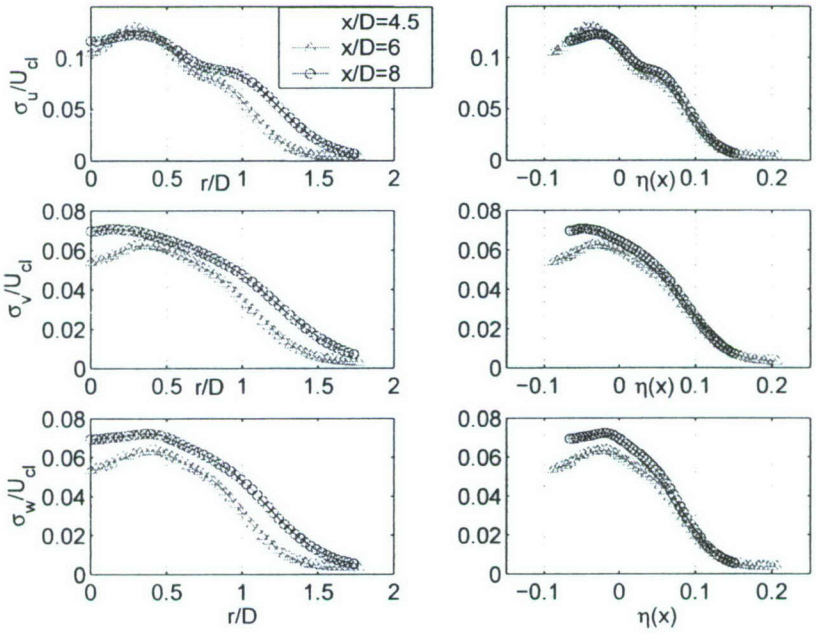

(b)

Figure 18. Turbulence intensity profiles (a)Cold jet (b)Hot jet.

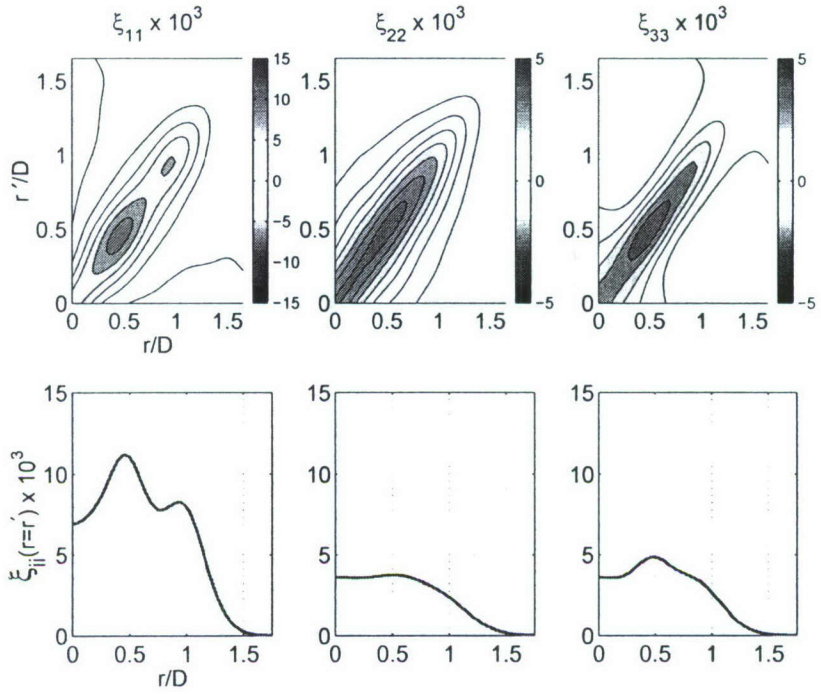

(a)

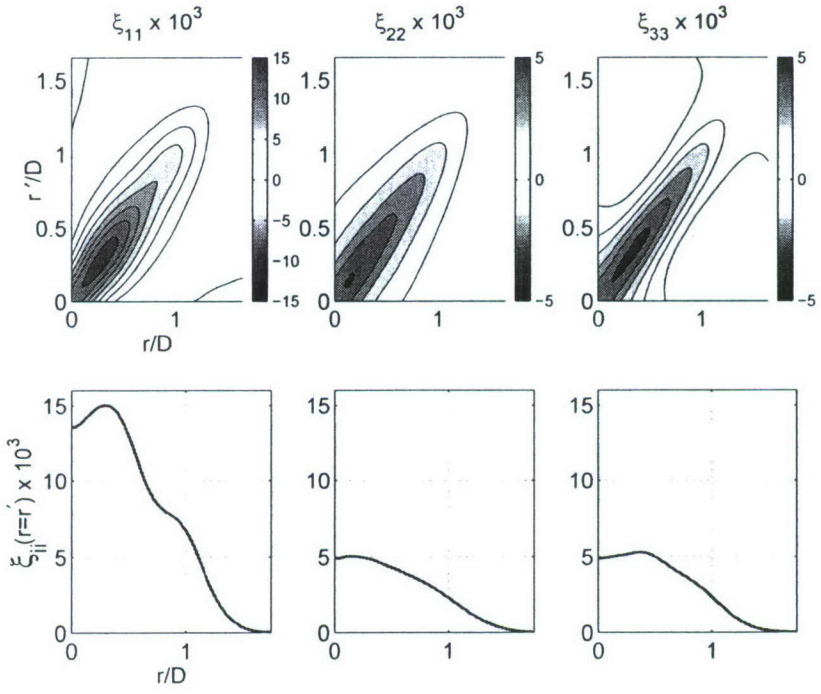

(b)

Figure 19. Normal Reynolds stresses at $x/D = 8$ (a)Cold jet (b)Hot jet.

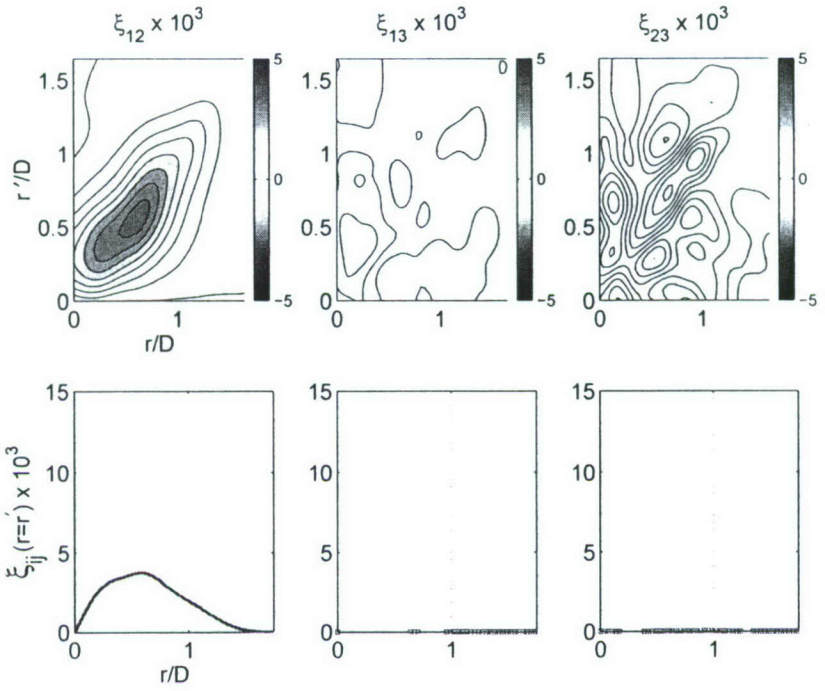

(a)

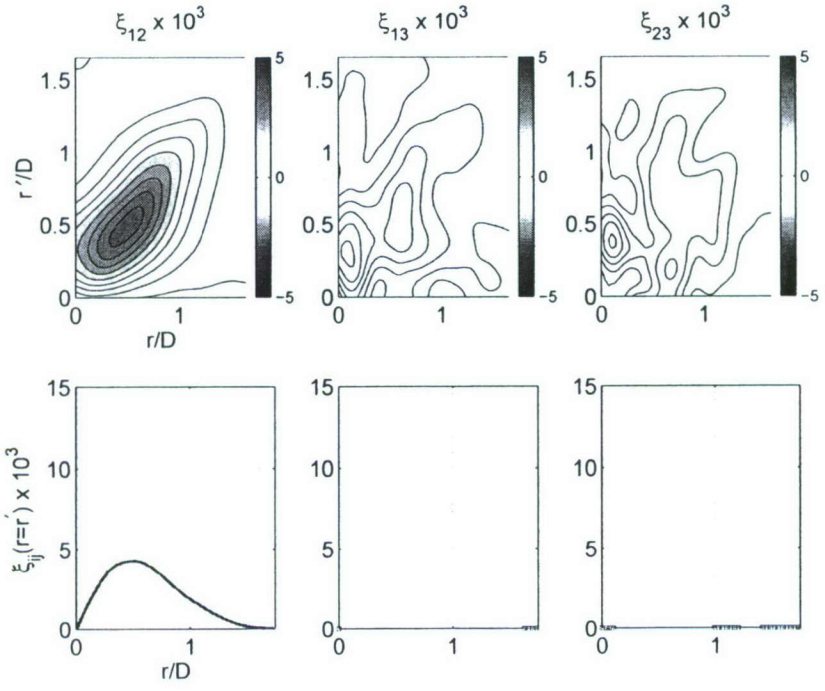

(b)

Figure 20. Shear Reynolds stresses at $x/D = 8$ (a)Cold jet (b)Hot jet.

seem to indicate a clear link between these stresses and the increase in overall sound pressure level shown earlier in an analysis of the far-field acoustics. However, as this term scales with density, the vast difference in mean density in each jet (ρ_{cold}=1.428 and ρ_{hot}=0.759) demonstrates that this is not the case. As such, the Reynolds stress terms contribution to noise generation in the hot jet would be diminished as compared to the cold jet. This again suggests the presence of an additional acoustic source with the addition of heat.

3. POD analysis

Known in mathematical circles as *Karhunen-Loève decomposition* or *principle component analysis*, POD serves as a method for extracting a basis set of modal functions from an ensemble of signals. Where the turbulence community is concerned, its serves to bring the orderly motion, of a seemingly random flow field, to the forefront. Similar to an energy budget, the POD greatly reduces the dimension of turbulence by decomposing the structure as a function of overall energy contribution. Based on the spectral theory of compact, adjoint operators, the method generates a basis set of spatial eigenfunctions resulting from the solution to the Fredholm eigenvalue problem. The ensemble of signals dictates these to be the most appropriate functions, resulting from a maximization of the signals' largest mean projection onto this basis set.

We start by seeking a deterministic set of functions that best describes our ensemble of signals (a velocity field, $u(\vec{x})$. From this set, a 'candidate structure' $\phi(\vec{x})$, which maximizes the normalized inner product with the velocity field, is found. *Vector notation is dropped for simplicity in the formulations below.*

$$\max \frac{\langle |(u \cdot \psi)|^2 \rangle}{(\psi \cdot \psi^*)} = \frac{\langle |(u \cdot \phi)|^2 \rangle}{(\phi \cdot \phi^*)} \tag{25}$$

This formulation leads to the Fredholm integral eigenvalue problem, as a necessary condition for this to hold is that, $\phi(\vec{x})$, be eigenfunctions of the two-point spatial correlation tensor of $u(\vec{x})$.

$$\int_D \langle u_i(\vec{x},t) u_j(\vec{x}',t) \rangle \, \phi_j(\vec{x}') d\vec{x}' = \lambda \phi_i(\vec{x}) \tag{26}$$

the two-point spatial correlation tensor known as the *kernel* is generally replaced by $R_{ij}(\vec{x},\vec{x}')$. Hilbert-Schmidt theory dictates that as a result of the inner product formulation in Hilbert (complex vector) space, the kernel R_{ij} will be a Hermitian operator. Additionally, solutions to the problem will consist of a infinite set of eigenfunctions, $\phi^{(n)}(\vec{x})$, and a corresponding ordered sequence of eigenvalues $\lambda^{(n)}$, where n denotes order in the sequence. The properties of the solution are such that,

- The maximization in Eq.(25) corresponds to the first eigenvalue, $\lambda^{(1)}$
- The set of eigenfunctions, $\phi_i^{(n)}$ are orthonormal,

$$\int_D \phi_i^{(p)}(\vec{x}) \phi_i^{(q)}(\vec{x}) d(\vec{x}) = \delta_{pq} \tag{27}$$

- The projection of the original ensemble onto the set of eigenfunctions yields a set of coefficients a_n,

$$a_n(t) = \int_D u_i(\vec{x},t) \phi_i^{(n)}(\vec{x}) d\vec{x} \tag{28}$$

- These POD coefficients a_n will be random and uncorrelated,

$$\langle a_n a_m \rangle = \lambda^{(n)} \delta_{nm} \tag{29}$$

- The original ensemble can be reconstructed by projecting the set of random POD coefficient a_n onto the set of eigenfunctions,

$$u_i(\vec{x},t) = \sum_{n=1}^{\infty} a_n(t) \phi_i^{(n)}(\vec{x}) \tag{30}$$

The dimension of the kernel N, in the eigenvalue problem is equivalent to the size of the domain $(\vec{x})$, which can be considerable large. The present formulation of a velocity field $u(\vec{x})$ would triple in dimension if each component was included, $(n_c \cdot N)$. Sirovich[31] realizing the inherent difficulties from a practical point of view attempted to derive a less computationally costly solution, which he referred to as 'snapshot' POD. The general basis of the problem is the same as in the 'classical' form, with the apparent distinction being the formulation of the kernel, and subsequent domain over which the eigenvalue problem is solved. We again, begin with an ensemble of a velocity field, however now separated by some time scale τ, on the order of or greater than the correlation time such that,

$$u^{(m)}(\vec{x}) = u(\vec{x}, m\tau) \tag{31}$$

Each m referring to a 'snapshot' or sufficient temporal separation making the velocity field uncorrelated in m. In similar fashion, the maximization leads to the integral eigenvalue problem, with the kernel now replaced by two-point *temporal* correlation tensor of $u^{(m)}(\vec{x})$.

$$C(\vec{x}, \vec{x}') = \frac{1}{M} \sum_{m=1}^{M} u^{(m)}(\vec{x}) u^{(m)}(\vec{x}') \tag{32}$$

equivalently written as,

$$C(t, t') = \frac{1}{T} \int_D u_i(\vec{x}, t) u_i(\vec{x}, t') d\vec{x} \tag{33}$$

where T is the period, D is the domain dictated by $(\vec{x})$, and t' represents a temporal separation. The resulting integral eigenvalue problem now becomes,

$$\int_T C(t, t') a_n(t') dt' = \lambda^{(n)} a_n(t) \tag{34}$$

The eigenvalue problem is now solved over the temporal domain, for the random POD coefficients, $a_n(t)$, now more clearly described as temporal eigenfunctions. Some key aspects of the solution are highlighted below.

- The POD coefficients a_n will again be random and uncorrelated, as a property of the basis of formulation.

$$\langle a_n a_m \rangle_T = \lambda^{(n)} \delta_{nm} \tag{35}$$

- The projection of the original ensemble onto the set of temporal eigenfunctions, a_n, now yields a set of spatial eigenfunctions $\phi_i^{(n)}$,

$$\phi_i^{(n)}(\vec{x}) = \frac{1}{T\lambda^{(n)}} \int_T a_n(t) u_i(\vec{x}, t) dt \tag{36}$$

- The coefficient $\frac{1}{T\lambda^{(n)}}$ must be applied to satisfy the condition that the set of spatial eigenfunctions, $\phi_i^{(n)}$ are orthonormal,

$$\int_D \phi_i^{(p)}(\vec{x}) \phi_i^{(q)}(\vec{x}) d(\vec{x}) = \delta_{pq} \tag{37}$$

The snapshot method aims to reduce the dimension of the integral eigenvalue problem from $n_c \cdot N$ to T. However, the pronounced difference shown in the formulation of the two techniques may ultimately serve to give no clear advantage. Both techniques can be applied to similar data sets. Should the flow configuration involve a coarser spatial grid size than temporal ($N \ll T$), or a temporal grid that is significantly dense, however still less coarse than the spatial ($T < N$, $N \gg 1$), then the snaphot method loses its advantage.

The snapshot proper orthogonal decomposition is performed giving a modal decomposition of the flow field, identifying the most energetic or 'coherent' structures, in an attempt to ascertain a measure of the

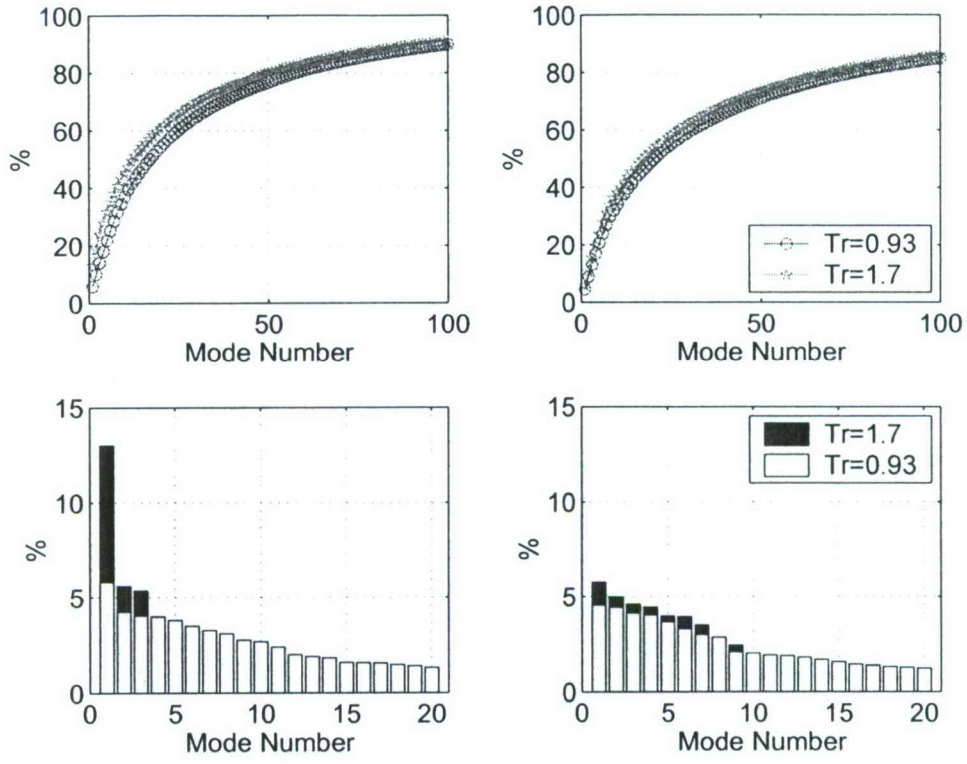

Figure 21. (a)Convergence of POD modes (left) at x/D=4.5 (right) and x/D=8.

large scale motion of the flow-field; *as it is the contribution of these structures that appears to be the marked difference in the cold and hot jet.* The 'snapshot' version of the method is used, comprising an average of 1980 PIV vector maps in each instance.

The formulation of the kernel matrix in the POD eigenvalue problem using the two-point fluctuating velocity correlations, dictates that the summation of the total number of eigenvalues generated gives the total turbulent kinetic energy of the flow field. The distribution of the system's energy in each jet, is very telling as to the dimensional nature. The ordering of the eigenvalues requires that the most energetic structures of the flow field will be represented by the first POD mode. In Figure 21, the distribution of energy is presented for both jets at streamwise locations x/D=4.5 & 8. The hot jet is shown to converge more rapidly at both locations, depicting a higher amount of the system's total energy over the lower modes. The largest disparity is seen at x/D=4.5, where the first mode of the hot jet nearly doubles the contribution of the cold, exhibiting more than 13% of the flow field's total energy. A similar trend is seen downstream, with a less pronounced difference. The turbulent kinetic energy distribution of each jet is tabulated below. Percentages represent % of total energy, and values, the number of modes. The low-dimensional nature, characteristic of the axisymmetric jet is seen here as 90% of the flow field's total energy can be recovered using an average of less than 7% of the total modes in all jets (*1980 total as dictated by the snapshot method*). Where the hot jet is concerned, it is seen that the features of this jet are 'more' low-dimensional in nature than that of the cold,exhibiting a steeper convergence slope. This is again more evident at the streamwise location x/D=4.5, closer to the jet exit. In the next section, the structure of these 'modes' is evaluated to gain some insight into the 'physical' flow features responsible for this distribution. Previous references to the modal structure of the source velocity field have been in the context of the Fourier-azimuthal modes. In the next section, the flow field is examined as a function of the *POD modal structure.* The 'structure' of the individual POD spatial modes, $\phi_i^{(n)}$ refers to an eigenfunction representation of the energy in the flow field, and ultimately not the jet's 'flow structure'. Interpretation of these is at times ambiguous. The features

Table 5. % Total Energy Convergence (*Number of POD modes*)

Jet/Location	30%	50%	70%	90%
Cold, x/D=4.5	7	17	37	101
Hot, x/D=4.5	5	12	30	93
Cold, x/D=8	8	20	48	139
Hot, x/D=8	7	17	42	131

of the flow will also be evaluated, by summing over the projection of the POD temporal modes, $a_n(t)$ onto these eigenfunctions, to reconstruct the original flow field.

$$u_i(\vec{x},t) = \sum_{n=1}^{\infty} a_n(t)\phi_i^{(n)}(\vec{x}) \tag{38}$$

The total number of modes used in this projection, dictates the total amount of energy in the representation of the flow field. As such, this technique allows the realization of the most energetic 'flow structure' within the random flow field, using only the 1st POD mode, greatly reducing the order of the system.

4. Modal structure

It has been suggested that the use of the snapshot POD method, along with reducing computational dimensions, does not 'presume' periodicity of the flow, as associated with a Fourier decomposition. It follows that the 'snapshot' POD decomposition gives a 'true' representation of the measured jet's characteristics, in the sense that it does not force fourier modes, and any asymmetries (*from flow field or measurement*), would be highlighted. In the azimuthal direction (θ), if the measured flow field is truly periodic and stationary in time, by definition, the POD decomposition mathematically reduces to a Fourier decomposition in this direction. Should the symmetry in measurement hold, then similar structures can be garnered in both cases. However, the 'snapshot' POD method used couples the decomposition of both the radial (r) and azimuthal direction (θ). As such, care must be taken where direct comparisons between the two modal structures is concerned.

Figures 22- 25 illustrate the flow features of the first 9 POD modes of the axial velocity component, $\phi_1^{(n)}$, for both the cold and hot jet, again at x/D=4.5 and 8. The cold jet exhibits a dominant structure resembling a Fourier-azimuthal mode 1 structure (22a). This is the most likely structure present in the flow, as it represents POD mode 1, contributing the most energy to the flow field. POD modes 7 & 8 are similar to a Fourier mode 4 structure, and suggesting a phasing relationship of approximately 45^o between the two. The higher mode 9 structure is similar to higher Fourier-azimuthal mode 5, suggesting an ordering similar to that of the Fourier modes. In line with this reasoning, combinations of POD modes 2-6 are examined to determine if lower ordered Fourier like modes may be present within these structures. Modes 4 & 5 are shown to form a POD mode 7-like structure (Figure 22b). The recent analysis of Pinier[67] highlights this result. Not clear here is whether these structures result from the radial inhomogeneities or the azimuthal. The higher ordered Fourier-modal distribution over POD modes present in [1,13,33] is not seen here as azimuthal directional decomposition is not performed prior to application of the POD.

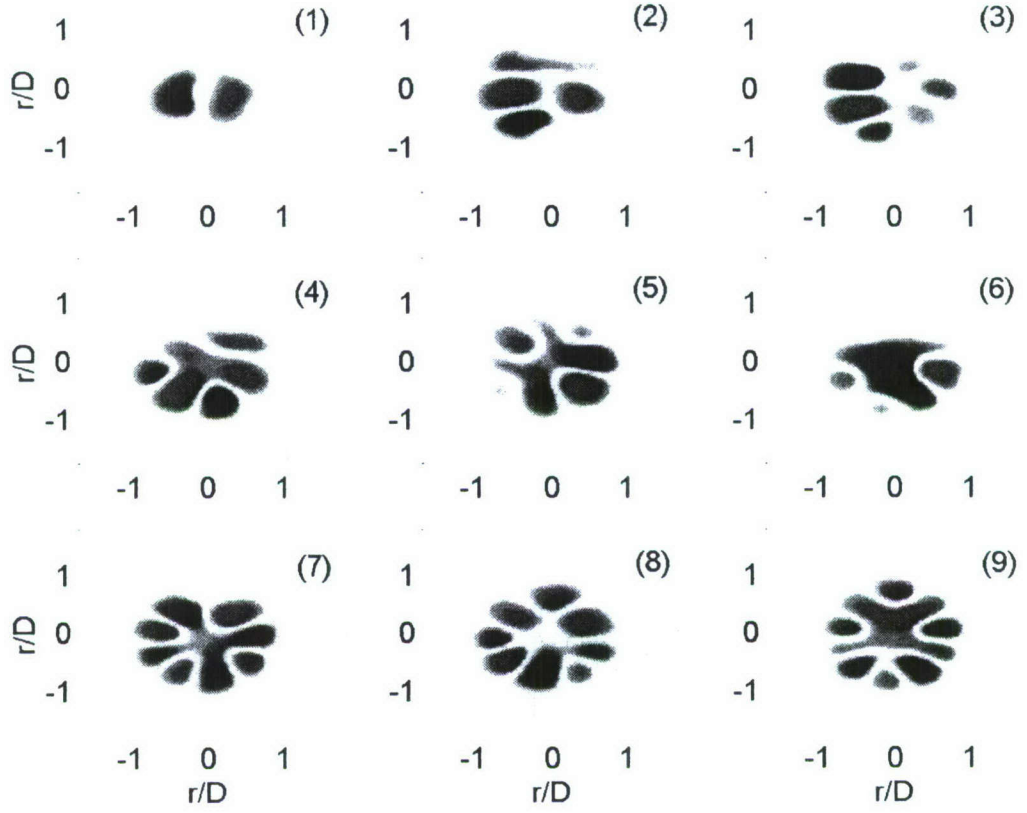

(a)

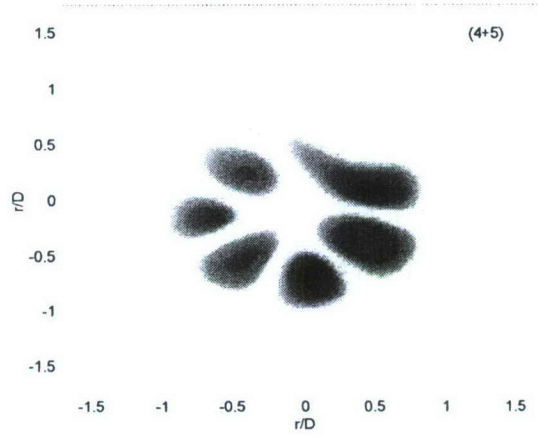

(b)

Figure 22. (a)POD eigenfunctions of the axial velocity component $\phi_1^{(n)}$ (*1st 9 modes*), of the cold jet at x/D=4.5. (b)Sum of $\phi_1^{(4)} + \phi_1^{(5)}$.

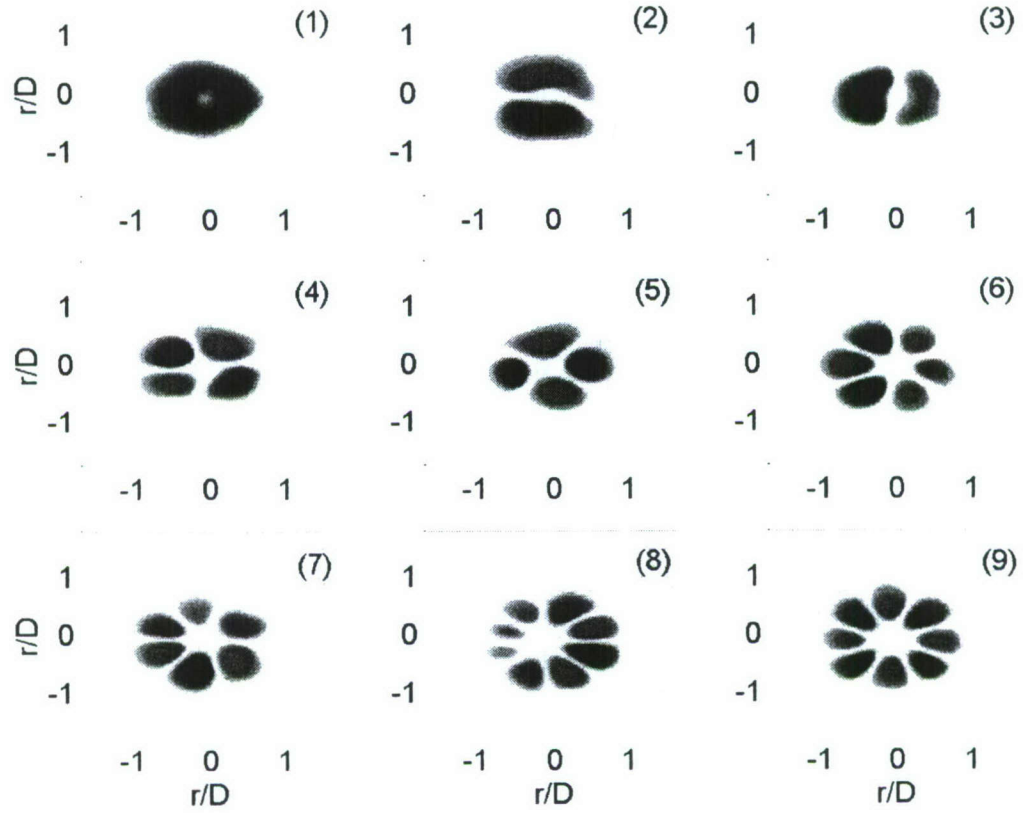

Figure 23. POD eigenfunctions of the axial velocity component $\phi_1^{(n)}$ (*1st 9 modes*), of the hot jet at x/D=4.5.

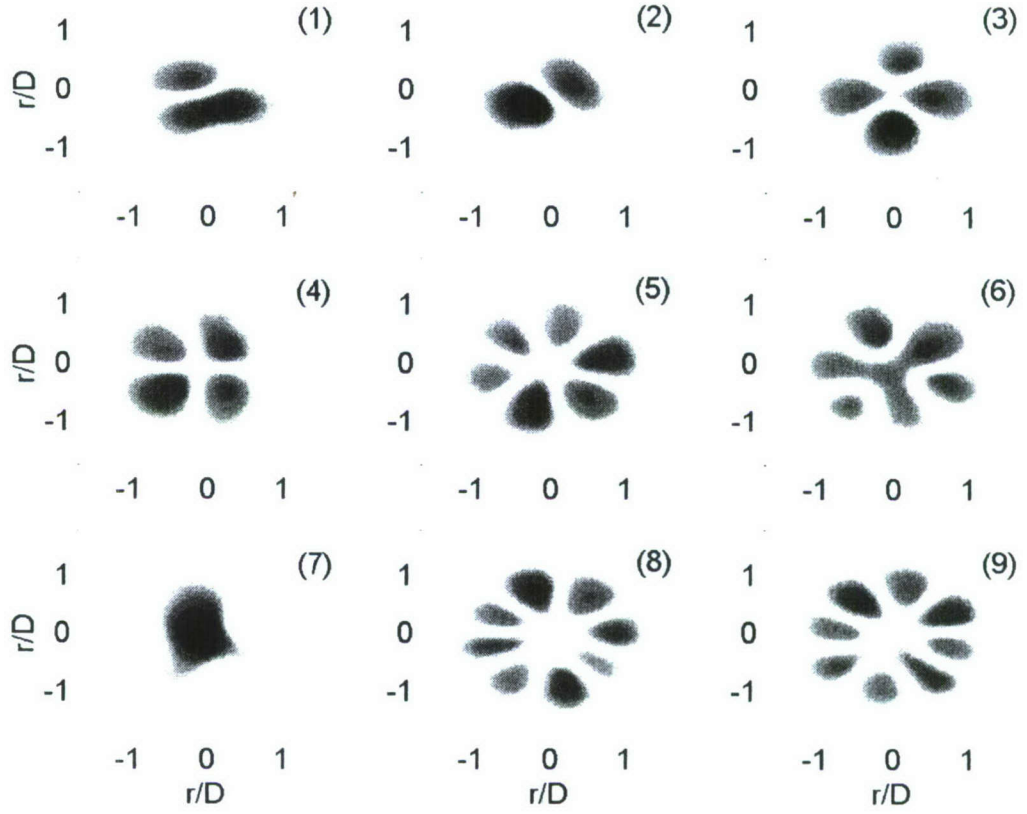

(a)

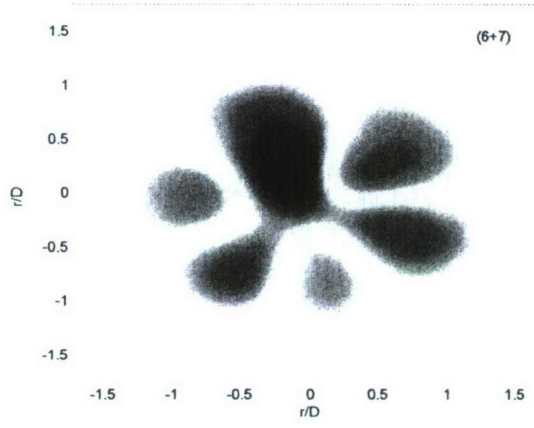

(b)

Figure 24. (a)POD eigenfunctions of the axial velocity component $\phi_1^{(n)}$ (*1st 9 modes*), of the hot jet at x/D=8. (b)Sum of $\phi_1^{(6)} + \phi_1^{(7)}$.

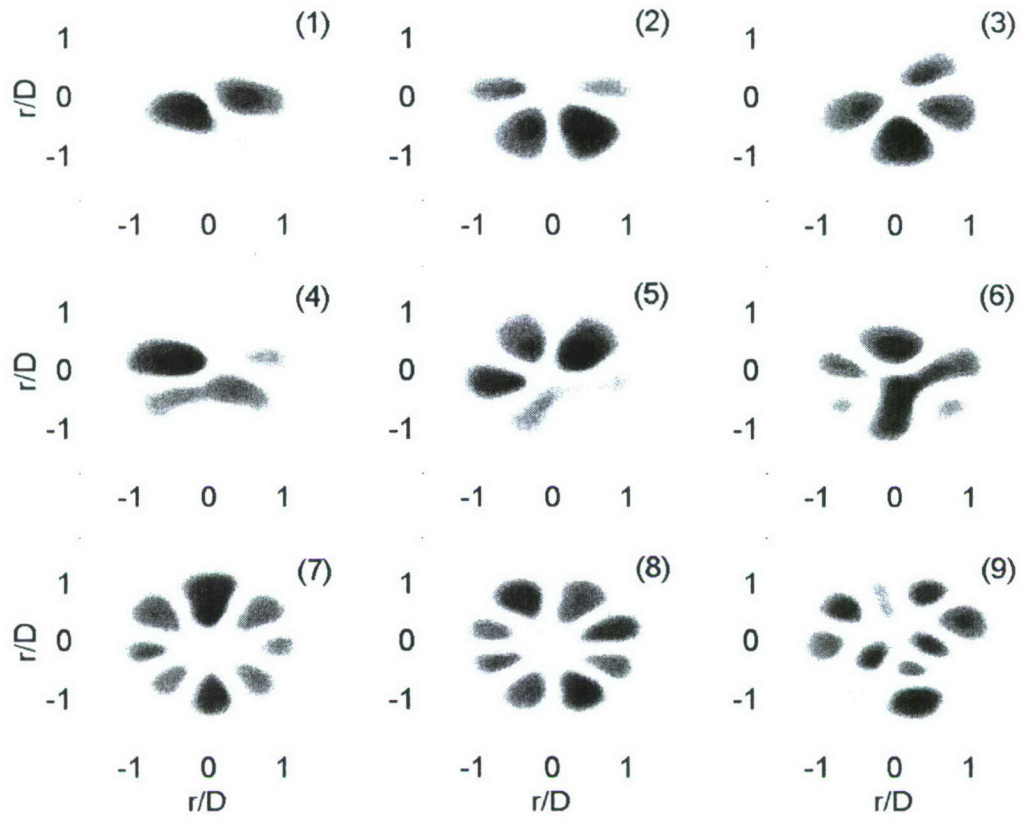

Figure 25. POD eigenfunctions of the axial velocity component $\phi_1^{(n)}$ (*1st 9 modes*), of the cold jet at x/D=8.

The more striking result is the clearly well-organized structures present in the hot jet at this streamwise location, closer to the jet exit, in Figure 23. The ***only*** flow structures exhibited here are those similar to Fourier-azimuthal mode structures. POD mode 1 resembles a Fourier mode 0, the column mode, as the most likely structure in the hot jet. The higher modes are paired, representing similar Fourier modes, each with a characteristic phasing relationship. Modes 2 & 3 at 90°, and consecutively higher modes at a decreasing phasing angle. This 'anomaly' is hypothesized next as the streamwise separation is increased to x/D=8.

At x/D=8, the structures of the hot jet remain fairly well-organized, exhibiting a larger radial extent (Figure 24). The dominant Fourier-azimuthal column mode has now switched to a helical mode 1, also seen at POD mode 2. The higher modes exhibit similar pairing and phasing, as seen at x/D=4.5. Mode 6 & 7 however, now combine to form an azimuthal mode 3 structure, a characteristic seen earlier in the cold jet. In Figure 25 the cold jet at this location illustrates a behavior similar to that at the upstream location, with an increased radial extent and the presence of what appears to be higher ordered Fourier modes at POD mode 9.

The observed trend now allows inferences to be made regarding the structure of the hot jet previously shown in Figure 23a. With the addition of heat, at a fixed acoustic Mach number, a lower Reynolds number is effected. As the flow field moves to a more 'laminar' flow, the structures become more organized radially, resulting in a more homogeneous and periodic jet, as the axisymmetric column mode structure is shown to persist longer in the source velocity field of the hot jet. This is in line with the previous analysis of fluctuating pressure field, as the hot jet also showed a pronounced column mode contribution as compared to the cold jet. The breakdown of the organization leads to the trend of 'splitting' Fourier modes observed, where the POD modes now sum to form Fourier modes, or simply exhibit non-representable eigenfunctions. This only

occurs downstream of the collapse of the potential core in the hot jet, where the axisymmetric shear layers have merged.

5. Velocity field reconstruction

The gain a better insight as to the features of the original flow field that are tied to the representation of the POD modal structure, the axial velocity component is now reconstructed (Figures 26 & 27). The flow field is first generated using a single mode (*POD mode 1, n=1*) to illustrate more clearly, the contribution of the most energetic, '*most likely*', flow feature. The streamwise location of x/D=4.5 is chosen, as this region exhibits the largest differences between both jets.

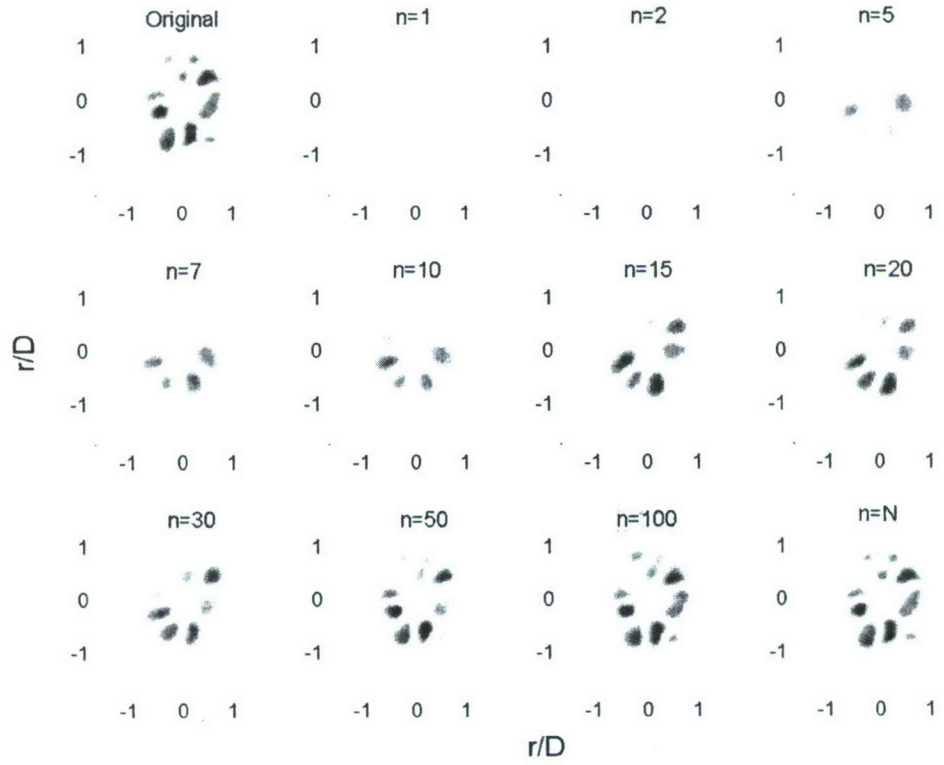

Figure 26. Velocity field reconstruction of axial component at x/D=4.5., in the cold jet.

The colormap scaling is normalized to the range of minimum to maximum magnitude of fluctuating velocity at this snapshot (±u'), to better illustrate the overall contribution of each mode. As seen in the figures, the hot jet depicts a brighter contour indicating a larger contribution of energy in the first POD mode (*as dictated by the steeper convergence curves presented in Figure 21*).

This trend continues until the 50 mode representation, where the levels of the contours in the cold jet begin to more closely resemble that of the original velocity snapshot. This level of similarity is reached in the hot jet at n=5. The more interesting feature here is the greater change in the 'richness' of the flow features seen in the cold jet, at similar mode count. The original velocity field in both jets exhibit a complex structure, with peaks lying with the region corresponding to the mixing layer. In the center of the curves, the potential core is represented. The hot jet depicts a smaller core region, and the presence of larger structure within the mixing layer. As POD mode contribution is increased, there is a greater disparity between the shapes and magnitudes of the peaks in the cold jet at similar mode count, as compared to the hot jet. This especially apparent at lower mode count.

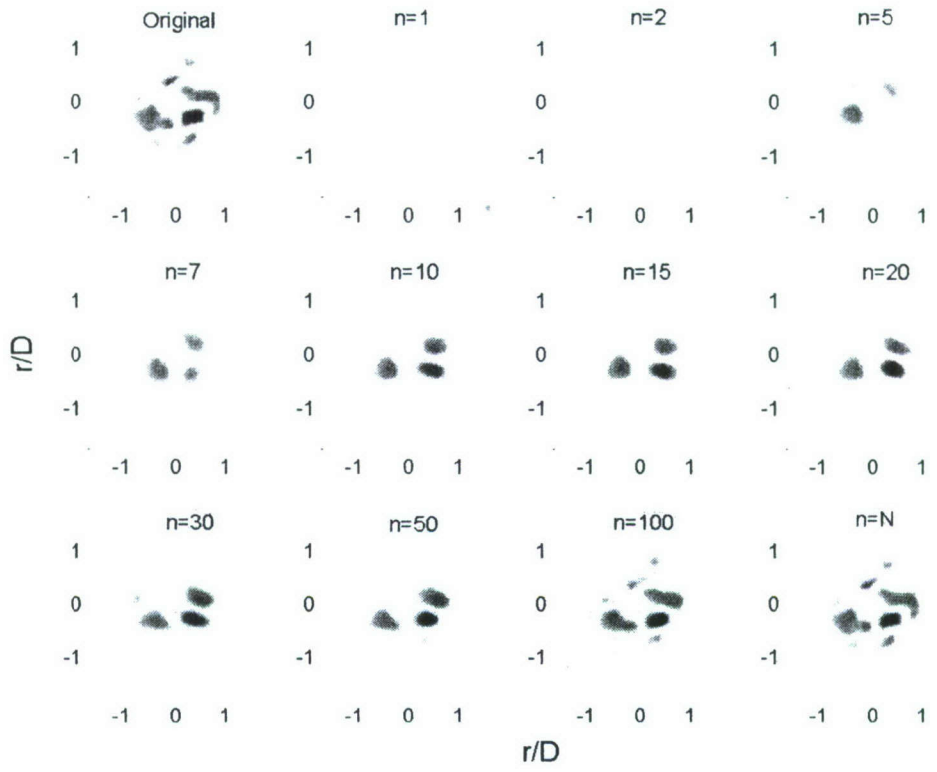

Figure 27. Velocity field reconstruction of axial component at x/D=4.5., in the hot jet.

The structure of the hot jet remains fairly similar over the addition of the first 20 POD modes, depicting only a gradual increase in the contribution of total energy. The energy distribution is such that the bulk flow features are realized using a lesser number of modes. The implies similar scaling of the low modes, whereby once the large scale, high energy contribution is realized, the higher ordered modes contribute little to the shape of the curves, until near n=20. This trend, as does the contours of the original velocity map (*although only an instantaneous snapshot*), suggests that a greater disparity in the scales of the dominant flow structure exists in the hot jet *i.e.* mainly large scales, as the low energy contribution of the small scales has little impact on the flow features. The cold jet conversely exhibits a trend of a greater 'disparity' in the scales, *i.e.* ranging in scales from large to small more evenly distributed, exhibiting more pronounced changes in the flow features with the addition of each mode.

Thus far, it has been found that the major differences between the hot and cold jet flow structure resides in the larger length scales exhibited in the hot jet. This feature is again highlighted here. The modal structure analysis has now demonstrated that it is the differences in the dominant modal ordering (*mode 0, hot and mode 1, cold*) of the two jets that stands as the source of this scaling. Larger scales persist owing to the stagnation of the natural development of the jet, with increased turbulent fluctuations due to a larger density gradient, ultimately serving to prematurely collapse the hot jet. The energy cascade from the large bulk mean flow to the smaller scales is now enhanced, as the smallest scales are now relatively larger (as seen in the structures of the shear layer in Figure 27).

It has been previously shown in the coupling of the near and far-field pressure, that the column mode exhibits a low frequency dependency, which is prevalent in the near-field signature of the hot jet, that drives the correlation with the far-field acoustics. This is now shown to be the case in the source velocity field, as well. Results presented here suggests that it may inherently be a Reynolds number effect, inhibiting the jets natural development, that contributes to the increased low frequency noise exhibited in the hot jet, as

supported by Viswanathan.[41]

H. Noise source statistics

The turbulent motion of compressible fluid is responsible for the generation of aeroacoustic noise. In the axisymmetric jet, this noise generation is governed by the interaction of fluctuating turbulent quantities convecting with the bulk mean flow. Lighthill's wave equation, describing the relationship between the source of noise in free shear flows and the resulting distribution of external fluctuations can be solved for the fluctuating density, in similar fashion as in Eq.1 described previously.

$$\rho(\mathbf{x},t) = \frac{1}{4\pi a_0^2}\int_V \frac{\partial^2 T_{ij}}{\partial x_i \partial x_j}(\mathbf{y},\tau)\frac{d\mathbf{y}}{|\mathbf{x}-\mathbf{y}|} \tag{39}$$

As the source strength in the acoustic analogy scales as a double divergence, $\frac{\partial^2}{\partial x_i \partial x_j}$, it follows that the fluid motion behaves as a volume distribution of acoustic quadrupoles. Following a formulation by Proudman[68] and Ribner,[69] the acoustic power output, or intensity, in the far-field defined by,

$$I(\mathbf{x}) = \frac{x^2 a_0^3}{\rho_0}\rho^2 \tag{40}$$

can then be expressed as a function of a series of fourth-order, quadrupole space-time correlations.

$$I(\mathbf{x}) = \frac{x_i x_j x_k x_l}{16\pi^2 a_0^5 \rho_0 x^5}\int_V \int_V' \overline{\frac{\partial^2 T_{ij}}{\partial \tau^2}\frac{\partial^2 T'_{kl}}{\partial \tau^2}}d\mathbf{y}d\mathbf{y}' \tag{41}$$

where only the perpendicular longitudinal axes in the differentiation $\frac{\partial^2 T_{ij}}{\partial x_i \partial x_j}$ are significant, scaling with

$$\frac{\partial T_{ii}}{\partial x_i \partial x_i} \sim \frac{x_i}{x}\frac{1}{a_0^2}\frac{\partial T_{ii}}{\partial \tau^2} \tag{42}$$

The ratio x_i/x is the direction cosine between source and observer location. After assumptions neglecting viscous and temperature effects, *i.e.* $T_{ij} = \rho u_i u_j$, the resulting acoustic power becomes,

$$I(\mathbf{x}) = \frac{\rho_0 x_i x_j x_k x_l}{16\pi^2 a_0^5 x^5}\int_V \overline{u_i u_j u'_k u'_l}d\mathbf{y} \tag{43}$$

Of the possible thirty-six components contributing to the quadrupole correlations, Ribner[69] proposes only nine contribute significantly to the broadband noise pattern of the jet. Terms involving the mean velocity component of the dominant flow direction in the jet deemed shear noise, and those only of fluctuating quantities, self noise. This is more clearly articulated as noise contribution from turbulence-mean flow interaction and turbulence-turbulence interaction, respectively. The contribution of each to the distribution seen in the far-field intensity, demonstrates an omnidirectional pattern (independent of ϕ), from the self noise and dipole-like ($B\cos^2\theta + \cos^4\phi$), from shear noise. The combined contribution of both exhibits an elongated elliptical pattern. When effects of convection and refraction are taken into account, the more common 'figure-eight' shaped pattern is generated, exhibiting a minimum at jet centerline, then peaking at shallow aft angle and diminishing with increased aft angle separation. The rearward angles demonstrating a minimum intensity. The broadband distribution can be decomposed to evaluate frequency content of the these noise terms. The modeled spectrums reveal that the *self noise* contribution peaks at substantially *higher frequency* than that of the shear noise, resulting from a quadratic dependence with the turbulent velocity field (*linear relationship with shear noise*).

Recalling the FS/LS spectrum of Tam *et al.*,[23] it is apparent that the two theories have similar foundations. Tam *et al.* suggesting that the shape of the far-field spectrum is governed by the dominant large scale contribution at shallow aft angles, and Ribner demonstrating that the largest contribution at these angles stems from shear noise, emanating primarily from the center of the mixing layer (*which is governed by large scale motion, driving it spreading*).

Shear Noise	Self Noise
$U_1U_1'\overline{u_1u_1'}$	$\overline{u_1^2u_1'^2}$
$U_1U_1'\overline{u_2u_2'}$	$\overline{u_1u_2u_1'u_2'}$
$U_1U_1'\overline{u_3u_3'}$	$\overline{u_1u_3u_1'u_3'}$
$U_2U_2'\overline{u_1u_1'}$	$\overline{u_1^2u_2'^2}$
$U_2U_2'\overline{u_2u_2'}$	$\overline{u_1^2u_3'^2}$
$U_2U_2'\overline{u_3u_3'}$	$\overline{u_2^2u_2'^2}$
$U_3U_3'\overline{u_1u_1'}$	$\overline{u_3^2u_3'^2}$
$U_3U_3'\overline{u_2u_2'}$	$\overline{u_2u_3u_2'u_3'}$
$U_3U_3'\overline{u_3u_3'}$	$\overline{u_2^2u_3'^2}$

The possible self-noise and shear-noise terms are as follows, These are now evaluated to asses their contribution in both the cold and hot jet. Only the first three shear noise terms are considered, as the mean flow direction (U_1) of the axisymmetric jet greatly out weighs the other two directions (*radial and azimuthal*), giving a largely more significant contribution. Also, following the reported experimental work of Ukeiley *et al.*,[66] and Bridges,[60] only the normal velocity correlations of the self-noise terms are examined here, as these have been shown to exhibit the largest magnitudes ($\overline{u_i^2u_i'^2}$). The formulation above assumes isotropic turbulence and neglects the contribution of the second source term, $(p - a_0^2\rho)$, which has been shown to scale with increases in temperature fluctuation. In line with this reasoning, it is the aim of this analysis to *qualitatively compare the contribution of the Reynolds stress term(s) in both jets and infer as to the contribution of the second source term from results.* The overbar in the above terms denotes both a spatial and temporal average of two-point space-time correlations. In the present investigation, the time separation is fixed at τ=0, as measurements are acquired using a single point in time, multi-point in space PIV system. This limits the ability to asses the frequency relationship of individual terms. However, it has been shown in the numerical analysis of Freund,[71] that maximum correlation are exhibited at this time separation.

The shear-noise terms representing axial, radial, and tangential source components (*top to bottom*), at fixed location of r/D=0, 0.5, & 1 (*left to right*), at a streamwise location of x/D=4.5 are seen in Figure 28 for both jets. As seen previously, the hot jet exhibits a larger spatial extent in nearly all contours. Similar magnitudes are exhibited in both jets, with a maximum along the centerline and decrease seen with increasing outward radial distance. This is consistent with results reported by Jordan & Gervais,[70] who modeled both isotropic and anisotropic turbulence, showing that the shearing of turbulence with the mean flow resulted in longitudenally aligned quadrupoles, with maxima at the centerline in both cases. The efficiency of these source terms depends greatly on the spatial extent over which the turbulence is correlated. It has been demonstrated that the radial distance proves to be the most significant length scale, as this is the direction over which the velocity gradient acts. The width of the peaks thus signify the regions of most efficient sound generation. As such, it follows that the hot jet would exhibit a more significant contribution to the far field spectrum. In line with this result, the hot jet contributes more low frequency acoustic energy in the direction of mean flow (*shallow aft angles*).

The axial source components are shown by Jordan & Gervais[70] and Freund[71] to give the most significant contribution, however Ukeiley *et al.*[66] demonstrates that it is the sources associated with the tangential

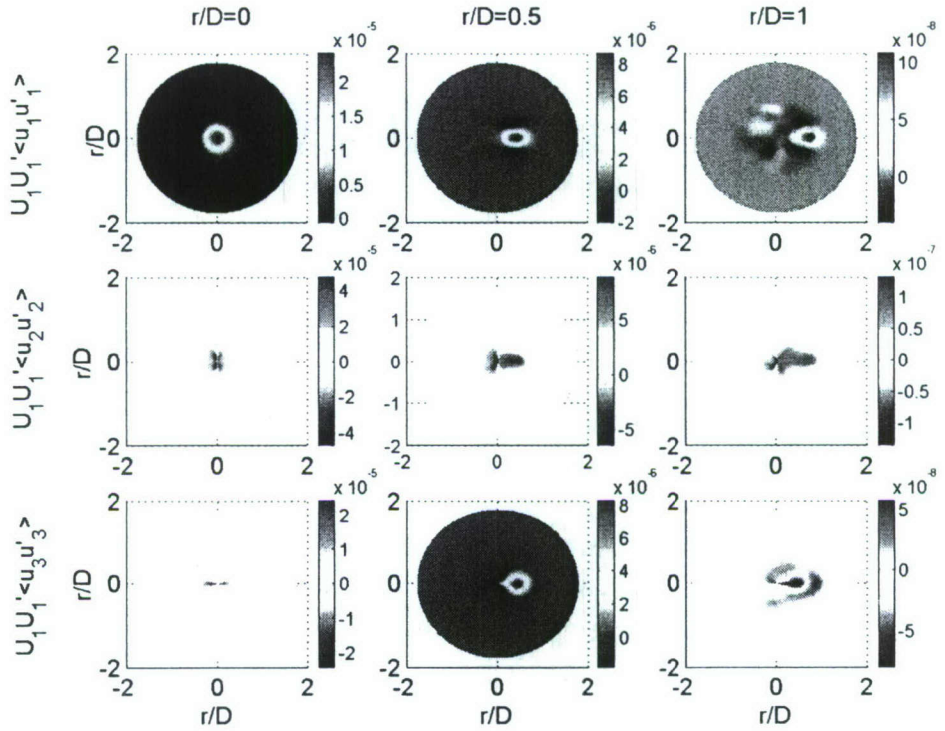

(a)

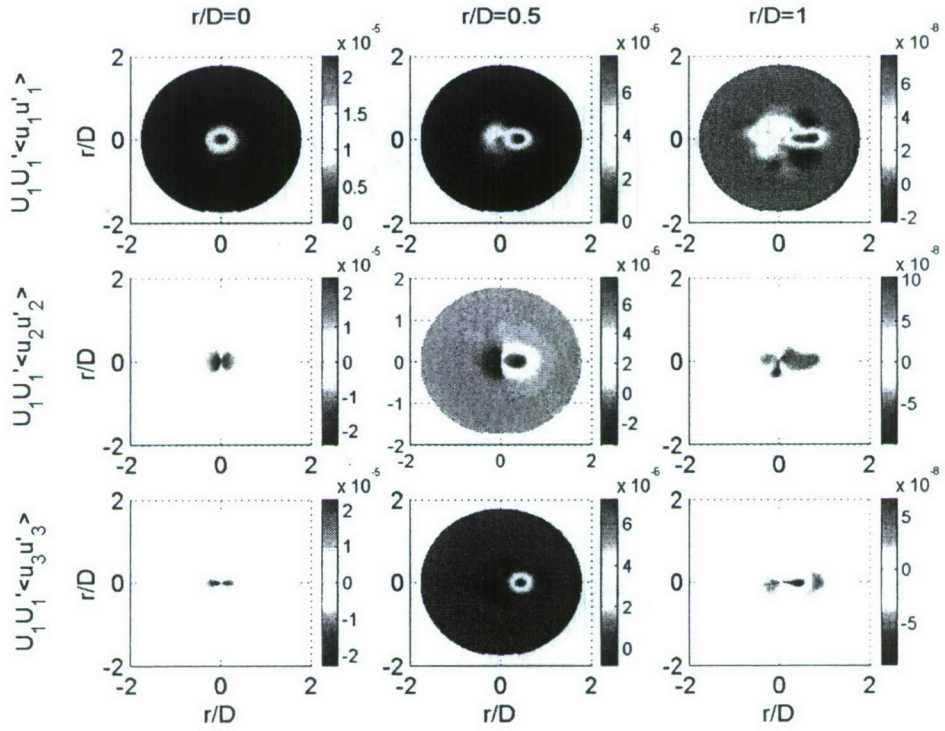

(b)

Figure 28. Shear-noise source correlations at x/D=4.5 (*normalized by* U_{cl}^4)(a)Cold jet (b)Hot jet

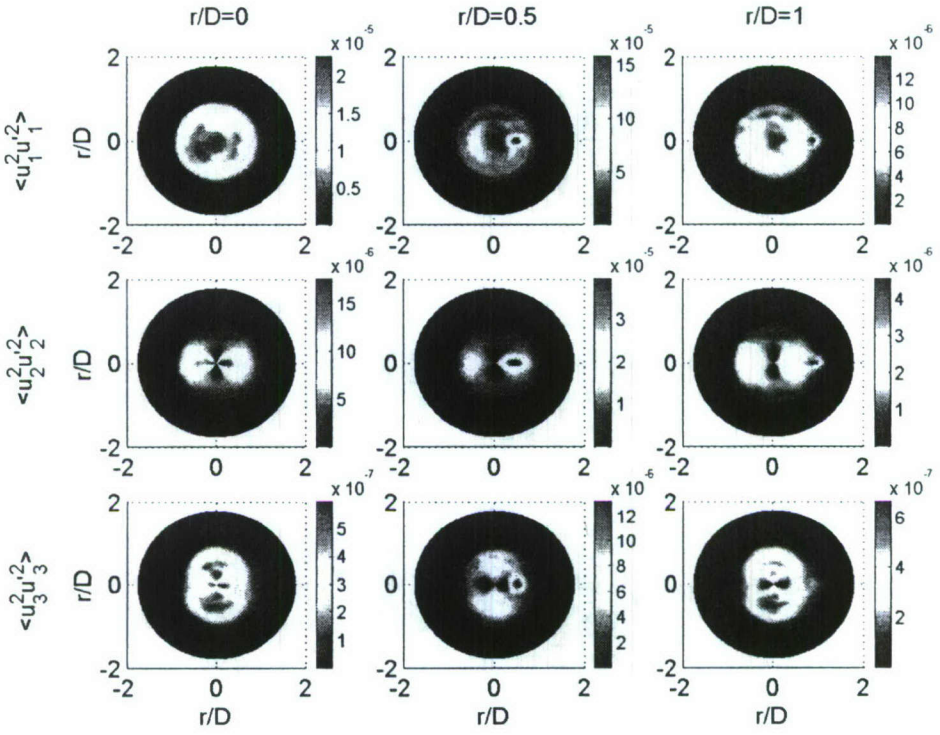

(a)

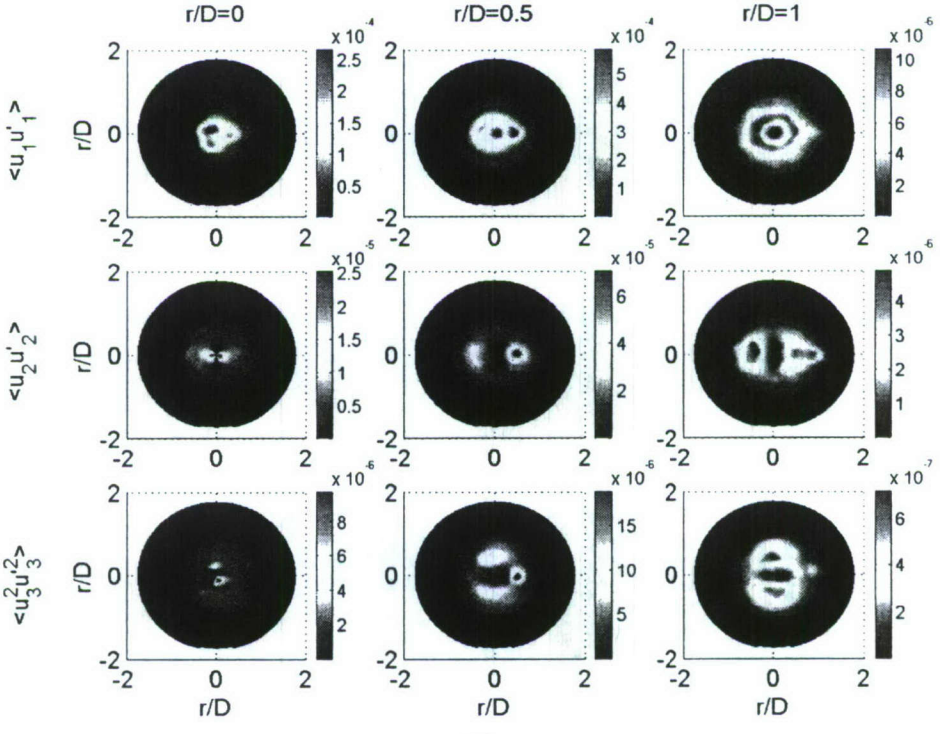

(b)

Figure 29. Self-noise source correlations at x/D=4.5 (*normalized by* U_{cl}^4) (a)Cold jet (b)Hot jet

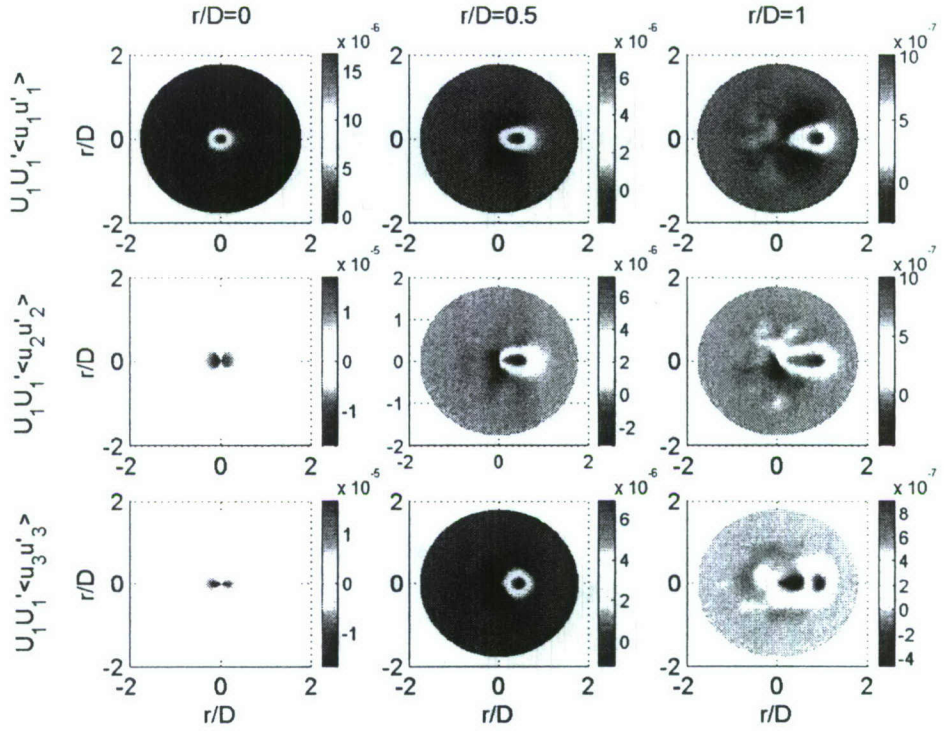

(a)

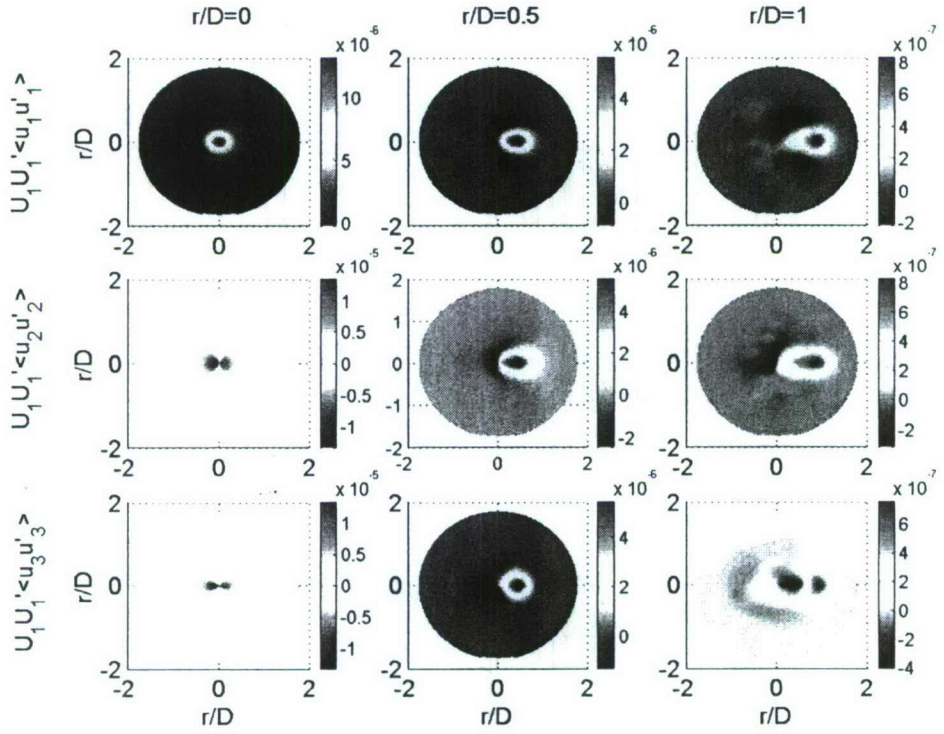

(b)

Figure 30. Shear noise source correlations at x/D=8 (*normalized by* U_{cl}^4) (a)Cold jet (b)Hot jet

velocity component, u_3, which exhibits a maxima. Here, no clear trend is discernable, but this will be revisited following the presentation of the remaining sources. The self-noise terms offer a different trend in Figure 29, as the cold jet exhibits a noticeably larger contours. Here, the scaling of this region is again significant as it implies an acoustic source region, however, not as dependent on radial distance as the shear-noise previously exhibited. These sources have a greater dependency on turbulence intensity. Although the magnitudes are consistently larger in the hot jet, owing primarily to the increased turbulent fluctuations, the region of effective noise generation is larger in the cold jet. An investigation of the total squared energy under the curves, as intensity scales with the integrated correlation, reveal a higher self-noise contribution from the cold jet. This suggests that the cold jet is a more efficient high frequency noise generator.

Downstream of x/D=8, the contours of the shear-noise exhibit similar regions over which the turbulence is correlated, resulting from the less pronounced differences between the two jets here, as shown previously. The self-noise sources also depict a similar behavior, with a more pronounced evidence of the potential core region collapse seen in the hot jet (Figures 30 & 31).

With downstream separation, at r/D=1, the self-noise sources suggest a breakdown in organization of the hot jet's structure with downstream evolution, consistent with a merging of the mixing layer. A similar trend is seen in the cold jet, though not as pronounced (*structures not as organized overall as shown by POD analysis*). There is also an increase in the magnitude of noise contribution and spatial extent, in both jets, with the exception of the centerline where 'peaks' are reduced (*overall correlated region still increases*). A seemingly more complicated trend is seen in the shear noise sources. The magnitudes here decrease with downstream distance at r/D=0, exhibit a slight decrease at r/D=0.5 (*more consistent in the hot jet*), and increase at r/D=1. This is not surprising as, these terms scale with the local mean velocity. A review of the streamwise profiles in Figure 16 highlights the reasoning behind the observed trend.

In each jet, at both streamwise locations observed, the self-noise sources contributions outweigh those of the shear-noise, as reported by others [71,70,66]. There is a less pronounced difference exhibited further downstream of the potential core. Trends regarding the dominance of individual components seen elsewhere, is not clearly discernable here. Only along the centerline do the axial components (1,1) consistently outweigh the radial (2,2) and tangential (3,3). As these are fourth order statistics of experimental measurements, the uncertainty in these correlations is greatly increased, and may prove to give vastly different results. This is especially true of the in-plane (*radial and tangential*) components, where fluctuations are of similar order as the mean value. Acquiring accurate turbulence statistics, is extremely challenging. However, the consistent trends exhibited in the values reported here, incur confidence in the relative behavior of the source terms. Thus this analysis, in the least, serves as a good qualitative comparison of the relative contribution of the noise sources in each jet.

As the contribution of the second source term, $(p - a_0^2\rho)$, is neglected here an incomplete picture of the source strength in the hot jet is left. However, as suggested by the modeling of Morfey *et al.*,[40] and shown numerically by Freund,[71] it's contribution serves to increase the radiation of noise in the direction of shallow aft angles. (*This is even apparent at the low Tr=0.86 in Freund's numerical simulation*). In this regard, the inclusion of this term would serve to increase the already dominant low frequency shear-noise (*peak radiation at shallow aft angles*) of the hot jet.

These results are, again, consistent with the findings of the acoustic far-field analysis. The hot jet is shown to demonstrate an increased contribution of low frequency, shear-noise, which is predominantly radiated in the direction of mean flow. The far-field spectrum correspondingly show an increased contribution of low frequency noise at shallow aft angles. The cold jet, conversely, demonstrates a greater contribution of high frequency, self-noise, at a similar streamwise location. It may be premature here to suggest that the diminished high frequency energy in the acoustic spectrum of the hot jet is tied to the lesser self-noise exhibited without further analysis over a larger number of axial locations, however the correlation is striking.

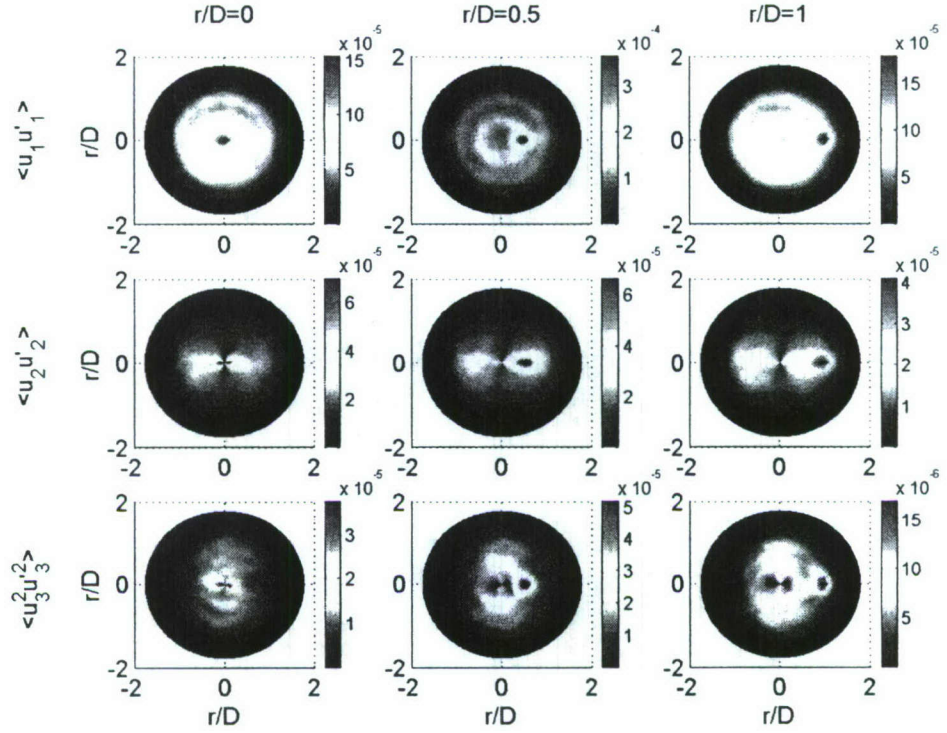

(a)

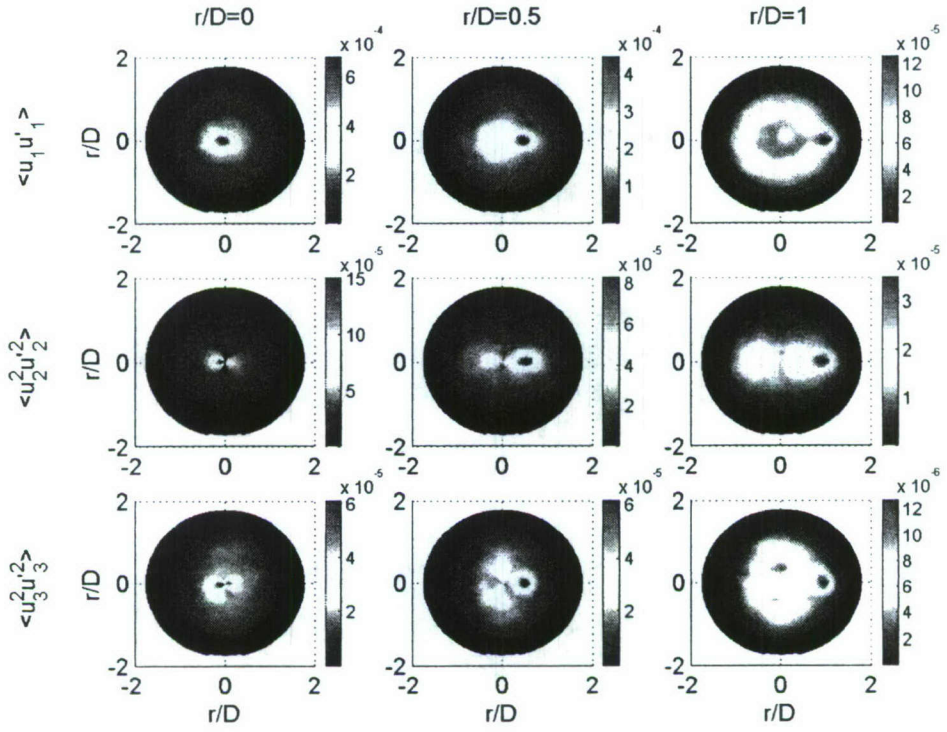

(b)

Figure 31. Self noise source correlations at x/D=8 (*normalized by* U_{cl}^4) (a)Cold jet (b)Hot jet.

I. Conclusions

The aeroacoustic source features of an 'acoustically matched' Mach 0.6 jet, with temperature ratio Tr=0.93 and 1.7, have been investigated. With exit velocity U_j fixed, and core flow temperature increased, the effect of elevated temperature on the source acoustics was isolated. As the jet Mach number (M_j) falls to 0.44 and Reynolds number almost half of the cold study, 2.8x10^5 from 6.9x10^5, it may be expected that less fluctuations would exist as the jet moves towards more laminar behavior. However, an analysis of the near-field pressure measured by an azimuthal array positioned near the jet exit (x/D=2), demonstrates a marked increase in low frequency energy, seen in the pressure power spectral density of the hot jet, accompanied by a slight decrease at high frequency. A modal decomposition reveals the presence of differing dominant modal contribution in each jet, (*column mode in the hot jet and helical in the cold*). The more distinct peaks exhibited in the coherency curves of the hot jet, suggests a more consistent scale. Conversely, broader peaks in the cold jet imply a greater distribution of scales over which energy is correlated.

The mean statistic of the source velocity field show that both jets have similar exit velocity and a similar spreading rate in the outer shear layer, exhibiting similar half-widths with the centerline. However, upon examination of the shortened potential core region in the hot jet (*x/D=5 versus 6 in the cold*), it is realized that the shear layer thickness is in fact larger, owing to the larger collapsing angle (*5.7° in the hot jet and 4.75° in the cold*). The turbulent fluctuations are seen to increase in all velocity components in the hot jet, with a predominance in the axial velocity component, at nearly 3%. The data from both jets collapses well using $\eta(x)$, half velocity scaling, as well as the Witze correlation parameter for jets of differing temperature ratios, which gives confidence in these measurement.

Reynolds stresses, are examined in both jets, again revealing trends consistent with a more rapid decay of potential core region of the hot jet, as peaks move closer toward the centerline at similar downstream separation. Examined along the centerline at r/D=0, the hot jet depicts the presence of larger scales closer to the jet exit. With increased downstream distance, the differences in scaling between the two jets exhibits only subtle differences, owing to the stunted development of the hot jet as the mixing layers have merged, no longer drawing energy from the potential core, (*which has since collapsed further upstream in the hot jet*). The length scales are shown to be consistently larger in the hot jet, as compared to it's cold counterpart, with the radial extent of the normalized stresses exhibiting the greatest differences in all terms, an effect which is shown to be less pronounced with increasing distance from centerline. The tangential normal stresses, serve as an exception to this trend, still exhibiting larger scales in the hot jet, but in azimuthal variation.

A low-dimensional analysis of the two source velocity fields, using the 'snapshot' POD method, reveals the dominance of a Fourier column mode-like structure in the hot jet. The cold jet is shown to exhibit a dominant Fourier helical mode-like structure. This explains the observed trend seen in the shear stresses, whereby the column mode structure of the core exhibits only a positive lobe with the helical structure of the radial component (*helical due to the opposing direction of motion across azimuthal separation due to spreading of the shear layer*). Correspondingly, the turbulent kinetic energy in the hot jet is shown to converge more rapidly, depicting a higher amount of the system's total energy over the lower ordered modes, (*more pronounced near the jet exit*). The largest disparity is seen at x/D=4.5, where the first POD mode of the hot jet more than doubles the contribution of the cold (6%), exhibiting more than 13% of the flow field's total energy. A rather striking result is observed as the, POD modal structure of the hot jet depicts only clearly well-organized structures, similar to those of Fourier modes. The cold jet exhibits some deviation from these kinds of structures, an effect which is show to exist in both jets at downstream location. As no periodicity of the flow field is presumed in the decomposition, this trends suggests that with the addition of heat the flow field tends to a more radially organized structure, resulting in a more homogeneous and periodic jet, as the axisymmetric column mode structure is shown to persist longer in the source velocity field of the hot jet. The breakdown of this organization leads to the trend of 'splitting' Fourier-like modes observed, where the POD modes now sum to form Fourier modes, or simply exhibit non-representable eigenfunctions. This only occurs downstream of the collapse of the potential core in the hot jet, where the axisymmetric shear layers have merged. However, at fixed acoustic Mach number, this may well be a lowered Reynolds number effect, as this behavior is typical of a more 'laminar' flow structure.

The results of the source velocity field analysis, are in line with those reported in separate analysis of the fluctuating pressure near-field. The increase in the turbulence levels of the hot jet are sense by the near-field

array suggesting that the region surrounding the flow has a strong dependency [34, 53, 35]. The dominant column mode of the hot jet is sensed as an increased low frequency contribution in the pressure near-field. The distinct peaks of the pressure coherency spectrum, suggesting the presence of a more consist scale in the hot jet and larger distribution of scales in the cold, is verified through the low-dimensional reconstruction of the dominant structures of the source velocity field. The more gradual change in the 'richness' (*shapes and magnitudes of the peaks*), of the flow features seen in the cold jet, with the addition of a similar number of POD modes, implies a similar weighting of modes. In the hot jet the energy distribution is such that once the high energy, bulk flow features are realized, the higher ordered modes contribute little to the shape or magnitude of the curves, until at a sufficiently large mode count.

The acoustic features of the each jet as sensed by the far-field array of microphones exhibits some distinction, in line with findings of others[38,60,27,56]. The directional dependence of the far-field spectrum with frequency is highlighted, as the spectral densities reveal an increase in the amplitude of the hot jet at nearly all observer angles, with a marked increase in the low frequency energy at shallow aft angles. The overall sound pressure levels demonstrate a $2dB$ increase seen at the shallowest aft angle of ϕ=15^o and a slight decrease of nearly a half dB seen at the ϕ=90^o location. This increase is a result of increased low frequency noise contribution in the hot jet, coupled with a decrease at high frequency, as compared to the cold jet, seen in the acoustic spectral densities. An analysis of the frequency contribution of each microphone location reveals more pronounced changes in amplitude with increasing frequency at shallow aft angles, substantiating the trend of low frequency noise dominance at shallow aft angles, reported in the OASPL increase. Correspondingly the reduction in high frequency noise, is reflected in the diminished contribution in OASPL of the microphone located at the largest observer angle of ϕ=90^o.

The far-field acoustic features are shown here to be reflective of the changes in the source velocity field, similarly to the near-field pressure. The marked increase in low frequency noise at shallow aft angles, can be linked to the dominant low frequency column mode present in the hot jet. In this similar regard, the reduction of the higher frequency noise can be linked to the increase in the scales of the structure (*small scales producing high frequency noise*). Thus, the shift to a dominant low frequency column mode observed in both the near-field pressure signature, along with the increase in low frequency acoustic energy seen predominantly at shallow aft angles, again, serves as evidence of the the large scale's contribution predominantly to the shallow aft angles.

The increase in OASPL demonstrates a greater influence on low frequency energy increase, than high frequency reduction. Where noise production is concerned, the Reynolds stresses, viewed as a simplified representation of the Lighthill's stress tensor, $T_{ij} = \rho u_i u_j$, exhibit increased magnitudes in the hot jet. As the turbulence levels do not show significant differences, the link between these stresses and the increase in OASPL is weakened by the vast difference in mean density of each jet (ρ_{cold}=1.428 and ρ_{hot}=0.759). Therefore, the Reynolds stress source term's contribution to noise generation in the hot jet would no doubt be diminished.

The mechanism responsible for the additional low frequency noise is sought in an investigation of the acoustic sources, using the quadrupole correlations. These fourth order space-time statistics are calculated directly from the fluctuating source quantities. The temporal domain is suppressed, at τ=0, due to the use of PIV to acquire the velocity field. The shear noise terms, contributing to low frequency fluctuations, are shown to depict similar magnitude in each jet, with a maximum along the centerline. As it is the radial extent of the correlation which greatly influences the efficiency of these source terms (*velocity gradient acts over spatial extent*), the width of the peaks thus signify the regions of most efficient sound generation. The hot jet, with larger scaled structures exhibiting a greater correlation length scale, in-turn demonstrates a more significant contribution to the far field spectrum. The peak angle of radiation as modeled by Ribner,[69] for these terms is in the direction of mean mean flow, or at shallow aft angles.

The self noise terms show a marked contribution in peak intensity in the cold jet, exhibiting noticeably larger spatial extent of correlation. As these sources have a greater dependency on turbulence intensity, the magnitudes are consistently larger in the hot jet (*owing primarily to the increased turbulent fluctuations*). However, intensity scales with the integrated correlation over the region of effective noise generation, which is larger in the cold jet, revealing a higher self-noise contribution from the cold jet. The cold jet is thus a more

efficient high frequency noise generator. These terms are know to exhibit an omnidirectional dependence. At each measured location, the self-noise sources contribution consistently outweighs those of the shear-noise. There is a less pronounced difference exhibited further downstream of the potential core. However, as the the self noise terms illustrate the contribution of high frequency energy to the acoustic spectrum, then the contribution of theses terms must outweigh the low frequency noise of the shear noise source terms, in both jets.

In a similar line of reasoning, the diminished contribution of high frequency noise in the hot jet should be less pronounced than the increase in low frequency noise, as the acoustic spectra demonstrates a larger low frequency change. As no clear distinction supporting this can drawn from the quadrupole correlations (*shear noise sources in both jets depicting similar magnitudes with only a slightly larger spatial extent in the hot*), the contribution of the entropy source term is deemed a significant contributor. The formulation used to derive these terms does not include the contribution of the second source term $(p - a_0^2\rho)\delta_{ij}$, however as evaluated numerically by Freund,[71] it's contribution is shown to exhibit a marked increase in noise, predominantly at shallow aft angles. This result is found in the cold jet at Tr=0.86. As such, it may be inferred that the contribution of this term will be more pronounced in the case where a temperature gradient exists, (*higher temperature ratio*). This contribution would serve to increase the already dominant low frequency shear-noise contribution (*in the direction of peak radiation at shallow aft angles*) of the hot jet, as compared to the cold.

The presence of the 'additional source' of acoustic energy in the hot jet can now be described as resulting from the increased organization of the velocity field, causing the column mode structure to persist longer than its cold counterpart. Larger scales are prevalent, owing to the stagnation of the natural development of the jet, and the increased turbulent fluctuations (*driven by a larger density gradient between core and entrained fluid*). This serves to prematurely collapse the hot jet. The scaling of these structures contributes greatly to the far-field spectrum in the form of low frequency shear noise, radiating primarily in the direction of propagation, *at shallow aft angles.* The resultant field is *loosely* described as a *more laminar jet with increased turbulent fluctuations.* This suggests that it may inherently be a *Reynolds number effect*, as this trend of 'laminarization' is associated with a decrease in the effective Reynolds number in the fixed Mach number experiment, as supported by Viswanathan.[41] (*Jet Mach number (M_j) falls to 0.44 form 0.6 and Reynolds number almost half of the cold study, 2.8x10^5 from 6.9x10^5*). However, the less pronounced difference in the source contribution of each, does speak to the increased contribution of the second, entropy source term.

1. Discussion

This study comprises several independent analysis, *i.e.* the source velocity field, fluctuating pressure surrounding it, and the acoustic far-field response. It has been demonstrated that the fluctuating pressure, sampled here at x/D=2, $r/D \simeq 1$, accurately captures the characteristic dynamics of the source velocity field[34,53,,35] In turn, it is also shown that the acoustic far-field exhibits a strong relationship with the fluctuating near-field signature.[52]

Next steps would include coupling the source velocity field with the surrounding near-field pressure, via the application of the modified complementary technique, as detailed by Bonnet *et al.*[42] As the technique relies greatly on the measure of correlation between the two fields, the current results, establishing a relationship between the two, are promising. Once a reliable set of estimation coefficients are obtained, the undersampled PIV velocity field can be estimated to realize a time-resolved field. This in turn provides a means by which the simplified stress term in Lighthill's acoustic analogy, $T_{ij} = \rho u_i u_j$, can be calculated and ultimately used to estimate the far-field acoustics. With the sampled acoustic field already available, comparisons can be made between the two to determine, firstly, whether the assumption of neglecting the entropy term $(p - a_0^2\rho)\delta_{ij}$ is justifiable in the cold jet. Secondly, this term's contribution in the hot jet can be evaluated, as the sampled acoustic far-field of the cold jet could serve as a benchmark, whereby levels above this would be deemed additional noise.

This analysis highlights the amount of information that is lacking as a result of the inability to sample inflow pressure and density directly. Panda *et al.*[72] has recently applied a Rayleigh scattering technique to get a measure of the density fluctuations, however with current technology, measurements of inflow pressure

would require bulky probes resulting in the contamination of the 'true' acoustic far-field signature. The use of numerical simulations such as Large Eddy Simulation and Direct Numerical Simulation provide solutions to evaluating the contribution of the entropy term. These, however rely greatly on the initial and boundary conditions employed to simulate the flow field. As well, extending the computational domain to the far-field requires further assumptions to be made.

Where control of noise is concerned, these results indicate that it is the intrinsic structure of the jet that must be manipulated. The increased low frequency noise is seen to result from differences associated with the scales and modal ordering of the dominant structures in each jet. A delicate balance must be reached in manipulating these through the use of upstream perturbation or fluid injection. Column mode forcing at the jet's preferred instability serves to increase the low frequency noise, whereas at higher modes, a small reduction can be achieved as a result of the combined effect of low frequency reduction and high frequency increase, Samimy.[75] It is in this regard that active flow control schemes must be adapted to include more complex forcing signals or strategies which couple differing modes, in hopes of achieving a more broadband reduction in noise.

V. Dynamical Systems Modeling

Several attempts have been made at investigating the dynamics of the high-speed jet, both quantitatively and in a time-resolved manner. This involves measuring flow quantities so as to capture from the smallest to the largest time-scale events in the flow field. From these type of experimental or computational measurements, dynamical information can be extracted from which much can be learned as to the types of coherent processes that occur and how they relate to the far-field sound.

Since the 1970's it is widely recognized that even in very high Reynolds number flows, there exists coherent structures that demonstrate distinctive features such as organized vorticity and exhibit repeating patterns of turbulent motion[4,16,15] Unlike previous beliefs that turbulent flows were dominated by random motion and chaos, through advanced measurements, simulations, and analytical data processing tools, such features are now recognized in highly turbulent flows as well. The problem lies in discerning a physical interpretation of these results to explain the mechanisms at work and build models to represent them. Such models are important in furthering our understanding of turbulent motion, as numerically solving the full Navier-Stokes equations for high Reynolds number flows is not a realizable goal in the foreseeable future of computing evolution. The development of dynamical systems models can therefore improve on Reynolds Averaged Navier-Stokes (RANS) techniques or validate Large Eddy Simulations (LES) of such flows.

Direct Numerical Simulations (DNS) of high-speed jets performed at very low Reynolds number, along with computations of the instantaneous aeroacoustic field, have provided great insight into the dynamics of these flows and their relation to the far-field sound. Freund *et al.*[11] have applied flow control using adjoint methods in a DNS simulation of a two-dimensional high-speed jet with the control objective of minimizing the far-field sound. The control is performed in a 'black-box' near the jet exit and modifications to the control input are made iteratively at retarded times to slightly modify the dynamics of the flow, minimizing the sound propagated to the far-field. A quiet jet was in this manner simulated and compared to the uncontrolled loud jet. Quite surprisingly, a simple comparison of the instantaneous dynamics of the controlled to the uncontrolled flow does not show a significant difference in the organization of the large-scale structures of the flow, which indicates that the noise production mechanism is quite subtle. Only once a processing of the data using proper orthogonal decomposition (POD) is performed does a difference in spatial phase appear between the first modes. This type of study of the dynamics of jets shows that a similarly subtle control strategy needs to found, when such a slight change in the flow has such a great impact on the far-field sound.

Early experimental measurements of the dynamics of high-speed jets were performed using rakes of hot-wires. Multi-point correlations of velocity components coupled with assumptions of homogeneity and periodicity in the jet flow flied, allowed the application of low-dimensional techniques such as Stochastic Estimation and POD.[1] Citriniti[7] took measurements of the dynamics of the axisymmetric incompressible jet at one downstream position using an in-house designed rake of 138 hot-wires. The experiment was then carried out at multiple near-field positions by Gamard[26] and multiple far-field positions by Jung,[7] to

study the evolution of the azimuthal modes as the jet develops downstream. Computational efforts towards measuring the dynamics of axisymmetric jet flows are today feasible at rather low Reynolds numbers ($5x10^3$) in direct simulations[71] and at intermediate Reynolds numbers ($5x10^4$) using LES.[56] These investigations have the advantage of containing time-resolved information of multiple flow quantities simultaneously (velocity, density, acoustics, hydrodynamics, vorticity, etc) from which much valuable information can be gained. However these methods are limited by the rather low Reynolds numbers attainable and the small amount of time series computed.

A. Measuring flow dynamics

Experimental time-resolved measurements of turbulent flow fields certainly emerged with the advent of hot-wire anemometry, principles of which date back to the beginning of the twentieth century. This proved to be an extremely effective and accurate tool, but limiting in terms of application. At higher velocities, the intrusive nature of the technique would cause probes to break under the high dynamic pressure loading, and generate turbulent vibrations. With the introduction of lasers came laser Doppler anemometry (LDA), which although technically much more challenging and costly for the experimenter, presented the advantage of being a non-intrusive technique. It was now possible to obtain 3-component single-point measurements of velocity in high-speed flows, without disturbing the flow. As this optics based measurement is based on the Doppler shift provoked by a particle crossing the measurement volume scattering light with a frequency shift proportional to its velocity, its main limitation is flow seeding. Non-intrusive multi-point velocity measurements were only developed toward the late 1980s when high powered lasers and fast response cameras were combined to form particle image velocimetry (PIV). This technique enabled accurate, spatially well-resolved velocity measurements simultaneously in an entire plane. Again, however, this technique proved to also be limited, as temporal resolution in high-speed flow was unattainable. However, much can be gained from such measurements if one has the desire to study the statistical properties of a flow such as mean velocity profiles, phase-averaged velocity fields, or simply collect databases of instantaneous snapshots of velocity fields to then perform multi-point spatial correlations and other post-processing techniques.

Experimentally measuring the dynamics of the high-speed jet flow can prove a challenging task. We are today experimentally limited to two-dimensional plane measurements (3 components). However, planar measurements can be very informative, especially when all three components of velocity can be measured simultaneously on a relatively fine grid, such as when using stereoscopic particle image velocimetry (PIV). This optics-based measurement technique is attractive not only because of its non-intrusiveness (the flow remaining undisturbed by the measurement) but also due to its range of application. It is not prudent to use rakes of hot-wires in high-speed compressible flows. PIV is therefore the only experimental instrument capable of providing planar velocity data at fine spatial resolution in high-speed flows such as the axisymmetric jet. The next step in dynamical measurements of such flows was the recent development of the multi-plane PIV measurement technique[7] which presents the advantage of being a non-intrusive technique applicable to many types of flows. This enables a direct measurement of the three-component acceleration field. Depending on application, Eulerian or Lagrangian acceleration can be realized by finite difference calculation of the consecutive PIV measurements; the latter being delayed by a carefully chosen time lapse that is tied to the time scales of the flow field under consideration.

B. Dual-time PIV experiment

The pioneering use of multiple PIV systems was proposed and later implemented by Kähler & Kompenhans[7] to develop a tool capable of measuring time derivatives of the velocity (*i.e.* acceleration) as well as spatial derivatives (*i.e.* velocity gradient tensors, strain rate tensors and vorticity field) in a whole plane. Several research groups have since performed dual-plane PIV using two PIV systems for measurements in two parallel and adjacent planes; as well as dual-time PIV using both systems in the same measurement plane separated in time by a short delay. The latter technique enables measurement of acceleration or more generally of the time derivative of the velocity field which, associated with the proper orthogonal decomposition (POD), enables dynamical systems development with a potential use for closed-loop flow control.

In the present configuration where the consecutive PIV measurements are performed at the same location, the Eulerian acceleration (or local acceleration) is computed directly. The Lagrangian acceleration (or material acceleration) is the whole left-hand side of the Navier-Stokes equations defined as,

$$\frac{D\vec{u}}{Dt} = \frac{\partial \vec{u}}{\partial t} + (\vec{u} \cdot \nabla)\vec{u} \tag{44}$$

the first term on the right-hand side being the Eulerian acceleration and the second term being the non-linear convective acceleration. To measure this quantity experimentally, one has to follow each particle as it moves through the velocity field to take into account both contributions to the acceleration of the particle, the unsteadiness of the velocity field and the change in velocity as the particle moves through this field. Two stereoscopic PIV systems are used in the present experiment in an identical cross-flow plane perpendicular to the jet axis, capturing all three components of acceleration. Using finite differencing, local acceleration is computed for each pair of velocity field obtained. The process is reiterated for different downstream positions ranging from 3 to 10 jet diameters so as to obtain a 3-dimensional acceleration field of the high-speed jet. A picture of the setup is shown in Figureŕeffig:dual.

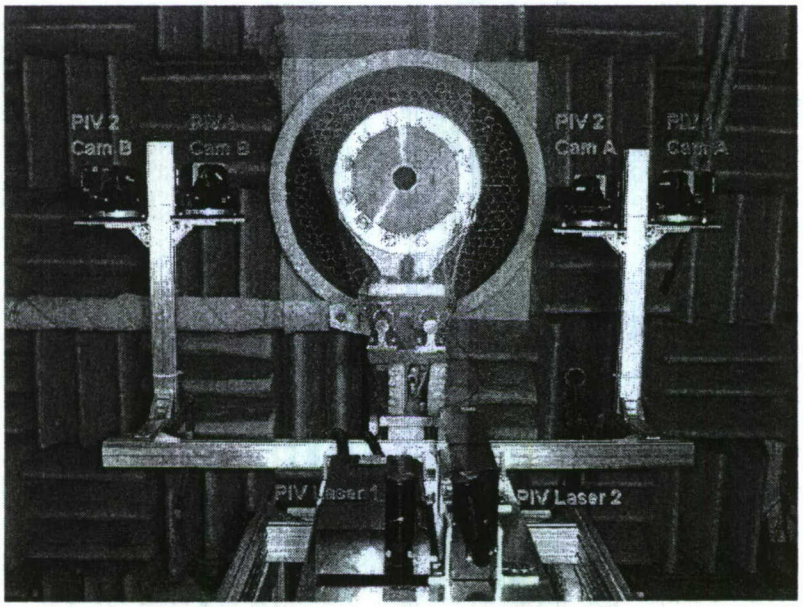

Figure 32. Dual-time PIV experiment setup.

The camera arrangement purposely makes the angle between the cameras in each pair equal to make the measurements from both systems as identical as possible. This minimizes the differences in the level of error which would be amplified when computing the time derivatives. The light sheets are orthogonally polarized and linear polarizing lenses are mounted on each camera to ensure separate measurements. Special care and time was taken in making the four laser sheets identical and aligning them to minimize the error between the measurements of both systems. The sheet thickness is 3 mm which is thick enough to enable the measurement of the out-of-plane component of velocity (u_x), which requires that a particle traveling through the light sheet is illuminated by both pulses of the lasers. In the present case, the delay between pulses is set to 5 μs, which allows a particle with a velocity of 200 m/s to move 1 mm within the 3 mm thick laser plane.

The choice of Δt is crucial in the finite difference computation of the time derivative of the velocity. If Δt is too small, $\Delta u = u(\vec{x}, t + \Delta t) - u(\vec{x}, t)$ will be of the same order of magnitude as the error associated with the PIV measurements themselves. If Δt is too large, then the dynamics of the flow at the time scales

of interest can not be resolved. Based on an extensive study on this subject was carried out a priori, a Δt of 25 μs was chosen for the downstream positions from x/D=3 to x/D=8 and a Δu of 35 μs for x/D=8.5 to x/D=10, as the time scales in the flow are larger further downstream.

C. Low-order dynamical system development

Given a complex system fluid flow, the goal in developing reduced order models (ROM) is to solve only a part of the infinite dimensional governing evolution equations (partial differential equations) by projecting these equations onto a subspace of finite dimensions, made up of a reduced basis of empirical eigenfunctions (like those provided by the POD). The level of complexity of a fluid flow increases with Reynolds number, but experiments at many different Reynolds numbers have shown that low-order analysis is effective throughout the whole range and that organized structures exist.

A Galerkin projection is the projection of a system of partial differential equations onto a finite basis of linearly independent functions. This projection can then be truncated to model only a part of the system. The proper orthogonal decomposition is a method that conveniently complements the Galerkin projection since the POD basis is orthonormal by construction and the functions are optimized in terms of the square of the velocity (i.e. the energy), hence when truncating the system at a low mode number, only the most energetic part of the flow is modeled in the system. Since an empirical method is used in the present work and the full Galerkin projection with explicit calculations of the projection coefficients is not performed, the analysis tied to the Galerkin projection in the case of incompressible flows is summarized in Bergmann.[7] The equations resulting from the projection are quadratic (as are the Navier-Stokes equations) but an important point lies in the fact that the Reynolds decomposition is used in the present case. Indeed, when separating the mean flow from the fluctuations in the projections, extra terms describing the interaction between the mean velocity and the turbulent fluctuations are derived by Ukeiley et *al.*[14] Since these terms are cubic in nature, an additional cubic term will be added to the modeling ODE to model this interaction. The second motivation for adding a cubic term in our case is that the flow cannot be considered incompressible, even though the previous developments were made using the incompressible version of the Navier-Stokes equations. Rowley *et al.*[8] apply a Galerkin projection to the full compressible Navier-Stokes equations and introduce a more appropriate inner product adapted for compressible flows. They also show that since the derived compressible equations are this time cubic in nature, a cubic model needs to be considered. Therefore, the following general ODE will be used in the development of an empirical low order dynamical system of the jet, as was similarly used by Perret,[21]

$$\frac{da_n}{dt} = D_n + \sum_{j=1}^{N_{LODS}} L_{nj}a_j + \sum_{j=1}^{N_{LODS}}\sum_{k=1}^{N_{LODS}} Q_{njk}a_j a_k + \sum_{j=1}^{N_{LODS}}\sum_{k=1}^{N_{LODS}}\sum_{l=1}^{N_{LODS}} C_{njkl}a_j a_k a_l \tag{45}$$

where D_n, L_{nj}, Q_{njk} and C_{njkl} are the constant, linear, quadratic and cubic terms of the dynamical system that need to be identified. As discussed above, these can be calculated directly using the analytical expressions derived from the Galerkin projection. Very finely resolved data (both in time and space) is however needed for such calculations and this direct technique would not be appropriate in the case of experimental PIV data where a significant amount of noise would be introduced by the double spatial derivatives and the computation of higher order terms. These coefficients will here be identified using an empirical method commonly referred to as the 'moments' method developed at the Laboratoire d'Etudes *Aérodynamiques* at the Univerity of Poitiers, France. The present work extends this technique and its application to a much higher speed flow to see how a more turbulent and less 'coherent' database affects the prediction capability of this method.

The moments method only requires an ensemble of statistically independent samples of the measurement and not a time-resolved signal. The method in fact converges faster when trained with independent samples rather than with slightly correlated measurements. The input database comprises for each independent time t_i a pair $(a_n(t_i), da_n/dt(t_i))$; i = 1, 2, ..., N. A linear forward differencing algorithm is used to compute the time derivative of the POD coefficients,

$$\frac{\partial a_n}{\partial t}(t_0) = \frac{a_n(t_0 + \triangle t) - a_n(t_0)}{\triangle t} \tag{46}$$

The advantage of using DT-PIV is that this term is measured directly. To determine each one of the constant, linear, quadratic and cubic coefficients one needs to derive as many equations as there are unknowns. In this aim, several moments of Eq. 45 are taken and ensemble averages are performed using the experimental database. The size of the problem can become very quickly unpractical especially when including cubic terms. One of the problems inherent to low-order dynamical systems in fluid dynamics is that the truncation performed, greatly reduces the dimensions of the problem but also neglects most of the smaller scales responsible for dissipating the energy through viscous forces. A common resulting behavior is for the dynamical system to rapidly diverge. To model the truncated scales and drain the energy in the system, an ad hoc artificial viscosity is introduced to consistently adjust the linear coefficient throughout all the modes. The number of modes kept in the low-order system is therefore always chosen to ensure the problem is well conditioned. This issue restricted the number of modes retained in the modeling to $N_{LODS} = 65$ in the quadratic case and $N_{LODS} = 12$ in the full modeling with the cubic terms.

A total of 6 low-order dynamical systems are developed at the downstream position of x/D=8 to study the influence of the different modeling parameters on the prediction of the dynamics and hence to find which are critical to building a successful dynamical system in a highly turbulent flow. These are detailed in Table6 below.

Table 6. Parameters used in the 6 different low-order dynamical systems.

System	Order	N_{LODS}	N_s	t_0	Total Eqns.	% TKE	Predicted time
LODS 1	cubic	12	4000	23	455	30	10ms
LODS 2	cubic	12	4000	35	455	30	10ms
LODS 3	quadratic	30	749	23	496	47	25ms
LODS 4	quadratic	48	3000	23	1225	57	10ms
LODS 5	quadratic	65	4000	23	2211	64	10ms
LODS 6	quadratic	65	4000	25	2211	64	10ms

The first two LODS were developed from the full cubic ODE and from a modeling stand point, contains the higher order terms necessary to model the interactions between the mean flow and the fluctuating velocities, since the Reynolds decomposition is used. Both systems are attracted towards the same dynamics even though the initial conditions were different. The predicted dynamics were low-dimensional in nature, as could be expected from the severe truncation of the higher modes, and tended to be drawn towards a sinusoidal limit cycle. The dominant frequency appeared around 500 Hz which is low compared to measurements performed with a laser doppler anemometer (LDA) in the same facility at $x/D = 6$. Hence, by extrapolation it would seem natural to find dominant frequency content in the vicinity of 1000 Hz at x/D=8, the present location under investigation. It can be concluded that severely truncated cubic models are not able to retrieve the higher frequency content in high-speed flows where the turbulence spectrum is broad and higher modes seem to play an important role.

The next four LODS are developed using the quadratic form of the ODE. The problem being much smaller compared to the cubic model, it is now possible to include many more modes in the system identification procedure. This is done with the aim of including additional smaller scales that are truncated in the cubic model and that seem to be crucial in highly turbulent flows to capture the higher frequency dynamics which are dominant in this flow. The quadratic model is able to be contained for a quite long period of time (25 ms) in a bounded domain. Although exhibiting significant periodicity in its dynamics, the frequency content is shown to be much more representative of the actual dynamics existing in such a flow, at around 1000 Hz, intermittently perturbed by higher frequency and amplitude fluctuations. The presence of high frequency dynamics are a large improvement on the previous cubic systems, which is largely due to the fact that a greater number of modes are kept in the modeling.

LODS 4, built with 48 POD modes and a greater number of training samples, is not able to stay bounded for as long as LODS 3. However much higher frequency dynamics than LODS 1 and LODS 2 is exhibited and the similar range of frequencies as LODS 3, around 1 kHz. Most likely a result of the amount of TKE

truncated from the system in the identification of the ODE coefficients. Purposely, LODS 5 is prescribed a high artificial viscosity of to study the consistency of the effect of this ad hoc parameter. Indeed the POD coefficients quickly converge to constant values due to an excessive action of the artificial viscosity in the system. The process of finding the right viscosity to compensate for the truncation is quite tedious but it is indispensable to prevent the system from either diverging (too low viscosity) or converging towards zero (too high viscosity). However once the parameters of the dynamical system are fixed and the coefficients of the system are identified, the successfully tuned viscosity will be efficient for all initial conditions and at least short time prediction is ensured. LODS 6 is developed with 65 modes, which represents the maximum size of the quadratic system without it being ill-conditioned. The higher number of training samples enables a better convergence of the statistics and hence a better conditioned matrix problem. This LODS presents the highest frequencies, which is consistent with the finding that the more modes are included in the system, the more realistic the frequency content retrieved in the system. Additionally, very important intermittency is observed in this case with high amplitude fluctuations followed by periods of rather low fluctuations. The study of the frequency content of the predicted velocity field demonstrates that a severe truncation of the higher modes in the case of the cubic modeling prevents any high frequency dynamics from being retrieved in the LODS.

D. Conclusions and recommendations

The moments method for systems identification has shown that it can be applied to low as well as high Reynolds number flows. The only shortcoming of low order modeling at high Reynolds numbers, and this is not specific to this method, is that the smaller scales that are truncated in the modeling play a considerably more important role for the dynamics of the flow as in the case of low Reynolds number flows. Indeed they are responsible for dissipating the TKE produced at the larger scales. Since production of TKE is much larger in highly turbulent flows, the dissipative scales become much more important and truncating them presents challenging consequences. This is not as much an issue in lower Reynolds number flows where for one part a lower number of modes captures a larger part of the TKE and also where the dissipative scales are not as crucial since production is not as important. Hence, in the low Reynolds number flows, a cubic model could be more effective at predicting the dynamics than a quadratic one. It is however shown here that modeling the interaction of the turbulence with the mean flow (through the cubic terms) is not as crucial as using as many modes as possible (hence 140 as much TKE as possible) in the development of the dynamical systems. It is therefore recommended that quadratic models with a larger number of modes be used when developing LODS's in high-speed and highly turbulent flows.

The choice in the truncation level has shown to be a crucial parameter and a careful study of the spatial distribution of the POD modes is highly recommended to prevent the system from being unstable. It was shown that the spatial POD modes can be associated to others by similarity of spatial features. This finding can guide the choice in the level of truncation to prevent groups of modes from being parted. This leads to the following recommendation, which is specific to axisymmetric flows.

When the measurement permits, it is suggested not to assume axisymmetry a priori and to learn from applying the 2D-POD to all three components of velocity instead of applying the Fourier transform in the azimuthal direction followed by the POD in the radial direction. In that case the phase relationship between the components is lost and the interpretation of the spatial POD modes becomes incomplete and perhaps misleading. Indeed interpreting the spatial structure of the POD modes has shown to be important in the choice of truncation level as well as insightful for the physical interpretation of the dominant structures in the flow in terms of turbulent kinetic energy. PIV measurements as well as CFD simulations enable estimations of the entire field, it can therefore be enriching to study the 2D-POD results without assuming axisymmetry in at least a first step.

References

[1]Glauser, M. N., Leib, S. J. & George, W. K., *Coherent structures in the axisymmetric jet mixing layer*, Turbulent Shear Flows **5** (1987), 134-145.

[2]Smith, J. T. M., *Cambridge aerospace series: Aircraft noise*, Cambridge University Press, New York, 1989.

[3]Ffowcs Williams, J. E. & Kempton, A. J., *The noise from the large scale structure of a jet*, J. Fluid Mech.**84** (1978), 673-694.

Kähler, C. J. and Kompenhans, J., *Fundamentals of multiple plane stereo particle image velocimetry*, Exp. Fluids (Suppl) **29** (2000), no. 7, S70-S77.

[4]Crow, S. C., & Champagne, F. H., *Orderly structure in jet turbulence* J. Fluid Mech. **48** (1971), 547-591.

[5]Lau, J. C., Fisher, M. J. & Fuchs, H. V., *The intrinsic structure of turbulent jets*, J. Sound & Vibration **22**:4 (1972), 379-406.

[6]Lighthill, M. J., *On sound generated aerodynamically: General theory*, Proceedings of the Royal Society, **211** (1952), no. 116, 564-587.

[7]Lighthill, M. J., *On sound generated aerodynamically II: Turbulence as a source of sound*, Proceedings of the Royal Society, **222** (1954), no. 1148, 1-32.

[8]Rowley, C. W., Colonius, T. & Murray, R. M., *Model reduction for compressible flows using POD and galerkin projection*, Physica D **189** (2004), no. 1-2, 115-129.

[9]Petersen, R. A., *Influence of wave dispersion on vortex pairing in a jet*, J. Fluid Mech. **89** (1978), 469-495.

[10]Fuchs, H. V., *Measurements of pressure fluctuations within subsonic turbulent jets*, J. Sound & Vibibration **22** (1972), 361-378.

[11]Wei, M. and Freund, J. B., *A noise-controlled free shear flow*, J. Fluid Mechanics **546** (2006), 123-152.

[12]Ukeiley, L., Seiner, J., & Ponton, M., *Azimuthal structure of an axisymetric jet mixing layer*, ASME FEDSM99-7252, (1999) July.

[13]Tinney, C. E., Glauser, M. N. & Ukeiley, L. S., *The evolution of the most energetic modes in a high subsonic Mach number turbulent jet*, AIAA Paper 2005-0417 (2005).

[14]Ukeiley, L., Cordier, L., Manceau, R., Delville, J., Glauser, M. N. & Bonnet, J-P., *Examination of the large-scale structures in a turbulent plane mixing layer. Part 2. Dynamical systems model*, J. Fluid Mechanics **441** (2001), 67-108.

[15]Hussain, A. K. M. F., *Coherent structures and turbulence*, J. Fluid Mechanics **173** (1986), 303-356.

[16]Brown, G. L. & Roshko, A., *On density effects and large structures in turbulent mixing layers*, J. Fluid Mech. **64** (1974), Part 4, 775-816.

[17]Goldstein M. E., *The low frequency sound from multipole sources in axisymmetric shear flows, with application to jet noise*, J. Fluid Mech. **70** (1975), Part 3, 595-604.

[18]Goldstein, M. E. & Lieb, S. J., *The role of instability waves in predicting jet noise*, J. Fluid Mech. **525** (2003), 3772.

[19]Lilley G. M., *Jet noise classical theory and experiments*, Aeroacoustics of Flight Vehicles: Theory and Practice, Volume 1: Noise Sources, NASA Reference Publication-1258, (1991), 211-285.

[20]Howe, M. S., *Contributions to the theory of aerodynamic sound, with application to excess jet noise and the theory of the flute*, J. Fluid Mech. **71** (1975), 625-673.

[21]Perret, L., *Etude du couplage instationnaire calculs-experiences en écoulements turbulents*, Ph.D. thesis, Université de Poitiers, Poitiers, France, 2004.

[22]Ribner, H. S., *The generation of sound by turbulent jets*, Adv. Appl. Mech. **8**, (ed. H. L. Dryden & Von Karman, T.) Academic Press, Inc., New York, 1964, 103-182.

[23]Tam, C. K. W., Golebiowski, M., & Seiner, J. M., *Two components of turbulent mixing noise from supersonic jets*, AIAA1996-1716 (1996).

[24]Crighton, D. J., *Basic principles of aerodynamic noise generation*, Progress in Aerospace Sciences **16** (1975), 31-96.

[25]Crighton, D. J. & Heurre, P., *Shear-layer pressure fluctuations and superdirective acoustic sources*, J. Fluid Mech. **220** (1990), 355368.

[26]Gamard, S., *Application of the slice POD to the far region of the axisymmetric jet*, Ph.D. thesis, State University of New York at Buffalo, 2002.

[27]Viswanathan, K., *Analysis of the two similarity components of turbulent mixing noise*, AIAA Journal **40** (2002), no. 9, 1735-1744.

[28]Bergmann, M., Optimisation aérodynamique par réduction de modèle pod et contrôle optimal. Application au sillage laminaire d'un cylindre circulaire, Ph.D. thesis, Institut National Polytechnique de Lorraine, Nancy, France, 2004.

[29]Arndt, R. E. A., Long, D. F., & Glauser, M. N., *The proper orthogonal decomposition of pressure fluctuations surrounding a turbulent jet*, J. Fluid Mech. **340** (1997), 1-33.

[30]Ko, N. W. M. & Davies, P. O. A. L., *The near field within the potential cone of subsonic cold jet*, J. Fluid Mech. **50** (1971), Part 1, 49-78.

[31]Sirovich, L., *Turbulence and the dynamics of coherent structures, Part 1: Coherent structures*, Quart. App. Math. **45** (1987), 561-571.

[32]Pinier, J. T., Ausseur, J. M., Glauser, M. N. & Higuchi, H., *Proportional closed-loop control of flow separation*, AIAA Journal **45** (2007), no. 1, 181-190.

[33]Cole, D. R., Glauser, M. N., & Guezennec, Y. G., *An application of stochastic estimation to the jet mixing layer*, Phys Fluids **4** (1991), no. 1, 192-194.

[34]Picard, C. & Delville, J., *Pressure velocity couping in a subsonic round jet*, Int. J. Heat & Fluid Flow **21** (2000), no. 3, 359-364.

[35]Tinney, C. E., Coiffet, F., Delville, J., Hall, A. M., Jordan, P., and Glauser, M. N., *On spectral linear stochastic estimation*, Exp. Fluids **41** (2006), no. 5, 763775.

[36]Lush, P. A., Fisher, M. J., & Ahuja, K. K., *Noise from hot jets*, British Acoustical Society, Proceedings. **2** (1973), no. 2, 1-14.

[37]Landau, L. D. & Lifshitz, E. M., *Fluid Mechanics*, Pergamon, London, UK, 1959.

[38]Tanna, H. K., *An experimental study of jet noise, Part 1: Turbulent mixing noise*, J. Sound & Vib. **50** (1977), no. 3, 405-428.

[39]Fisher, M. J., Lush, P. A., & Harper Bourne, M., *Jet noise*, J. Sound & Vib. **28** (1973), no. 3, 563-585.

[40]Morfey, C. L., Szewczyk, V. M., & Tester, B. J., *New scaling laws for hot and cold jet mixing noise based on a geometric acoustics model*, J. Sound & Vib. **61** (1978), no. 2, 255-292.

[41]Viswanathan, K., *Aeroacoustics of hot jets*, J. Fluid Mech. **41** (2004), 39-82.

[42]Bonnet J. P., Cole D. R., Delville J., Glauser M. N., & Ukeiley L. S. *Stochastic estimation and proper orthogonal decomposition: Complementary techniques for identifying structure*, Exp. in Fluids **17** (1994), 307-314.

[43]Hall, A. M., Tinney, C. E., & Glauser M. N., *Investigating the 'modified' complementary technique using pressure-velocity correlations of an axisymmetric jet* , AIAA Paper 2005-0039 (2005).

[44]Ukeiley L. S. & Murray, N. E. *Modified quadratic stochastic estimation of resonating subsonic cavity flow*, J. Turbulence, (*submitted for review*).

[45]Tinney, C. E. *Low-dimensional techniques for sound source identification in high speed jets*, Ph.D. thesis, Syracuse University, Syracuse, New York, 2005.

[46]Ewing D., & Citriniti, J., *Examination of a LSE/POD complementary technique using single and multi-time information in the axisymmetric shear layer*, Proceedings of the IUTAM Symposium on simulation and identification of organized structures in flows, (ed. Sorensen, Hopfinger, Aubry) Kluwer, Lyngby, Denmark, (1999), 375384.

[47]Dosanjh, D. S., Bhutiani, P. K., & Ahuja, K. K., *Supersonic jet noise suppression by coaxial multi-nozzle cold/heated jet flows*, Department of Transportation Final Report, Washington DC (1977).

[48]Tinney, C. E., Hall, A. M., Glauser, M. N. Ukeiley, L. S. & Coughlin, T., *Designing an anechoic chamber for the experimental study of high speed heated jets*, AIAA Paper 2004-0010 (2004).

[49]Melling, A., *Tracer particles and seeding for particle image velocimetry*, Meas. Sci. Tech. **8** (1997), 1406-1416.

[50]ANDERSON, J. D., *Modern compressible flow with historical perspective*, 3rd Ed., McGraw-Hill, New York, 2003.

[51]Coiffet, F., Delville, J., Ricaud, F., & Valiere, J.C., *Nearfield pressure of a subsonic free jet, estimation and separation of hydrodynamic and acoustic components*, Proceedings of the 10^{th} European Turbulence Conference (ed. Anderson, H. I. & Krogstad, P. A.), Trondheim, Norway, (2004) 168.

[52]Hall, J. W., Hall, A. M., Pinier, J. T., & Glauser, M. N., *The spectral relationship between the near-field and far-field pressure in a turbulent jet*, AIAA Journal (*submitted for review*).

[53]Hall, A. M., *An experimental investigation of the pressure-velocity correlation of an axisymmetric jet*, Master's thesis, Syracuse University, Syracuse, New York, 2004.

[54]Hall, A. M., Pinier, J. T., & Glauser M. N., *Identifying the most energetic modes of the pressure near-field region of a Mach 0.85 axisymmetric jet*, AIAA Paper 2006-0314 (2006).

[55]Mollö-Christensen, E. & Narasimha, R., *Sound emission from jets at high subsonic velocities*, J. Fluid Mech. **8**(1960), 49-60.

[56]Bodony, D. J. & Lele, S. K., *Jet noise presdiction of cold and hot subsonic jets using large-eddy simulation*, AIAA Paper 2004-3022 (2004).

[57]Tam, C. K. W. & Ariault, L., *Jet mixing noise from fine-scale turbulence*, AIAA Journal **37** (1999) , no. 2, 145-153.

[58]Ribner, H. S., *Comment on "Jet mixing noise from fine-scale turbulence*, AIAA Journal **38** (2000), no. 2, 377-379.

[59]Fisher, M. J., *Comment on "Jet mixing noise from fine-scale turbulence*, AIAA Journal **38** (2000), no. 2, 379-380.

[60]Bridges, J. & Wernet, M., *Measurements of the aeroacoustic sound source in hot jets*, AIAA Paper 2003-3130 (2003).

[61]Lew, P., Blaisdelly, G. A., & Lyrintzisz, A. S., *Recent progress of hot jet aeroacoustics using 3-D large-eddy simulation*, AIAA Paper 2005-3084 (2005).

[62]Witze, P. O., *Centerline velocity decay of compressible free jets*, AIAA Journal **12** (1974), no. 4, 417-418.

[63]Alkislar, M. B., Krothapalli, A. & Butler, G. W., *The effect of streamwise vortices on the aeroacoustics of a Mach 0.9 jet*, J. Fluid Mech. **578** (2007), 139-169.

[64]Arakeri, V. H., Krothapalli, A., Siddavaram, V., Alkislar, M. B., & Lourenco, L. M., *On the use of microjets to surpress turbulence in a Mach 0.9 axisymmetric jet*, J. Fluid Mech. **490** (2003), 75-98.

[65]Tinney, C. E., Glauser, M. N., & Ukeiley, L. W., *Low-dimensional characteristics of transonic jet. Part 1: Proper orthogonal decomposition*, J. Fluid Mech. (*submitted for review*).

[66]Ukeiley, L., Tinney, C. E., Mann, R., & Glauser, M. N., *Spatial correlations in a transonic jet*, AIAA Journal, **45** (2007), no. 6, 1357-1369.

[67]Pinier, J. T., *Low-dimensional techniques for active control of high-speed jet aeroacoustics*, Ph.D. thesis, Syracuse University, Syracuse, New York, 2007.

[68]Proudman, I., *The generation of noise by isotropic turbulence*, Proceeding of the Royal Society of London A, **214** (1952), no. 1116, 129-132.

[69]Ribner, H. S., *Quadrupole correlation governing the pattern of jet noise*, J. Fluid Mech., **38** (1969), no. 1, 1-24.

[70]Jordan, P. & Gervais, Y., *Modelling self- and shear-noise mechanisms in inhomogeneous, anisotropic turbulence* , J. Sound & Vib. **279** (2005), Issues 3-5, 529-555.

[71]Freund, J. B., *Noise source turbulence statistics and the noise from a Mach 0.9 jet*, Phys. Fluids **15** (2003), no. 6, 1788-1799.

[72]Panda, J., Seasholtz, R. G., Elam, K. A., Mielke, A. F., & Eck, D. G., *Effect of heating on turbulent density fluctuations and noise generation from high speed jets*, AIAA Paper 2004-3016, (2004).

[73]Crighton, D. J., *The excess noise field of subsonic jets*, J. Fluid Mech. **56** (1972), Part 4, 683-694.

[74]Powell, A., *Aerodynamic and jet noise*, Handbook of Acoustics, John Wiley & Sons, Inc., 1998.

[75]Samimy, M., Kim, J.-H., Kastner, J., Adamovich, I., & Utkin, Y., *Active control of a Mach 0.9 jet for noise mitigation using plasma actuators*, AIAA Journal **45** (2007), no. 4, 890-901.